Catalyst Development for Dry Reforming of Methane and Low-temperature Water-gas Shift Reaction

A Thesis

by

Rothman Y.F. Kam

B.Eng. (Chemical and Materials Engineering)

Submitted to the Monash University in Partial Fulfillment of the Requirements for the Degree of

Doctor of Philosophy in **Chemical Engineering**

Chemical Engineering Department

Monash University

Australia

August 2010

Copyright Notices

Notice 1

Under the Copyright Act 1968, this thesis must be used only under the normal conditions of scholarly fair dealing. In particular no results or conclusions should be extracted from it, nor should it be copied or closely paraphrased in whole or in part without the written consent of the author. Proper written acknowledgement should be made for any assistance obtained from this thesis.

Notice 2

I certify that I have made all reasonable efforts to secure copyright permissions for third-party content included in this thesis and have not knowingly added copyright content to my work without the owner's permission.

ABSTRACT

Both dry reforming of methane (DRM) and low-temperature water-gas shift (LT-WGS) processes can be integrated into a fuel cell plant and are utilised for the production of hydrogen as an important energy source for fuel cells. Improvement of current catalytic systems, and identification and development of alternative catalysts for DRM and LT-WGS reactions have formed the basis of this study.

In the first stage of the work, the influence of WO_3 on a Pt/CeO_2 catalyst was investigated for the dry reforming of methane. It was found that Pt/CeO_2 catalysts loaded with WO_3 at 10 mol% to 20 mol% were very stable during 20 hours of dry reforming of methane operation in comparison to a commercial Ni catalyst. However further addition of WO_3 (>70%) promoted coking on the Pt/CeO_2 sample, ultimately leading to catalyst deactivation.

It was also desirable to develop catalysts with higher activity to reduce operating cost, thus the physicochemical properties of different materials were assessed to identify parameters important for LT-WGS activity. Copper catalysts on metal oxide support (CeO_2, ZnO, TiO_2, SiO_2, Al_2O_3, ZrO_2, MgO and SnO_2) were screened, while characterisation showed the catalyst adsorbing H_2O and CO was crucial in generating LT-WGS activity, with Cu/ZnO attaining the highest LT-WGS activity. Lanthanum (La) was known to have high affinity for H_2O, hence the effects of La doping on Cu/ZnO catalysts for use in LT-WGS reaction was investigated. The findings

indicated the La promoter improved activity at a loading of 2.3 wt%, above which the activity significantly decreased.

A systematic investigation has also been conducted on the effects of oxygen introduction on the Cu-based and Pt-based catalysts during LT-WGS operation with particular attention on the pyrophoricity (i.e. vulnerability to oxidative sintering) of the catalysts, and the impacts on key material characteristics. The objective was to examine whether the catalysts were suitable for fuel cell applications. It was observed that the Cu-based catalysts were pyrophoric and therefore not a suitable catalyst. No pyrophoricity was observed for Pt-based catalysts. Pt/CeO_2 was the only catalyst that retained its activity, displaying no loss in specific surface area or metal dispersion throughout the entire process, rendering it a suitable candidate for fuel cell systems.

ACKNOWLEDGEMENTS

I express my deepest gratitude to Dr. Cordelia Selomulya for her tireless supervision, faith and advice throughout the Ph.D. project, both as mentor and friend. I am equally thankful to my co-supervisors at CSIRO, Dr. Nick Burke and Dr. Ken Chiang, whose patience and kindness, as well as their academic experience, has been invaluable to me. I am extremely grateful to my co-supervisors at UNSW, Dr. Jason Scott and Prof. Rose Amal, who have been critical towards my knowledge in catalysis and for hosting my stay at the Particle and Catalysis Research Group of UNSW. They have been the source of continuous inspirations through which many new ideas were developed within this project.

Completion of the project would not have been possible without the assistance of Dr. Wey Yang Teoh (UNSW) for his assistance during FSP synthesis, Katie Levick (UNSW) on TEM imaging, Dr. Bill Gong (UNSW) and Dr Robert Jones (La Trobe University) on XPS analysis. The contribution of Mr. Finlay Shanks of Monash University on RAMAN analysis is acknowledged. Note of thanks to lab manager John Starling (UNSW) and Kim Phu (Monash) for constantly procuring chemicals. The technical support of Phil Thompson, Paul Brockbank and Geoff Vaughn was critical in ensuring smooth operations of the WGS reactor.

I am indebted to my many student colleagues for providing a stimulating and fun environment in which to learn and grow. I am especially grateful to Dr. Andrew Sim, Dr. Richard Kydd, Yung Kent Kho, Yuan Fang, Carrie Chen, Hue Chen Au-Yong,

Ria Amelia, Clain Law, Amanthi Jayemanne, Xiao Pei Hoo, Ruby He and Alice Yuen for their friendship and support. Dr. Peter Bradford was particularly helpful for patiently teaching me English while we were conducting experiments in the laboratory.

Lastly, and most importantly, this thesis is dedicated to my parents, Serena Kam and Peter Kam, without whom none of this would have been even possible.

RESEARCH PAPERS AND PUBLICATIONS

Journal publications:

1. Rothman Kam, Cordelia Selomulya, Rose Amal, Jason Scott. (2010) The influence of La-doping on the activity and stability of Cu/ZnO catalyst for the low-temperature water-gas shift reaction, *Journal of Catalysis*. **273**: 73-81.

2. Rothman Kam, Jason Scott, Rose Amal, Cordelia Selomulya. (2010) The role of metal oxides in promoting Cu as catalyst for the low-temperature water-gas shift reaction, (**submitted** to *Chemical Engineering Journal*).

3. Rothman Kam, Jason Scott, Rose Amal, Cordelia Selomulya. (2010) Pyrophoricity and stability of copper and platinum based water-gas shift catalysts during oxidative shut-down/start-up operation, (s**ubmitted** to *Chemical Engineering Science*).

4. Rothman Kam, Nick Burke, Ken Chiang, Andrew Sim, Cordelia Selomulya. (2010) CeO_2/WO_3 as support for Pt catalyst: Implications for dry reforming of methane, (**in preparation** for submission to *Chemical Engineering Science*).

TABLE OF CONTENTS

CHAPTER ONE

Introduction

1.1 Overview

Global warming caused by the combustion of fossil fuel has resulted in damaging effects to the environment [1]. Currently there is an initiative to limit or 'phase out' the use of non-renewable carbon-based energy sources to minimise the risk of irreparable damage to our ecosystem. Thus rigorous research and development on alternative carbon-free or 'green' energy have been put forward to overcome the greenhouse gas emission problem. However, the transition toward clean energy is relatively slow because of perceived lack of economic competitiveness with established technologies [2].

Fuel cell is an emerging technology for efficient energy production. The concept behind fuel cell is that it directly produces electricity from chemical energy of fuels rather than from combustion, rendering fuel cells twice as efficient as the internal combustion engine [3]. The general functionality of a fuel cell involves the dissociation of hydrogen over a platinum catalyst at the anode into protons and electrons. The electrons proceed through an external circuit where their energy can be harnessed in the form of electricity and applied to a load. The protons arrive at the cathode where they combine with oxygen to form water [4]. Thus, only environmentally friendly by-products (water and heat) are produced when hydrogen is used as the source of energy.

Hydrogen is an attractive alternative fuel and a prime candidate for replacing conventional fossil fuels, provided methods can be found to generate hydrogen cheaply and efficiently [2]. A number of strategies have been developed to generate hydrogen by utilising a range of resources, but the most heavily employed method is by extracting hydrogen from natural gas. It is also possible to extract hydrogen from water using electrolysis techniques, but this is still a highly inefficient process with a high energy cost for extraction. The studies described in this thesis are focused on two chemical reactions to generate hydrogen; the dry reforming of methane and the water-gas shift reaction, both of which are among the typical fuel processing methods in conjunction with fuel cells.

Hydrogen production from methane (CH_4) as the main constituent of natural gas usually consists of two steps. The first step is the steam reforming of methane ($CH_4 + H_2O \rightarrow CO + 3H_2$) where CH_4 reacts with steam to form synthesis gas [5] or 'syngas'.
Steam reforming of methane is usually carried out over a Ni/Al_2O_3 catalysts at a temperature of about 750 ºC to 800 ºC, giving a mixture of CO and H_2 with a relative CO/H_2 ratio around 0.33. In the second step, CO is further oxidised to CO_2, leading to more H_2 by employing a water-gas shift ($CO + H_2O \rightarrow CO_2 + H_2$) reaction.

In this thesis, an alternative process called the dry reforming of methane ($CH_4 + CO_2 \rightarrow 2CO + 2H_2$) will be assessed. The main advantage of this reaction over steam reforming is the ability to convert two greenhouse gases (methane and carbon dioxide) to syngas [6].

Catalyst development has played a crucial role in the advancement of these processes, nevertheless, the fundamental needs for catalysts to promote higher product selectivity while at the same time exhibiting high stability are still the greatest motivation for any catalytic research. The main research described in this thesis will focus on catalysts development for the dry reforming of methane and catalyst study for the low-temperature water-gas shift reaction, both of which are important processes for the production of hydrogen.

1.2 Dry reforming of methane

Dry reforming of methane (DRM) does not require generation of expensive steam as required for steam reforming. The DRM uses methane which is reacted with CO_2 gas in the presence of a catalyst, producing CO and H_2 with a ratio of 1:1 (Eq. 1.1), a trait desirable for methanol and Fischer-Tropsch synthesis.

$$CH_4 + CO_2 \rightarrow 2CO + 2H_2 \qquad \Delta H°_{298} = +247 \text{ kJ mol}^{-1} \qquad \text{(Eq. 1.1)}$$

Rhodium and ruthenium noble metal catalysts demonstrate high activity for the dry reforming reaction, with no observed carbon formation [7]. Whilst nickel catalysts traditionally used in the steam reforming reaction are also active for dry reforming reaction, rapid deactivation via carbon deposition and sintering of the active metal phase always occurs with this system [8]. There is a marked decrease in the rate of reforming observed for the dry reforming reaction in comparison to steam reforming. This could be explained by the increased ratio of CO formed, resulting in higher levels of coking from the Boudouard reaction (Eq. 1.2) and more rapid catalyst deactivation [9].

$$2CO \rightarrow C + CO_2 \qquad \Delta H°_{298} = -172 \text{ kJ/mol} \qquad \text{(Eq. 1.2)}$$

Addition of TiO_x demonstrates an increased activation barrier for the CO dissociation reaction, inhibiting carbon formation by blockage of active sites at which carbon deposition may occur. MgO is also used to react with Ni to form a solid solution, aiding in prevention of carbon dissolution into the nickel crystal [10]. Ceria (CeO_2) has demonstrated unique properties in being able to oxidize carbon species to regenerate the catalyst and prevent deactivation even at low temperatures [11]. Ceria as a catalyst has proven highly effective, while ceria as a promoter has demonstrated both increasing catalytic stability and enhanced prevention of catalyst coking by the removal of adsorbed carbon species. Studies have shown that platinum (Pt) catalysts supported on CeO_2 has been used successfully in the dry reforming of methane because of its moderate activity and stability [12]. The superiority of the Pt/CeO_2 catalysts over Ni-based catalysts stems from the excellent stability because of minimal metallic phase sintering [13] and prevention of coking [12]. However, the activity is still too low to be of commercial interest, hence the effort to find a suitable promoter to increase the catalytic activity of Pt/CeO_2.

1.3 Water-gas shift reaction

The water-gas shift (WGS) reaction is present in several industrial processes including coal gasification, steam reforming, and ammonia production. It is the reaction between CO and steam to produce CO_2 and H_2 as shown in Eq. 1.3.

$$CO + H_2O \leftrightarrow CO_2 + H_2 \qquad \Delta H°_{298} = -41.1 \text{ kJ mol}^{-1} \qquad \text{(Eq. 1.3)}$$

The WGS reaction is a slightly exothermic reaction, with equilibrium constant decreasing with increasing temperature. Since the 1960s, the WGS reaction has mainly been used in H_2 production for ammonia synthesis, and hydro-treatment for petroleum

and coal processing. Typically, when high purity H_2 is required, the WGS reaction is carried out in two stages; a low-temperature reaction stage operated at about 200 °C to 300 °C over the ternary copper/zinc oxide/alumina mixed oxides and a high-temperature reaction stage operated at about 350 °C to 450 °C over the iron oxide/chromium oxide type catalysts [14].

The high temperature iron oxide-based catalyst is promoted with chromium oxide which increases the catalyst lifetime by suppressing sintering. Iron oxide catalysts can tolerate low sulphur concentrations and can effectively reduce inlet CO concentrations from about 40 mol% down to the equilibrium CO value dictated by the operating temperature (i.e. ~3% at about 450 °C [15, 16]. The Cu-based WGS reaction catalysts which typically operate in plants for about 2 to 4 years can effectively reduce CO concentrations down to about 0.1% [15]. In addition to their high catalytic activity, the low temperature Cu-based catalysts exhibit higher reaction selectivity and fewer side reactions at elevated pressure compared to the high temperature shift catalysts. A disadvantage of the Cu-based catalysts, however, is their lack of sulphur tolerance, being poisoned by very low sulphur concentrations. In this work, the emphasis will be on the low-temperature WGS reaction because of the favourable thermodynamics for the formation of hydrogen and the ability to reduce CO, which is a poison to the Pt electrodes in fuel cells [17].

1.4 Research aims and thesis outline

The purpose of the current research was to explore the intrinsic properties of the catalysts that govern the mechanisms for the aforementioned chemical reactions. Based

on this knowledge, new combination of catalysts have been developed and characterised for the dry reforming of methane and water-gas shift reaction in order to tackle the challenges as mentioned in **Sections 1.2** and **1.3**.

In view of these current challenges, the specific research aims are:

Catalyst development for dry reforming of methane

- To investigate the effects of WO_3 promoter on Pt/CeO_2 catalyst during the dry reforming of methane with emphasis on oxygen mobility and capacity of CeO_2. Here, the influence of WO_3 on Pt/CeO_2 catalyst activity and stability were studied under a continuous flow condition. The catalysts were compared with a benchmark commercial Ni/Al_2O_3 catalyst for the dry reforming of methane.

Catalyst study for the low-temperature water-gas shift reaction

- Physicochemical properties of copper/metal oxide catalysts were assessed to identify parameters important for low-temperature water-gas shift activity. Metal oxides supports investigated were CeO_2, ZnO, TiO_2, SiO_2, Al_2O_3, ZrO_2, MgO and SnO_2, with the selection designed to provide a range of characteristics including surface area, reducibility, and acid/base strength.

- To explore the effect of lanthanum (La) as a promoter in the Cu/ZnO catalytic system during water-gas shift reaction, in particular the influence of La on Cu/ZnO catalyst activity and stability. Insights on the mechanisms governing catalyst performance of La promoted Cu/ZnO catalysts were also investigated. The catalysts

were bench-marked against a commercial $Cu/ZnO/Al_2O_3$ formulation for the low-temperature water-gas shift reaction.

- To investigate the activity and stability of Cu/ZnO-based catalysts and Pt-based catalysts during oxidative shut-down/start-up low-temperature water-gas shift operating conditions. The pyrophoric properties of the catalyst were also examined.

The literature review (**Chapter Two**) outlines the current catalyst developments for the dry reforming of methane and the water-gas shift reaction and also the challenges imposed during the application of the catalysts. The DRM is one method of hydrogen production; however, the conventional Ni catalyst employed for this reaction usually succumbs to deactivation through both sintering of the active metal and carbon formation. Similarly, the WGS catalysts are also prone to sintering during operation. Identification of alternative catalytic systems that may improve the activity without deactivation under similar circumstances is tentatively identified.

Based on the information from literature survey and the extrapolation of the mechanism, clear guidelines were developed for the promotion and development of Pt catalyst on a binary ceria (CeO_2) and tungsten trioxide (WO_3) supports for the dry reforming of methane, with the performance of several Pt/CeO_2-WO_3 catalyst formulations investigated in a fixed bed reactor (**Chapter Three**).

Chapter Four to **Six** focuses on catalyst study and development for low-temperature WGS reaction. **Chapter Four** outlines the results from the screening of copper catalyst supported on various metal oxides for low-temperature WGS activity. The aim is to find

the intrinsic properties of the metal oxide support on the performance of Cu catalysts responsible for WGS activity.

From the screening tests, CO and H_2O-temperature programmed desorption (TPD) studies showed that the bifunctionality of the catalyst in adsorbing H_2O and CO was crucial in generating low-temperature WGS activity. Lanthanum oxide (La_2O_3) is known to have high affinity towards H_2O and has demonstrated to provide structural stability for Al_2O_3 based catalysts. With this notion, the H_2O absorbing property of the La_2O_3 is exploited and used to promote the Cu/ZnO-based catalyst for the low-temperature WGS reaction. **Chapter Five** summarises the extensive characterisation and activity testing done on the novel La-doped Cu/ZnO catalyst. Additionally, the mechanism that governs the performance of the catalyst is also investigated.

In **Chapter Six**, the pyrophoricity of Cu/ZnO-based and Pt-based catalysts will be studied during oxidative shut-down/start-up of the low-temperature WGS reaction to assess whether these catalysts are suitable for fuel cell application. The cyclic oxidative shut-down/start-up operation is frequently encountered in a fuel cell set-up. Hence, the aim is to investigate the activity and stability of Cu/ZnO-based catalysts, including those loaded with refractory oxides such as Al_2O_3 and La_2O_3, and Pt-based catalyst under such conditions. The pyrophoric properties of the catalysts were also examined. To the best of knowledge, this is the first time an investigation has been conducted on the effects of oxygen introduced to the Cu-based and Pt-based catalysts during low-temperature WGS operation.

Chapter Seven concludes the work with discussion on the major findings and recommends the scope for further exploration of catalyst development for DRM and low-temperature WGS reactions.

1.5 References

1. R.A. Houghton and G.M. Woodwell, 'Global Climatic Change', *Scientific American* 260(4) (**1989**) 36-44.
2. J. Ogden, 'High hopes for hydrogen', *Scientific American* 295 (**2006**) 94-101.
3. D.L. Trimm, 'Minimisation of carbon monoxide in a hydrogen stream for fuel cell application', *Applied Catalysis A: General* 296 (**2005**) 1-11.
4. J. Larminie and A. Dicks, *Fuel Cell Systems Explained*, Wiley, New York, **2000**.
5. S. Matar, M.J. Mirbach, and H.A. Tayim, *Catalysis in Petrochemical Processes*, Kluwer Academic Publishers, Dordrchtm, Holland, **1989**.
6. J.H. Lunsford, 'Catalytic conversion of methane to more useful chemicals and fuels: a challenge for the 21st century', *Catalysis Today* 63 (**2000**) 165-174.
7. J.R. Rostrup-Nielsen and J.H.B. Hansen, 'CO_2-Reforming of Methane over Transition Metals', *Journal of Catalysis* 144 (**1993**) 38-49.
8. J.W. Snoeck, G.F. Froment, and M. Fowles, 'Steam/CO_2 Reforming of Methane. Carbon Formation and Gasification on Catalysts with various Potassium Contents', *Industrial & Engineering Chemistry Research* 41 (**2002**) 4252-4265.
9. J.R. Rostrup-Nielsen and J.H.B. Hansen, 'CO_2-Reforming of Methane over Transition Metals', *Journal of Catalysis* 144(1) (**1993**) 38-49.
10. M.C.J. Bradford and M.A. Vannice, 'Catalytic reforming of methane with carbon dioxide over nickel catalysts. 1. Catalyst characterization and activity', *Applied Catalysis A - General* 142(1) (**1996**) 73-96.
11. E. Aneggi, M. Boaro, C. de Leitenburg, G. Dolcetti, and A. Trovarelli, 'Insights into the redox properties of ceria-based oxides and their implications in catalysis', *Journal of Alloys and Compounds* 408 (**2006**) 1096-1102.
12. S. Damyanova, B. Pawelec, K. Arishtirova, M.V.M. Huerta, and J.L.G. Fierro, 'The effect of CeO_2 on the surface and catalyric properties of Pt/CeO_2-ZrO_2

catalysts for methane dry reforming', *Applied Catalysis B: Environmental* 89 (**2009**) 149-159.

13. Y. Nagai, T. Hirabayashi, K. Dohmae, N. Takagi, T. Minami, H. Shinjoh, and S.i. Matsumoto, 'Sintering inhibition mechanism of platinum supported on ceria-based oxide and Pt-oxide–support interaction', *Journal of Catalysis* 242 (**2006**) 103–109.
14. D.S. Newsome, 'The Water-Gas Shift Reaction', *Catalysis Reviews: Science and Engineering* 21(2) (**1980**) 275-318.
15. C.H. Bartholomew and R.J. Farrauto, *Fundamentals of Industrial Catalytic Processes*. 2nd Edition ed, John Wiley & Sons, Ltd, Hoboken, NJ, **2006**.
16. G. Ghiotti and F. Bocuzzi, 'Chemical and Physical Properties of Copper-Based Catalysts for CO shift Reaction and Methanol Synthesis', *Catalysis Reviews: Science and Engineering* 29(2 & 3) (**1987**) 151-182.
17. D.L. Trimm and Z.I. Onsan, 'Onboard fuel conversion for hydrogen-fuel-cell-driven vehicles ', *Catalysis Reviews* 43 (2001) 31–84.

CHAPTER TWO

Literature Review

2.1 Introduction

With concerns of global warming caused by the possibility of anthropogenic greenhouse gas emission, a correlation of mean global temperature rise with atmospheric CH_4 and CO_2 is established [1]. Consequently, there has been increased interest in a better understanding of CH_4 and CO_2 removal, disposal, and utilisation. The 'dry reforming of methane' (Eq. 2.1) is one such method to transform CO_2 and CH_4 to synthesis gas (i.e. CO and H_2), which can then be used in chemical energy transmission system [2-4] or utilised in the Fisher-Tropsch reaction to produce liquids [5, 6].

$$CH_4 + CO_2 \rightarrow 2CO + 2H_2 \qquad \Delta H°_{298} = +247 \text{ kJ mol}^{-1} \qquad \text{(Eq. 2.1)}$$

CH_4 and CO_2 are relatively inexpensive due to their natural abundance; hence, conversion of these two molecules to higher-value compounds is of interest. Reforming with CO_2, rather than H_2O, is attractive because it yields synthesis gas with lower H_2/CO ratios, which is a preferable feedstock for the Fischer–Tropsch synthesis of long-chain hydrocarbons [7]. In addition, other reaction pathways have also been explored. The formation of acetic acid from CH_4 and CO_2 gases over Pd and Cu catalysts has been reported [8], and the oxidative coupling of CH_4 to produce C_2 hydrocarbons using CO_2 as the oxidant has been observed, although yields are very low [9, 10]. However, the preeminent reaction to convert these two reactants is CO_2 reforming of CH_4 or 'dry reforming' (DRM). In 1999, Bradford and Vannice [11] published a comprehensive

review of the dry reforming of methane which critically reviewed the reaction chemistry with emphasis on CH_4 and CO_2 activation mechanisms on the catalyst's active sites, carbon deposition on catalyst surface and the kinetics that governs the dry reforming reaction over supported transition metal catalysts.

The water-gas shift (WGS) reaction is an important industrial process which usually proceeds after hydrocarbon reforming. It is a reversible, exothermic chemical reaction for controlling the H_2 and CO levels in product streams for industrial processes such as hydrogen production, methanol, ammonia and Fischer–Tropsch synthesis. The reaction describes the reaction between carbon monoxide and water vapour to produce carbon dioxide and hydrogen (Eq. 2.2).

$$CO + H_2O \leftrightarrow CO_2 + H_2 \qquad \Delta H°_{298} = -41.1 \text{ kJ mol}^{-1} \qquad \text{(Eq. 2.2)}$$

Interest in fuel cells as an alternate means for efficient energy production has given rise to research in fuel processing. The WGS reaction is among the typical fuel processing reactions studied in conjunction with fuel cells. The DRM can be integrated into the fuel cell plant (Fig. 2.1). Natural gas (predominantly methane) is fed to the reformer which converts the methane and CO_2 into CO and H_2 at elevated temperatures in a catalytic process called dry reforming. Next, the product gas from the dry reforming reactor undergoes WGS reaction in two stages, high-temperature (HT) and low-temperature (LT). Thus both stages work to convert the energy trapped in the unwanted carbon monoxide into additional usable hydrogen for the fuel cell. The last step in the fuel processing section is the preferential oxidation unit (PrOx). This step provides further oxidation of the remaining CO to CO_2 in the reformate stream by oxygen before it is sent to the fuel cell [12]. Ultimately, the amount of CO in the feed to the fuel cell should be below the tolerable level of 50 ppm, as it is toxic to the fuel cell operation [13, 14].

Typically, the PrOx is operated at lower temperatures than the water-gas shift reaction and occurs over a highly selective Cu metal on which oxygen reacts with the unwanted CO without wasting substantial hydrogen [12]. Once the reformate stream has achieved the desired composition, it proceeds to the anode of the fuel cell stack assembly where the protons are separated from the electrons as they pass through the electrolyte membrane (in the case of the PEM fuel cell) while the electrons travel through the circuit creating electric current. This current may then be utilised to perform electric work before the protons and electrons reunite at the cathode with oxygen (typically from air) to form the environmentally benign by-products water and heat in addition to CO_2 from reformate which in turn can be fed back into the dry reformer.

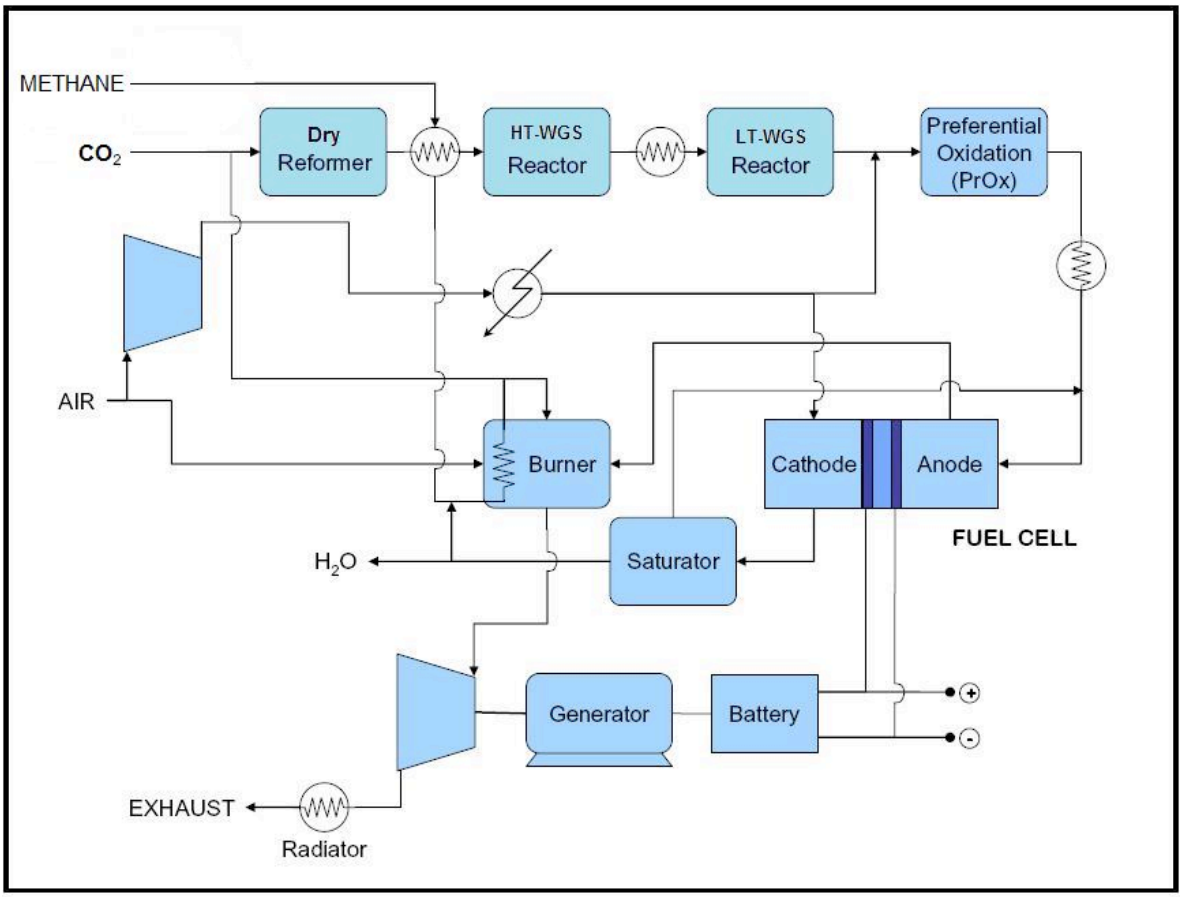

Fig. 2.1: **Schematic of a fuel cell plant integrated with dry reforming of methane and water-gas shift processes.**

This chapter will begin with a brief introduction to catalysts development and preparation for dry reforming of methane, including catalytic strategies to tackle the problem of carbon deposition and deactivation commonly encountered during DRM. More detailed focus will be placed on HT-WGS and LT-WGS reaction with an aim at providing aspects related to catalyst development. Finally, the status of WGS reaction mechanisms and associated kinetics are briefly examined.

2.2 Catalysts for dry reforming of methane

2.2.1 Nickel-based catalysts

Whilst nickel catalysts traditionally used in the steam reforming reaction are also active for the dry reforming reaction, however, rapid deactivation via carbon deposition and particle sintering always accompanies this system [15]. There is a marked decrease in the rate of reforming observed for the dry reforming reaction in comparison to steam reforming. This could be explained by the increased ratio of CO formed, resulting in higher levels of coking from the Boudouard reaction (Eq. 2.3) and more rapid catalyst deactivation [16].

$$2CO \rightarrow C + CO_2 \qquad \Delta H^\circ_{298} = -172 \text{ kJ/mol} \qquad \text{(Eq. 2.3)}$$

Braford & Vannice (1996) found the addition of TiO_x to Ni catalyst demonstrated an increased activation barrier for the CO dissociation reaction, inhibiting carbon formation by blockage of active sites at which carbon deposition may occur [17, 18]. MgO is also used to react with Ni to form a solid solution, aiding in prevention of carbon dissolution into the nickel crystal [19]. In contrast, a lack of metal support

interaction in Ni/SiO_2 permitted substantial formation of filamentous whisker carbon and hence catalyst deactivation during DRM. Recently, Barros et al. [20] developed a $La_2NiO_4/\alpha\text{-}Al_2O_3$ catalyst prepared by a unique microwave assisted self-combustion method. The following reaction conditions were employed: total flow rate of 50 ml min^{-1} (Ar = 40 ml min^{-1}, CH_4 = 5 ml min^{-1}, CO_2 = 5 ml min^{-1}); temperature of 700 °C; 200 mg of reduced catalyst. The sample showed initial CH_4 conversion (84%) with low carbon deposition which caused slight deactivation over 60 h of time on stream from CH_4 conversion of 84% to 78%. Modified Ni/Al_2O_3 catalysts was also studied by Luna et al. [21] using 0.5 wt% K, Sn, Mn and Ca as alkali promoters prepared by sol-gel method. Alkali promoters are known to affect the reducibility, morphology and the electronic properties of the Ni catalyst [22] hence improving its performance during DRM [21]. Luna et al. [21] found the growth of carbon filaments occurs on an unmodified Ni/Al_2O_3 catalyst particularly on the Ni metal surface where the active metal is carried at the tip of the carbon filament and, as a consequence, the catalytic activity remains constant since the active Ni is still accessible to the reactants. In the case of the Ca, Mn and Sn-modified catalysts, a dramatic reduction of catalytic activity and a significant increase in carbon deposition were observed during their reaction condition of 750 °C, 1 atm, CH_4/CO_2 = 1, $W/F°_{CH4}$: 0.5 g h mol^{-1}; 0.100 g of reduced catalyst. The K modified catalyst showed low carbon (17 wt% reduction compared to the neat Ni/Al_2O_3) and high stability of its catalytic activity during 30 h of operation at the expense of a slight decrease in CH_4 conversion (from 80% to 76%). Luna et al.'s [21] data confirm that the incorporation of potassium hinders the accumulation of carbon on the catalyst surface because the potassium migrates from the support to the surface of nickel and neutralises a fraction of the most active sites for the reforming

reaction producing, as a consequence, a decrease in methane conversion and carbon formation.

Ceria (CeO_2) has demonstrated unique properties in being able to oxidize carbon species to regenerate the catalyst and prevent deactivation even at low temperatures [23]. Ceria as a support has proven highly effective, and ceria as a promoter has demonstrated not only increased catalytic stability, but also enhanced prevention of catalyst coking by the removal of adsorbed carbon species. Several catalysts with varying Ni loading on a CeO_2 support has been prepared using "combustion synthesis" by Gonzalez-Delacruz et al. [24]. The catalysts have been tested for dry reforming of methane. Even CeO_2 was unable to maintain the activity and stability of the Ni catalyst as shown by Gonzales-Delacruz et al. [24] after subjecting the catalyst for 12 h of time on stream under the reaction conditions of 750 °C; CH_4:CO_2:He of 18:18:64 (ml min^{-1}); catalyst loading of 20 mg. Severe carbon deposition have been observed in the form of narrow and long nano-fibre [24].

The effect of zirconium ions on the Ni catalytic behaviour is not simple. A binary co-precipitated CeO_2/ZrO_2 support for impregnated Ni catalyst was also investigated by Kambolis et al. [25]. The Ni catalysts supported on binary oxides are much more active than that supported on pure ceria. This is attributed to the higher surface density of metallic Ni active sites on the ternary catalysts. However, in the presence of Zr^{4+}, filamentous carbon is still formed.

2.2.2 Noble metal-based and other catalysts

In general, supported noble metals, such as Rh, Ru, Pd, Pt, and Ir, on MgO and Al_2O_3 support, can lead to lower carbon deposition in the DRM reaction [11, 26]. In particular, rhodium (Rh) and ruthenium (Ru) noble metal catalysts demonstrate high activity for the dry reforming reaction, with no observed carbon formation regardless the metal oxide support as long as the metallic phase is well dispersed [26]. However, from a practical point of view, Rh and Ru are unsuitable for industrial use, considering their high cost and restricted availability. Bradford & Vannice [11] studied the dry reforming of methane over Pt supported on TiO_2, ZrO_2, SiO_2 and Cr_2O_3. Although, Pt/SiO_2 and Pt/Cr_2O_3 catalyst deactivated significantly within 5 h and 15 h on stream, respectively, the Pt/ZrO_2 and Pt/TiO_2 catalysts exhibited much higher stability even after 80 h to 100 h on stream. Temperature-programmed hydrogenation analysis showed Pt/ZrO_2 and Pt/TiO_2 suppressed carbon deposition under mild reaction condition of 500 °C; total flow rate of 20 ml min^{-1} (CH_4 and CO_2 of 5 ml min^{-1} each and the balance He); catalyst loading 50 mg. Pt catalysts supported on nanocrystalline mesoporous CeO_2 and CeO_2/ZrO_2 carriers were investigated at atmospheric pressure by Damyanova et al. [27]. No carbon deposition was observed for the neat Pt/CeO_2 and $Pt/CeO_2–ZrO_2$ catalysts. Temperature-programmed reduction (TPR) results showed good reductive properties for $Pt/CeO_2–ZrO_2$ catalysts due to both, the high surface shell reduction of zirconia and the synergetic effect between Pt and CeO_2. The high stability of $Pt/CeO_2–ZrO_2$ catalysts was related to the close contact between Pt and CeO_2 because of strong Pt-O-Ce bond [28].

Other non-nickel and non-noble metal based catalysts were also studied. Co/TiO_2 catalysts were prepared by wet synthesis and tested under DRM conditions [29]. All Co/TiO_2 catalyst showed strong resistance to coke deposition (< 0.01 wt%) in the CH_4/CO_2 reaction at 750 °C. Interestingly, the cobalt metal on rutile TiO_2 had lower CH_4 conversion as compared to Co on anatase TiO_2 because the bulk structure of the TiO_2 substrate has an effect on the dispersion of the active cobalt metallic sites. Deactivation of this catalyst was observed due to particle sintering [29].

2.3 Water-gas shift catalysts

2.3.1 Copper-based catalysts

Copper-based catalysts are generally employed for LT-WGS reaction because of their instability at high operating temperatures (>300 °C). Newsome (1980) screened through unsupported metallic copper and copper supported on Al_2O_3, SiO_2, MgO or Cr_2O_3 for LT-WGS reaction and found all to be slightly active [30]. It was in the late 1920's that the ability of Cu/ZnO to catalyse the WGS reaction was recognised, but it was not until 1963 that this type of catalyst was used in a commercial plant [31]. The susceptibility of the catalyst to rapid thermal sintering and poisoning limited the effective life of the catalyst until alumina (Al_2O_3) was found to reduce the likelihood of sintering by enhancing the strength and minimising pellet shrinkage [31-33]. The typical composition of a commercial $Cu/ZnO/Al_2O_3$ is approximately 30-35 wt%CuO, 30-50 wt%ZnO and 8-20 wt%Al_2O_3 prepared via co-precipitation [30, 31, 34]. Presently, this type of catalyst can be expected to have lifetime of about 2 to 4 years [31]. However, the $Cu/ZnO/Al_2O_3$ catalyst is highly sensitive to sulphur poisoning and could only be

used industrially in a routine manner after effective feedstock desulphurisation, which can bring process gas sulphur levels down to 10-100 ppb [31, 35].

The nature of the copper catalyst active sites for LT-WGS reaction is still controversial, with groups claiming that Cu^{+} cations dissolved in ZnO lattices are the active sites [36-40] while other groups suggest that only the metallic copper surface area plays an important role in activating the LT-WGS reaction irrespective of support [34, 41, 42].

A Cu/Zn/Al Raney catalyst was reported to be more active for LT-WGS reaction than a co-precipitated Cu/Zn/Al catalyst [43]. Raney Cu/ZnO formulations, additionally modified with chromium oxide [44] appear to bring better durability and activity under steady state conditions. Improved activity of Cu-ZnO formulations has also been reported upon promotion with alkaline-earth metals [45]. All of the above Cu-ZnO based catalysts, however, suffer from the drawback of being pyrophoric and highly susceptible to poison such as sulphur [35].

Extensive studies on the activity of the CeO_2 supported Cu catalyst were carried out because the catalyst showed indications of activity for the LT-WGS reaction and the ability to circumvent sulphur poisoning [41, 46-48]. Kusˇar et al. [47] compared the activity of a sol-gel and co-precipitated Cu/CeO_2 catalyst to a commercial $Cu/ZnO/Al_2O_3$ catalyst during LT-WGS reaction. The performance of the sol-gel and co-precipitated Cu/CeO_2 were very similar, however, the $Cu/ZnO/Al_2O_3$ achieved 80% CO conversion as compared to 10% from the Cu/CeO_2 catalysts at an operating temperature of 230 °C [47]. The LT-WGS activity of Cu/CeO_2 is generally lower than of $Cu/ZnO/Al_2O_3$ type catalysts because of lower copper surface area which is believed

to be the active sites for WGS reaction [49]. In other cases, binary metal oxide supports for Cu catalysts were considered. Li et al. [46] examined the activity of the $Cu/CeLaO_x$ catalyst and found it was more active than the commercial $Cu/ZnO/Al_2O_3$ catalyst. Huber et al. [50] looked at a Zr-CeOx binary substrate for Cu catalyst and found it was not superior to $Cu/ZnO/Al_2O_3$ catalyst in terms of activity and short-term stability. Ko et al. [51] also considered the Cu/ZrO_2 catalyst for LT-WGS reaction [51]. However, the experimental set-up in their study induced high residence times so that mass transfer limitation may have affected the results to suggest that the Cu/ZrO_2 catalyst was comparable to or better than the activity of a conventional $Cu/ZnO/Al_2O_3$ catalyst at relatively low operating temperature (>200°C). The main problem with Cu/CeO_2-based catalyst is the stability is not as good as $Cu/ZnO/Al_2O_3$ [48].

2.3.2 Iron-based catalysts

The iron oxide (Fe_2O_3) based catalysts are some of the earliest heterogeneous catalysts used industrially and are commonly called high temperature water-gas shift (HT-WGS) catalysts which operate in the temperature range of about 300-450°C [52]. Iron oxides based catalysts are usually applied exclusively in industrial high temperature shift reactors and are structurally promoted with chromium oxide (Cr_2O_3) [31]. Cr_2O_3 is believed to act as a stabiliser by retarding sintering of iron oxide crystallites and loss of catalyst surface area [31].

Various Fe_2O_3/Cr_2O_3 catalyst compositions have been tested, whilst 14 wt% Cr_2O_3 produces the greatest resistance to sintering, a concomitant reduction in activity per unit area means that an 8 wt% Cr_2O_3 addition has been accepted as compromise [53]. The

BET surface area of commercial Fe-Cr catalysts amounts to 30-80 m^2 g^{-1} depending on the Cr_2O_3 content and the calcination temperature [54]. Plant practices demonstrate that such stabilised catalysts can be operated in plants for 2-10 years before relatively slow thermal sintering leads to a reduction in activity sufficient to require catalyst replacement.

It is known that promoters or dopants, even at small amounts, can significantly improve the catalytic activity of a Fe_2O_3/Cr_2O_3 catalyst. Lei et al. [55] found that 0.5 wt% to 1 wt% rhodium doped on Fe_2O_3/Cr_2O_3 exhibited higher HT-WGS activity, selectivity and stability compared to a neat Fe_2O_3/Cr_2O_3 catalyst. The superior driving force is believed to be enhance CO adsorption on Rh and strong interaction between Rh and Fe_2O_3 [55]. In addition, the presence of Pb^{4+} in Fe_2O_3/Cr_2O_3 catalyst results in an increase activity of the catalysts [56]. The same authors reported that Pb^{4+} modified the structure of the Fe_2O_3 solid in a way that expanded the tetrahedral sites and contracted the octahedral sites, leading to increased covalence in the system and improved electron "hopping" capabilities which enhanced the already very high conductance of the Fe_2O_3 solid [32].

A recent advancement in the promotion of Fe_2O_3/Cr_2O_3 catalysts was the addition of first row transition metal oxides as promoters [57, 58]. An earlier study of the effect of the addition of CuO, CoO and ZnO (5 wt%) on the activity of Fe_2O_3/Cr_2O_3 catalysts (in terms of their CO conversion), showed that the doped samples had a higher activity than the undoped catalysts, with maximum activity occurring at lower temperature. The Cu-doped Fe_2O_3/Cr_2O_3 sample was shown to have the highest activity over the wide temperature range. Andreev et al. [58] suggested that Cu provided new active sites for

the WGSR, reacting in the same manner as the metallic copper within the $Cu/ZnO/Al_2O_3$ catalyst during LT-WGS reaction.

2.3.3 Gold-based catalysts

Andreeva et al. [59] was the first to report the use of a gold catalyst for WGS reaction. The same group co-precipitated an Au/Fe_2O_3 catalyst which exhibited higher catalytic activity than that of the industrial copper catalyst at the temperature range of 200 °C to 300 °C. It can be drawn that the high catalytic activity of Au/Fe_2O_3 is due to a specific interaction between gold and the ferric oxide support [59]. Later on, Boccuzzi et al. [60] compared the LT-WGS activity of an Au/Fe_2O_3 to an Au/TiO_2 catalyst and found similar catalytic activity. The Au/CeO_2 came to light as it is more stable than the Au/TiO_2 [61] and intensive study on this catalytic system for WGS reaction has been reported [62-65]. The origin of the highly active Au/CeO_2 catalysts is still debatable, some argue that the highly active Au/CeO_2 is attributed to the loss of metallic character and an increase in electronegativity or ionic character of the Au particles [66, 67] while others believe the activity stems from intrinsic oxygen vacancies available [64, 68]. Unfortunately, these gold catalysts can be prone to thermal instability and rapid deactivation similar to most Cu catalysts. Fu et al. [69] reported the deactivation of Au/CeO_2 during LT-WGS operation was due to the loss of CeO_2 support area during steady-state reaction. Kim et al. [66] also found the formation of thermally stable carbonate species covering the surface of Au/CeO_2, which blocked the active sites. Denkwit et al. [63] elaborated that the carbonate was of monodenate carbonate species which predominately inhibited the LT-WGS reaction while their formation was enhance by CO_2 in the feed gas.

2.3.4 Noble metal catalysts

Due to the toxicity and environmental restriction associated with chromium compounds and the lack of stability in the Cu-based and Au-based catalysts, attempts to develop other chromium-free, non-toxic and stable catalyst systems for WGS have been undertaken by various researchers. A number of different supports used for noble metal catalysts for WGS reaction have been reported. Grenoble et al. [70] examined Al_2O_3-supported Pt, Pd, Rh and other group VIIB, VIII and IB metals. Bunluesin et al. [71] studied ceria supported Pd, Pt, and Rh (1 wt%) while Thinon et al. [72] screened through the noble metal catalysts supported on Fe_2O_3, TiO_2, ZrO_2 and CeO_2. The catalysts are ranked from descending order in terms of CO conversion: Rh > Pt >> Pd and generally, rhodium is the most active noble metal catalyst; however, the catalyst is very poor in selectivity because it produces a lot of methane (Eq. 2.4) during WGS reaction [72].

$$CO + 3H_2 \rightarrow CH_4 + H_2O \qquad \text{(Eq. 2.4)}$$

Because platinum is the well-rounded performing catalysts out of all the noble metals, a shift in focus on this catalysts prevailed. The Pt/TiO_2 [73-76], Pt/CeO_2 [77-79] and Pt/ZrO_2 [80-82] are the most popular catalytic system for WGS in literature owing to their large window of operating temperature, non-pyrophoric and non-toxic nature. The most active Pt catalysts on metal oxide supports followed the order $TiO_2 > CeO_2 > ZrO_2$ and the difference in activity was due to the influence of the oxide supports as they play a significant role in determining the mechanistic reaction sequence for the WGS reaction over Pt-based catalysts [83, 84]. Using transient kinetic studies Azzam et al. [83] concluded that a simultaneous ‘redox’ and ‘associative formate’ route contributed

on Pt/TiO_2. The 'associative formate' route dominated on the Pt/CeO_2 and the 'carbonate' route for Pt/ZrO_2.

Unfortunately, Pt/TiO_2 deactivates readily during WGS operation, caused by sintering of the metallic Pt [75, 85, 86]. Attempts to stabilise the metallic Pt have been successfully reported by Azzam et al. [84] and Iida et al. [86], where both groups had used Re as a promoter to not only prevent Pt from coalescing together but also to improve WGS activity.

2.3.5 Other catalysts

Another material recognised since the late 1970s as an industrial, sulphur resistant water-gas shift catalyst, is sulphide activated cobalt oxide-molybdenum oxide-based catalysts. These catalysts are widely applied in synthesis gas production from heavy oil and coal which have extremely high levels of sulphur and were found to have potential interest for the HT-WGS reaction due to their high tolerance to sulphur. Two sulphur-resistant Co-Mo industrial catalysts promoted by potassium [87, 88] and/or magnesium [89] showed high values of catalytic activity. In the investigation of the effect of potassium on the texture and activity of $Co\text{-}Mo/\gamma\text{-}Al_2O_3$ catalysts for WGS reaction, Xie et al. [87] found that the deposition of K onto $Co\text{-}Mo/\gamma\text{-}Al_2O_3$ resulted in an uniform distribution of oxomolybdenum species in the support and improved activity in the WGS reaction at 400 °C with a gas mixture of 27.4 %CO in He and H_2O/CO ratio of 1:2 after being subjected to sulphidation with $10\%H_2S/H_2$ at the volume rate of 400 h^{-1}. The Mg^+ promoter increased the dispersion of Mo on the surface of the support and enhances the interaction between active components Mo in the $Co\text{-}Mo/\gamma\text{-}Al_2O_3$ catalyst

and also increased the amount of octahedral Mo species which were responsible for WGS activity [89].

2.4 Water-gas shift kinetics

Rhodes et al. [32] presented an excellent paper which critically reviewed the mechanism of the WGS reaction over both iron-based and copper-based catalysts. The current section will briefly introduce the kinetics of the HT-WGS reaction over Fe_2O_3/Cr_2O_3 catalysts and LT-WGS reaction over $Cu/ZnO/Al_2O_3$ that have been studied widely over the past 40 years, and more than 20 different kinetics equations have been proposed. Newsome (1980) extensively discussed the proposed kinetics equations published till 1975 [30]. There is, however, still some disagreement on the precise form of the rate equation and values of the rate constants or activation energies. The reasons for this conflict have been attributed to the presence of impurities in the gases used, to varying degrees of mass-transfer limitation, and to the fact that kinetic measurements have been mostly obtained with integral rather than differential reactors which often operate only at or near atmospheric pressure [90].

Five main classes of reaction models, together with their associated kinetics expressions have been proposed for the WGS reaction over both Fe_2O_3/Cr_2O_3 and $Cu/ZnO/Al_2O_3$ catalysts. The rate equations for five proposed models of WGS are shown as followings [31]:

(i) Langmuir-Hinshelwood model:

$$r = \frac{\kappa K_{CO} K_{H_2O} \{[CO][H_2O] - [CO_2][H_2]/K\}}{\{1 + K_{CO}[CO] + K_{H_2O}[H_2O] + K_{CO_2}[CO_2] + K_{H_2}[H_2]\}^2} \quad \text{(Eq. 2.5)}$$

Where, K_i is the adsorption equilibrium constant for component i, κ is the rate constant and K is the equilibrium constant.

(ii) Hulburt-Vasan model:

$$r = \frac{\kappa[H_2O]}{1 + K[H_2O]/[H_2]} \quad \text{(Eq. 2.6)}$$

Where, κ is the rate constant and K is the equilibrium constant.

(iii) Kodama model:

$$r = \frac{\kappa\{[CO][H_2O] - [CO_2][H_2]/K\}}{1 + K_1[CO] + K_2[H_2O] + K_3[CO_2] + K_4[H_2]} \quad \text{(Eq. 2.7)}$$

Where, κ is the rate constant, K is the equilibrium constant and K_i is the equilibrium constant of reaction step *i*.

(iv) Oxidation-reduction model:

$$r = \frac{\kappa_1\kappa_2\{[CO][H_2O] - [CO_2][H_2]/K\}}{\kappa_1[CO] + \kappa_2[H_2O] + \kappa_{-1}[CO_2] + \kappa_{-2}[H_2]} \quad \text{(Eq. 2.8)}$$

Where, κ_i is the rate constant of reaction step *i*, κ_{-i} is the rate constant of reverse step *–i*, and K is the equilibrium constant.

(v) Power law model:

$$r = a\kappa[CO]^m[H_2O]^n[CO_2]^p[H_2]^q \quad \text{(Eq. 2.9)}$$

$$r = \kappa_1 p^a{}_{CO}\, p^b{}_{H_2O}\, p^c{}_{CO_2}\, p^d{}_{H_2}(1 - \beta) \quad \text{(Eq. 2.10)}$$

Where, r is reaction rate, p_i is corresponding partial pressure of component i, a , b, c, and d is the apparent reaction order of component CO, H_2O, CO_2 and H_2 respectively; κ_i is the rate constant, and $\kappa_1 = A\exp(-\frac{E_a}{RT})$, where A is the pre-exponential factor, Ea is the apparent activation energy, R is the universal gas constant 8.314 J mol^{-1} K^{-1} and T is the reaction temperature (K). β is the term for backward reaction or approach to equilibrium factor and is defined as:

$$\beta = \frac{1}{K} \bullet \frac{p_{CO_2} p_{H_2}}{p_{CO} p_{H_2O}} \qquad \text{(Eq. 2.11)}$$

Where, K is the equilibrium constant for WGS reaction.

2.5 Water-gas shift mechanisms

Two types of reaction mechanisms, the associative mechanism and the regenerative (redox) mechanism, were proposed on the basis of this kinetic studies [30, 32]. The associative mechanism is based upon interaction of adsorbed carbon monoxide and water to form an intermediate which break down to form products. Shido and Iwasawa [91] explored the WGS reaction in terms of a associative formate mechanism:

$CO_{(g)} \rightarrow CO_{(a)}$ (Eq. 2.12)

$H_2O_{(g)} \rightarrow H_2O_{(a)} \rightarrow OH^{\bullet}_{(a)} + H^{\bullet}_{(a)}$ (Eq. 2.13)

$CO_{(a)} + OH^{\bullet}_{(a)} \rightarrow HCOO^{\bullet}_{(a)}$ (Eq. 2.14)

$HCOO^{\bullet}_{(a)} \rightarrow CO_2 + H^{\bullet}_{(a)}$ (Eq. 2.15)

$2H^{\bullet}_{(a)} \rightarrow H_{2(g)}$ (Eq. 2.16)

They were believed to have been the first to detect formate species using FTIR-spectroscopy and present the effects of the WGS reaction on ZnO crystal. Fajin et al.

[92] looked at the effect of the surface steps in the mechanism of the WGS reaction catalyzed by Cu surfaces has been studied by means of periodic density functional calculations using the stepped Cu(3 2 1) surface as a realistic model of the catalyst surface. They found the intermediate did not necessarily have to be of formate species and that a carboxyl-type ($OCOH^{\bullet}_{(a)}$) could be formed instead [92].

The regenerative (oxidation-reduction cycles) mechanism is thought to be the dominant pathway for HT-WGS catalysts. The mechanism can be described as following elementary steps [41, 93, 94]:

$$H_2O + * \rightarrow H_2 + O^* \qquad \text{(Eq. 2.17)}$$

$$CO + O^* \rightarrow CO_2 + * \qquad \text{(Eq. 2.18)}$$

Where * is an oxygen vacancy site and O^* is an adsorbed surface oxygen.

In the first step (Eq. 2.17) water adsorbs and dissociates on reduced sites on the catalysts surface to produce hydrogen while oxidising the oxygen deficient site. In the following step (Eq. 2.18) CO is oxidised to CO_2 on the oxidised site. The redox mechanism over low-temperature Cu-based catalysts was first widely accepted. Chen et al. [95] further studied the WGS reaction over Cu/SiO_2 and found that the WGS reaction to proceed on Cu crystallites by H_2O dissociation and no formate or carbonate intermediate was detected on the surface therefore the redox mechanism seems to be most probable. This result agrees well with the findings from an investigation of WGS on a clean Cu(1 1 1) single crystal surface and with H_2O adsorption on polycrystalline copper [40].

However, Herwijnen et al. [96] observed that both forward and reverse WGS proceeded via relatively stable intermediates formed from CO/H_2O and CO_2/H_2, respectively and

the decomposition of these complexes was rate determining. Salmi & Hakkarainen [97] interpreted their kinetic results using a mechanistic model involving a fast CO and H_2O adsorption, a slow dissociation of adsorbed H_2O, surface intermediate formation and decomposition and H_2 adsorption.

2.6 Concluding remarks

The literature survey revealed that although currently available catalysts work well in dry reforming of methane and in low-temperature water-gas shift reaction, significantly improved catalysts are required to meet the needs to reduce the size of WGS reactors and subsequently their costs, particularly to meet the transient operation and size constraints imposed by vehicular fuel cell applications. Thus, there is a need for developing new alternative DRM and LT-WGS catalysts to comply with the new requirements.

For the past decade, many efforts of developing alternative DRM catalysts have been focusing on active and cost effective nickel catalysts [17, 18, 22, 24, 25]. Platinum metal catalysts are of particular interest in this application, with ceria supports – which promote oxygen storage and DRM activity [27]. Published studies suggest that CH_4 dissociates on the metal and reacts with oxygen from the ceria (support) which in turn is oxidised by CO_2. In contrast, only a few studies have been carried out to find alternative DRM catalysts.

For the LT-WGS reaction, there has been a debate regarding the reaction mechanism over Cu-based catalysts, namely whether the mechanism is associative and is taking

place through intermediates (formats or carbonates), or regenerative via redox reaction. Combined mechanisms are probable [32] depending on the reaction conditions. As a result, the current research project is directed toward finding which intrinsic properties of the Cu-catalyst governing the LT-WGS activity, and subsequently utilising this strategy to develop new catalysts for LT-WGS.

2.6 References

1. D. Schneider, 'Global Warming Is Still a Hot Topic: Arrival of the seasons may show greenhouse eÝect', *Scientific American* 272(2) (**1995**) 13-14.
2. J.H. McCrary, G.E. McCrary, T.A. Chubb, J.J. Nemecek, and D.E. Simmons, 'An experimetnal study of the CO_2-CH_4 reforming-methanation cycle as a mechanism for converting and transporting solar energy ', *Solar Energy* 29(2) (**1982**) 141-151.
3. J.D. Fish and D.C. Hawn, 'Closed Loop Thermochemical Energy Transport Based on CO_2 Reforming of Methane: Balancing the Reaction Systems', *Journal of Solar Energy Engineering* 109 (**1987**) 215-220.
4. T.A. Chubb, 'Characteristics of CO_2-CH_4 reforming-methanation cycle relevant to the solchem thermochemical power system', *Solar Energy* 24 (**1980**) 341-345.
5. M.A. Vannice, 'The Catalytic Synthesis of Hydrocarbons from Carbon Monoxide and Hydrogen', *Catalysis Reviews: Science and Engineering* 14 (**1976**) 153-191.
6. J.R.H. Ross, A.N.J. van Keulen, M.E.S. Hegarty, and K. Seshan, 'The catalytic conversion of natural gas to useful products', *Catalysis Today* 30(1-3) (**1996**) 193-199.

7. A.M. Gadalla and B. Bower, 'The role of catalyst support on the activity of nickel for reforming methane with CO_2', *Chemical Engineering Science* 43(11) (**1988**) 3049-3062.

8. M. Kurioka, K. Nakata, T. Jintoku, Y. Taniguchi, K. Taskaki, and Y. Fujiwara, *Chemistry Letters* 244 (**1995**).

9. T. Nishiyama and K.-I. Aika, 'Mechanism of the Oxidative Coupling of Methane Using CO_2 as an Oxidant over PbO-MgO', *Journal of Catalysis* 122 (**1990**) 346-351.

10. K. Asami, T. Fujita, K.-i. Kusakabe, Y. Nishiyama, and Y. Ohtsuka, 'Conversion of methane with carbon dioxide into C_2 hydrocarbons over metal oxides', *Applied Catalysis A: General* 126 (**1995**) 245-255.

11. M.C.J. Bradford and M.A. Vannice, 'CO_2 reforming of CH_4', *Catalysis Reviews: Science and Engineering* 41(1) (**1999**) 1-42.

12. R. Kydd, W.Y. Teoh, K. Wong, Y. Wang, Jason Scott, Q.-H. Zeng, A.-B. Yu, J. Zou, and R. Amal, 'Flame-Synthesized Ceria-Supported Copper Dimers for Preferential Oxidation of CO', *Advance Functional Materials* 19 (**2009**) 369-377.

13. D.L. Trimm and Z.I. Onsan, 'Onboard fuel conversion for hydrogen-fuel-cell-driven vehicles ', *Catalysis Reviews* 43 (**2001**) 31–84.

14. J. Larminie and A. Dicks, *Fuel Cell Systems Explained*, Wiley, New York, **2000**.

15. J.W. Snoeck, G.F. Froment, and M. Fowles, 'Steam/CO_2 Reforming of Methane. Carbon Formation and Gasification on Catalysts with various Potassium Contents', *Industrial & Engineering Chemistry Research* 41 (**2002**) 4252-4265.

16. J.R. Rostrup-Nielsen and J.H.B. Hansen, 'CO_2-Reforming of Methane over Transition Metals', *Journal of Catalysis* 144(1) (**1993**) 38-49.

17. M.C.J. Bradford and M.A. Vannice, 'Catalytic reforming of methane with carbon dioxide over nickel catalysts. I. Catalyst characterization and activity', *Applied Catalysis A: General* 142 (**1996**) 73-96.

18. M.C.J. Bradford and M.A. Vannice, 'Catalytic reforming of methane with carbon dioxide over nickel catalysts. II. Reaction kinetics', *Applied Catalysis A: General* 142 (**1996**) 97-122.

19. M.C.J. Bradford and M.A. Vannice, 'Catalytic reforming of methane with carbon dioxide over nickel catalysts. 1. Catalyst characterization and activity', *Applied Catalysis A - General* 142(1) (**1996**) 73-96.

20. B.S. Barros, D.M.A. Melo, S. Libs, and A. Kiennemann, 'CO_2 reforming of methane over La_2NiO_4/α-Al_2O_3 prepared by microwave assisted self-combustion method', *Applied Catalysis A: General* 378 (**2010**) 69–75.

21. A.E.C. Luna and M.E. Iriarte, 'Carbon dioxide reforming of methane over a metal modified Ni-Al_2O_3 catalyst', *Applied Catalysis A: General* 343 (**2008**) 10–15.

22. F. Arena, F. Frusteri, and A. Parmaliana, 'Alkali promotion of Ni/MgO catalysts', *Applied Catalysis A: General* 187 (**1999**) 127–140.

23. E. Aneggi, M. Boaro, C. de Leitenburg, G. Dolcetti, and A. Trovarelli, 'Insights into the redox properties of ceria-based oxides and their implications in catalysis', *Journal of Alloys and Compounds* 408 (**2006**) 1096-1102.

24. V.ı.M. Gonzalez-Delacruz, F.a. Ternero, R. Pere˜n´ıguez, A. Caballero, and J.P. Holgado, 'Study of nanostructured Ni/CeO_2 catalysts prepared by combustion synthesis in dry reforming of methane', *Applied Catalysis A: General* doi:10.1016/j.apcata.2010.05.027 (**2010**).

25. A. Kambolis, H. Matralis, A. Trovarelli, and C. Papadopoulou, 'Ni/CeO_2-ZrO_2 catalysts for the dry reforming of methane', *Applied Catalysis A: General* 377 (**2010**) 16–26.

26. J.R. Rostrup-Nielsen and J.H.B. Hansen, 'CO_2-Reforming of Methane over Transition Metals', *Journal of Catalysis* 144 (**1993**) 38-49.

27. S. Damyanova, B. Pawelec, K. Arishtirova, M.V.M. Huerta, and J.L.G. Fierro, 'The effect of CeO_2 on the surface and catalyric properties of Pt/CeO_2-ZrO_2 catalysts for methane dry reforming', *Applied Catalysis B: Environmental* 89 (**2009**) 149-159.

28. Y. Nagai, T. Hirabayashi, K. Dohmae, N. Takagi, T. Minami, H. Shinjoh, and S.i. Matsumoto, 'Sintering inhibition mechanism of platinum supported on ceria-based oxide and Pt-oxide–support interaction', *Journal of Catalysis* 242 (**2006**) 103–109.

29. K. Takanabe, K. Nagaoka, K. Nariai, and K.-i. Aika, 'Influence of reduction temperature on the catalytic behavior of Co/TiO_2 catalysts for CH_4/CO_2 reforming and its relation with titania bulk crystal structure', *Journal of Catalysis* 230 (**2005**) 75–85.

30. D.S. Newsome, 'The Water-Gas Shift Reaction', *Catalysis Reviews: Science and Engineering* 21(2) (**1980**) 275-318.

31. L. Lloyd, D.E. Ridler, and M.V. Twigg, 'Catalyst Handbook, 2nd Ed., ed. M. V. Twigg', *Wolfe Publishing, London* (**1989**) ch. 6.

32. C. Rhodes, G.J. Hutchings, and A.M. Ward, 'Water-gas shift reaction: finding the mechanistic boundary', *Catalysis Today* 23(1) (**1995**) 43-58.

33. G. Ghiotti and F. Bocuzzi, 'Chemical and Physical Properties of Copper-Based Catalysts for CO shift Reaction and Methanol Synthesis', *Catalysis Reviews: Science and Engineering* 29(2 & 3) (**1987**) 151-182.

34. M.J.L. Gines, N. Amadeo, M. Laborde, and C.R. Apesteguia, 'Activity and structure-sensitivity of the water-gas shift reaction over Cu-Zn-Al mixed oxide catalysts', *Applied Catalysis A: General* 131 (**1995**) 283-296.

35. M.S. Spencer, 'The role of zinc oxide in Cu/ZnO catalysts for methanol synthesis and the water-gas shift reaction', *Topics in Catalysis* 8 (**1999**) 259-266.

36. Y. Okamoto, K. Fukino, T. Imanaka, and S. Teranishi, 'Surface Characterization of CuO-ZnO Methanol-Synthesis Catalysts by X-ray Photoelectron Spectroscopy. 2. Reduced Catalysts', *Journal of Physical Chemistry* 87 (**1983**) 3747.

37. R. Kam, C. Selomulya, R. Amal, and J. Scott, 'The influence of La-doping on the activity and stability of Cu/ZnO catalyst for the low-temperature water–gas shift reaction', *Journal of Catalysis* 273 (**2010**) 73–81.

38. A.J. Bridgewater, M.S. Wainwright, D.J. Young, and J.P. Orchard, 'Methanol synthesis over raney copper-zinc catalysts. III. optimization of alloy composition and catalyst preparation', *Applied Catalysis* 7 (**1983**) 369-382.

39. K.R. Harikumar and C.N.R. Rao, 'Interaction of CO with Cu/ZnO catalyst surfaces prepared in situ in the electron spectrometer: evidence for CO_2 and related species relevant to methanol synthesis', *Applied Surface Science* 125 (**1998**) 245-249.

40. C.-S. Chen, T.-W. Lai, and C.-C. Chen, 'Effect of active sites for a water–gas shift reaction on Cu nanoparticles', *Journal of Catalysis* 2010 (**2010**) 18-28.

41. N.A. Koryabkina, A.A. Phatak, W.F. Ruettinger, R.J. Farrauto, and F.H. Ribeiro, 'Determination of kinetic parameters for the water-gas shift reaction on copper

catalysts under realistic conditions for fuel cell applications', *Journal of Catalysis* 217 (**2003**) 233-239.

42. F. Nishida, I. Atake, D. Li, T. Shishido, Y. Oumi, T. Sano, and K. Takehira, 'Effects of noble metal-doping on Cu/ZnO/Al2O3 catalysts for water–gas shift reaction Catalyst preparation by adopting "memory effect" of hydrotalcite', *Applied Catalysis A: General* 337 (**2008**) 48-57.
43. A. Andreev, V. Kafedjiiski, T. Halachev, B. Kunev, and M. Kaltchev, 'Raney type copper-zinc-aluminium catalyst for water-gas shift reaction', *Applied Catalysis* 78 (**1991**) 199-211.
44. L. Ma, D.L. Trimm, and M.S. Wainwright, 'Structural and catalytic promotion of skeletal copper catalysts by zinc and chromium oxides ', *Topics in Catalysis* 8 (**1999**) 271-277.
45. T. Shishido, M. Yamamoto, I. Atake, D. Li, Y. Tian, H. Morioka, M. Hondac, T. Sano, and K. Takehira, 'Cu/Zn-based catalysts improved by adding magnesium for water–gas shift reaction', *Journal of Molecular Catalysis A: Chemical* 253 (**2006**) 270-278.
46. Y. Li, Q. Fu, and M. Flytzani-Stephanopoulos, 'Low-temperature water-gas shift reaction over Cu- and Ni-loaded cerium oxide catalysts', *Applied Catalysis B: Environmental* 27 (**2000**) 179-191.
47. H. Kusˇar, S. Hocˇevar, and J. Levec, 'Kinetics of the water–gas shift reaction over nanostructured copper–ceria catalysts', *Applied Catalysis B: Environmental* 63 (**2006**) 194–200.
48. P. Djinovic, J. Batista, J. Levec, and A. Pintar, 'Comparison of water–gas shift reaction activity and long-term stability of nanostructured CuO-CeO_2 catalysts

prepared by hard template and co-precipitation methods', *Applied Catalysis A: General* 364 (**2009**) 156–165.

49. A.S. Quiney and Y. Schuurman, 'Kinetic modelling of COconversion over a Cu/ceria catalyst', *Chemical Engineering Science* 62 (**2007**) 5026 – 5032.

50. F. Huber, H. Meland, M. Rønning, H. Venvik, and A. Holmen, 'Comparison of Cu–Ce–Zr and Cu–Zn–Al mixed oxide catalysts for water-gas shift', *Topics in Catalysis* 45 (**2007**) 101-104.

51. J.B. Ko, C.M. Bae, Y.S. Jung, and D.H. Kim, 'Cu-ZrO_2 catalysts for water-gas-shift reaction at low temperatures', *Catalysis Letters* 105 (**2005**) 157-161.

52. C.H. Bartholomew and R.J. Farrauto, *Fundamentals of Industrial Catalytic Processes*. 2nd Edition ed, John Wiley & Sons, Ltd, Hoboken, NJ, **2006**.

53. F. Domka, A. Basinska, and R. Fiedorow, 'Porous structure of Fe2O3-Cr2O3 catalysts prepared from iron oxide-hyroxide systems', *Surface Technology* 18 (**1983**) 275-282.

54. C.N. Satterfield, *Heterogeneous Catalysis in Industrial Practice*. 2 ed, McGraw-Hill, New York, **1991**.

55. Y. Lei, N.W. Cant, and D.L. Trimm, 'The origin of rhodium promotion of Fe_3O_4–Cr_2O_3 catalysts for the high-temperature water–gas shift reaction', *Journal of Catalysis* 239 (**2006**) 227–236.

56. H. Topsoe and M. Boudart, 'Mossbauer Spectroscopy of CO Shift Catalysts Promoted with Lead', *Journal of Catalysis* 31 (**1973**) 346-359.

57. M.A. Edwards, D.M. Whittle, C. Rhodes, A.M. Ward, D. Rohan, M.D. Shannon, G.J. Hutchings, and C.J. Kiely, 'Microstructural studies of the copper promoted iron oxide/chromia water-gas shift catalyst', *Physical Chemistry Chemical Physics* 4 (**2002**) 3902-3908.

58. A. Andreev, V. Idakiev, D. Mihajlova, and D. Shopov, 'Iron-based catalysts for the water—gas shift reaction promoted by first-row transition metal oxides', *Applied Catalysis* 22 (**1986**) 385-387.

59. D. Andreeva, V. Idakiev, T. Tabakova, and A. Andreev, 'Low-Temperature Water–Gas Shift Reaction over Au/α-Fe_2O_3', *Journal of Catalysis* 158 (**1996**) 354–355.

60. F. Boccuzzi, A. Chiorino, M. Manzoli, D. Andreeva, T. Tabakova, L. Ilieva, and V. Iadakiev, 'Gold, Silver and copper catalysts supported on TiO2 for pure hydrogen production', *Catalysis Today* 75 (**2002**) 169-175.

61. M. Haruta and M. Daté, 'Advances in the catalysis of Au nanoparticles', *Applied Catalysis A: General* 222 (**2001**) 427–437.

62. Q. Fu, A. Weber, and M. Flytzani-Stephanopoulos, 'Nanostructured Au–CeO_2 catalysts for low-temperature water–gas shift', *Catalysis Letters* 77 (**2001**) 87-95.

63. Y. Denkwitz, A. Karpenko, V. Plzak, R. Leppelt, B. Schumacher, and R.J. Behm, 'Influence of CO_2 and H_2 on the low-temperature water-gas shift reaction on Au/CeO2 catalysts in idealized and realistic reformate', *Journal of Catalysis* 246 (**2007**) 74-90.

64. J.A. Rodriguez, S. Ma, P. Liu, J. Hrbek, J. Evans, and M. Pérez, 'Au(111) in the Water-Gas Shift Reaction Activity of CeO_x and TiO_x Nanoparticles', *Science* 318 (**2007**) 1757-1760.

65. T. Tabakova, F. Boccuzzi, J. Manzoli, and D. Andreeva, 'FTIR study of low-temperature water-gas shift reaction on gold/ceria catalyst', *Applied Catalysis A: General* 252 (**2003**) 385-397.

66. C.H. Kim and L.T. Thompson, 'Deactivation of Au/CeOx water gas shift catalysts', *Journal of Catalysis* 230 (**2005**) 66-74.

67. G.C. Bond and D.T. Thompson, 'Catalysis by Gold ', *Catalysis Reviews Science and Engineering* 41(3 & 4) (**1999**) 319 – 388.

68. Q. Fu, S. Kudriavtseva, H. Saltsburg, and M. Flytzani-Stephanopoulos, 'Gold–ceria catalysts for low-temperature water-gas shift reaction', *Chemical Engineering Journal* 93 (**2003**) 41-53.

69. Q. Fu, W. Deng, H. Saltsburg, and M. Flytzani-Stephanopoulos, 'Activity and stability of low-content gold–cerium oxide catalysts for the water–gas shift reaction', *Applied Catalysis B: Environmental* 56 (**2005**) 57–68.

70. D.C. Grenoble, M.M. Estadt, and D.F. Ollis, 'The Chemistry and Catalysis of the Water Gas Shift Reaction', *Journal of Catalysis* 67 (**1981**) 90-102.

71. T. Bunluesin, R.J. Gorte, and G.W. Grahamb, 'Studies of the water-gas-shift reaction on ceria-supported Pt, Pd, and Rh: implications for oxygen-storage properties', *Applied Catalysis B: Environmental* 15 (**1998**) 107-114.

72. O. Thinon, F. Diehl, P. Avenier, and Y. Schuurman, 'Screening of bifunctional water-gas shift catalysts', *Catalysis Today* 137 (**2008**) 29-35.

73. P. Panagiotopoulou, A. Christodoulakis, D.I. Kondarides, and S. Boghosian, 'Particle size effects on the reducibility of titanium dioxide and its relation to the water-gas shift activity of Pt/TiO2 catalyst', *Journal of Catalysis* 240 (**2006**) 114-125.

74. H. Iida and A. Igarashi, 'Characterization of a Pt/TiO_2 (rutile) catalyst for water gas shift reaction at low temperature', *Applied Catalysis A: General* 208 (**2006**) 152-160.

75. K.G. Azzam, I.V. Babich, K. Seshan, and L. Lefferts, 'Single stage water gas shift conversion over Pt/TiO_2—Problem of catalyst deactivation', *Applied Catalysis A: General* 338 (**2008**) 66–71.

76. I.D. Gonzalez, R.M. Navarro, M.C. Alvarez-Galvan, F. Rosa, and J.L.G. Fierro, 'Performance enhancement in the water–gas shift reaction of platinum deposited over a cerium-modified TiO_2 support', *Catalysis Communications* 9 (**2008**) 1759–1765.

77. Y.D. Bi, W. Zhang, H.Y. Xu, and W.Z. Li, 'Nanocrystalline CeO2 in SBA-15: Performance of Pt/CeO2/SBA-15 Catalyst for Water-gas-shift Reaction', *Catalysis Letters* 119 (**2007**) 126-133.

78. A.M.D.d. Farias, P. Bargiela, M.d.G.C. Rocha, and M.A. Fraga, 'Vanadium-promoted Pt/CeO_2 catalyst for water-gas shift reaction', *Journal of Catalysis* 260(1) (**2008**) 93-102.

79. A. Goguet, F. Meunier, J.P. Breen, R. Burch, M.I. Petch, and A.F. Ghenciu, 'Study of the origin of the deactivation of a Pt/CeO_2 catalyst during reverse water gas shift (RWGS) reaction', *Journal of Catalysis* 226 (**2004**) 382-392.

80. P.O. Graf, D.J.M.d. Vlieger, B.L. Mojet, and L. Lefferts, 'New insights in reactivity of hydroxyl groups in water gas shift reaction on Pt/ZrO2', *Journal of Catalysis* 262 (**2009**) 181-187.

81. D. Nguyen-Thanh, A.M.D.d. Farias, and M.A. Fraga, 'Characterization and activity of vanadia-promoted Pt/ZrO2 catalysts for the water–gas shift reaction', *Catalysis Today* 138 (**2008**) 235-238.

82. J.M. Pigos, C.J. Brooks, G. Jacobs, and B.H. Davis, 'Low temperature water-gas shift: Characterization of Pt-based ZrO_2 catalyst promoted with Na discovered by combinatorial methods', *Applied Catalysis A: General* 319 (**2007**) 47–57.

83. K.G. Azzam, I.V. Babich, K. Seshan, and L. Lefferts, 'Bifunctional catalysts for single-stage water-gas shift reaction in fuel cell applications. Part 1. Effect of the support on the reaction sequence', *Journal of Catalysis* 251 (**2007**) 153-162.

84. K.G. Azzam, I.V. Babich, K. Seshan, and L. Lefferts, 'A bifunctional catalyst for the single-stage water–gas shift reaction in fuel cell applications. Part 2. Roles of the support and promoter on catalyst activity and stability', *Journal of Catalysis* 251 (**2007**) 163–171.

85. X. Zhu, T. Hoang, L.L. Lobban, and R.G. Mallinson, 'Significant Improvement in Activity and Stability of Pt/TiO_2 Catalyst for Water Gas Shift Reaction Via Controlling the Amount of Na Addition', *Catalysis Letters* 129 (**2009**) 135–141.

86. H. Iida, K. Yonezawa, M. Kosaka, and A. Igarashi, 'Low-temperature water gas shift reaction over $Pt–Re/TiO_2$ catalysts prepared by a sub-critical drying method', *Catalysis Communications* 10 (**2009**) 627-630.

87. X. Xie, H. Yin, B. Dou, and J. Huo, 'Characterization of a potassium-promoted cobalt- molybdenum/alumina water-gas shift catalyst', *Applied Catalysis* 71(2) (**1991**) 187-198.

88. H. Wang, Y. Lian, Y. Li, W. Fang, and Y. Yang, 'W-promoted Co–Mo–K/γ–Al_2O_3 catalysts for water–gas shift reaction', *Catalysis Communications* 10 (**2009**) 1864–1867.

89. Y. Lian, H. Wang, Q. Zheng, W. Fang, and Y. Yang, 'Effect of Mg/Al atom ratio of support on catalytic performance of Co-Mo/MgO-Al_2O_3 catalyst for water gas shift reaction', *Journal of Natural Gas Chemistry* 18 (**2009**) 161-166.

90. K. Kochloefl, *Handbook of Heterogeneous Catalysus*, ed. G. Ertl, H. Knozinger, and J. Weitkamp. Vol. 4, VCH, Germany, **1997**.

91. T. Shido and Y. Iwasawa, 'Reactant-Promoted Reaction Mechanism for Water-Gas Shift Reaction on ZnO, as the Genesis of Surface Catalysis', *Journal of Catalysis* 129 (**1991**) 343-355.

92. J.L.C. Fajin, M.N.D.S. Cordeiro, Francesc Illas, and J.R.B. Gomes, 'Influence of step sites in the molecular mechanism of the water gas shift reaction catalyzed by copper', *Journal of Catalysis* 268 (**2009**) 131-141.

93. C.V. Ovesen, P. Stoltze, J.K. Nørskov, and C.T. Campbell, 'A kinetic model of the water gas shift reaction', *Journal of Catalysis* 134 (**1992**) 445-468.

94. T. Shishido, M. Yamamoto, D. Li, Y. Tian, H. Morioka, M. Honda, T. Sano, and K. Takehira, 'Water-gas shift reaction over Cu/ZnO and Cu/ZnO/Al_2O_3 catalysts prepared by homogeneous precipitation', *Applied Catalysis A: General* 303 (**2006**) 62-71.

95. C.-S. Chen, J.-H. Lin, T.-W. Lai, and B.-H. Li, 'Active sites on Cu/SiO_2 prepared using the atomic layer epitaxy technique for a low-temperature water–gas shift reaction', *Journal of Catalysis* 263 (**2009**) 155–166.

96. T.v. Herwijnen and W.A.D. Jon, 'Kinetics and Mechanism of the CO shift on Cu/ZnO', *Journal of Catalysis* 63 (**1980**) 83-93.

97. T. Salmi and R. Hakkarainen, 'Kinetic Study of the Low-Temperature Water-Gas Shift Reaction over a Cu-ZnO Catalyst', *Applied Catalysis* 49 (**1989**) 285-306.

CHAPTER THREE

CeO_2/WO_3 as support for Pt catalyst: Implications for dry reforming of methane

3.1 Introduction

Reforming of natural gas into synthesis gas is the prime route to convert methane (the main component in natural gas) to ammonia, methanol, liquid fuels and other oxygenated compounds [1]. Particular interest has been focused on catalyst-assisted dry reforming of methane (CH_4), described by Eq. 3.1. This process directly converts two greenhouse gases to synthesis gas with a lower H_2/CO ratio when compared to the conventional steam reforming of methane (Eq. 3.2). However, the fact that the product gas contains a H_2 and CO ratio of 1 is ideal for methanol synthesis and Fischer-Tropsch reaction [2].

$CH_4 + CO_2 \rightarrow 2CO + 2H_2$ $\Delta H°_{298} = +247$ kJ mol^{-1} (Eq. 3.1)

$CH_4 + H_2O \rightarrow CO + 3H_2$ $\Delta H°_{298} = +206$ kJ/mol (Eq. 3.2)

The major obstacle that restrains dry reforming of methane from commercialisation is the severe catalyst deactivation from thermodynamically favoured coke formation [3]. Nickel catalysts traditionally used in steam reforming reactions are active dry reforming catalysts, however they are prone to rapid deactivation via carbon deposition due to the high endothermic nature of the reaction [4]. Bodrov and Apel'baum [5] reasoned that

the reaction rate for the dry reforming reaction is much lower in comparison to steam reforming because the dissociation of H_2O is more efficient than CO_2 [2].

It is well known that Pt/CeO_2 catalysts are active in dry reforming of CH_4 and immune to coke formation [6]. Platinum (Pt) has shown to be responsible for decomposing CH_4 into carbon and hydrogen, while ceria (CeO_2) as a support has demonstrated unique oxygen storage and mobility properties [6], which can be attributed to the ability to remove carbon deposits. During the redox cycle of CeO_2, the oxide is readily reduced upon removal of lattice oxygen to form Ce_2O_3, which in turn is oxidised back to CeO_2 in the presence of an oxidant [7]. This redox property is responsible for oxidising carbon species and catalysts regeneration to prevent deactivation from coking. The synergistic effect between Pt and CeO_2 as a catalyst has not only proven to be highly effective in resisting catalyst coking, but also renders them very stable during high temperature reaction. Nagai et al. [8] observed that the metallic phase of Pt on CeO_2 did not sinter even after subjecting the catalysts to oxidative treatment at 800 °C for 5 hours. They found the strong metal-support interaction through the formation of Pt-O-Ce bond had the ability to anchor the metallic Pt by preventing the migration and coalescence of the metal crystallites [8].

Previous studies have shown that the use of promoters can enhance the catalytic properties of CeO_2 support, resulting in increased activity and stability for the dry reforming reaction. The addition of zirconia (ZrO_2) to CeO_2 has shown to significantly increase the oxygen storage capacity as well as decreasing temperature of reduction of ceria [6, 9]. These improvements have also been shown to impart beneficial effects to

their use as the three-way catalysts [10] for soot combustion [9] and in water-gas shift reactions [11].

The effect of one promoter for CeO_2 that has not been explored in detail is tungsten trioxide (WO_3) with distinctive stepwise redox capabilities from $WO_3 \leftrightarrow WO_2 \leftrightarrow W$ [12]. This oxide also has large oxygen capacities as evidenced by its reduction in the presence of H_2 [12] and CH_4 [13, 14]. Kodama et al. [13] demonstrated that WO_3 was highly selective towards CO and H_2 when subjected to the cyclic steam reforming of methane at 800 °C to 1000 °C in a chemical looping scheme as described by reaction (3) and (4) [13, 14]. Although WO_3 was not involved in the reaction as a catalyst under these conditions, Kodama et al. [13] demonstrated that ZrO_2 promoted WO_3 gave a marked improvement in methane reforming as compared to a neat WO_3. Based on these findings, it is worth to examine whether WO_3 could also assist in the dry reforming of methane and/or act as a co-catalyst to improve the Pt/CeO_2 catalyst, according to these reactions:

$$WO_3 + 3CH_4 \rightarrow W + 3CO + 6H_2 \qquad \Delta H°_{298} = +245 \text{ kJ mol}^{-1} \qquad \text{(Eq. 3.3)}$$

$$W + 3H_2O \rightarrow WO_3 + 6H_2 \qquad \Delta H°_{298} = -39.1 \text{ kJ mol}^{-1} \qquad \text{(Eq. 3.4)}$$

The objective of this study is to investigate the effects of WO_3 promoter on Pt/CeO_2 catalyst during the dry reforming of methane with emphasis on oxygen mobility and capacity of CeO_2. Here, the influence of WO_3 on Pt/CeO_2 catalyst activity and stability were studied under a continuous flow condition, which differs from the cyclic switching between CH_4 and the oxidant as employed by Kodama et al. [13]. Continuous flow allows a better control over reaction conditions, and thus is more applicable for

industrial processing. The catalysts were compared with a benchmark commercial Ni/Al_2O_3 catalyst for the dry reforming of methane.

3.2 Experimental

3.2.1 Catalyst preparation

Urea co-precipitation-gelation method [15] was used to synthesize CeO_2, WO_3 and binary CeO_2-WO_3 with different ratios of oxide supports, as this method gives a better control of the homogeneity and surface area of samples than co-precipitation with ammonium carbonate [16]. The metal salt precursor used in this study was $(NH_4)_2Ce(NO_3)_6$ (Aldrich, 99.99%) for ceria and WCl_6 (Aldrich, 99.9+% metals basis) for tungsten trioxide. The preparation of the oxide supports comprised dissolving the metal salts (nitrates or chlorides) at desired ratios in deionised water to form 0.1 M solution. A solution of urea of 0.4 M was mixed with the metal salt solution with a ratio of 2:1 (v/v) respectively, under reflux conditions [17]. The solution was stirred vigorously whilst heated to 110 °C. After aging the precipitate in boiling solution for 12h, subsequent filtering and washing steps were employed. The precipitate was dried at 120°C overnight. Samples were calcined in a muffle furnace with a temperature ramp rate of 5ºC min^{-1} and held at 700 °C for 2h. The calcined material was grinded and sieved into particle size between 150-250 μm in diameter.

Pt catalysts were then loaded on CeO_2, WO_3 and CeO_2-WO_3 oxides by wet impregnation. Appropriate amount of $H_2PtCl_6 \cdot 6H_2O$ (Aldrich) in ethanol was added to the oxide support and the mixture was stirred in a rotary evaporator until the ethanol

was evaporated. The solids were dried overnight at 120°C and calcined at 700°C for 2h. In all cases, the Pt loading was maintained at approximately 1 wt%. The samples were denoted as Pt/$x$$CeO_2$–$y$$WO_3$, where x and y were the theoretical molar ratios of CeO_2 and WO_3 contents, respectively. Commercial Ni catalysts (ICI, Katalco) were used for comparative studies in this work.

3.2.2 Catalyst characterization

X-ray diffraction (XRD) spectra were collected on a Philips X'Pert MPD instrument using Cu Kα (λ = 1.542 Å) with scan range from 10° to 100° at a scan rate of 0.22° min^{-1} and step size of 0.026°. X-ray Photoelectron Spectroscopy (XPS) surface analysis of the catalysts was performed on a Kratos AXIS Nova (Kratos Analytical Ltd, UK) using a monochromatised Al $K\alpha$ radiation at a pass energy of 20 eV and at $P < 3 \times 10^{-9}$ Torr. The energy scale was calibrated and corrected for charging using the C1s (285.0 eV) line as the binding energy reference. The Pt contents in catalysts were analysed using a Perkin-Elmer OPTIMA DV3000 inductive coupled plasma spectrophotometer (ICP-OES). A Pt sample under consideration was dissolved in an acid mixture of nitric, hydrochloric and hydrofluoric with a 2:6:5 volume ratio, while being heated at 180 °C until the solution was almost dried. The resultant solution was then cooled and made up to volume with a 5 % hydrochloric acid matrix before ICP-OES analysis. The specific surface areas (SSA) of the prepared catalysts were analysed by nitrogen adsorption at 77 K, on the Micromeritics Tristar 3000, using the BET model. Raman spectra were collected using a Renishaw inVia microscope at an excitation wavelength of 514 nm. Sampling time was 30 s at incident energy of 5.0 mW. Spectra were normalised to the maximum intensity of each individual run.

3.2.3 Temperature-programmed reduction, oxidation and CO chemisorption

Temperature-programmed reduction (TPR) and oxidation (TPO) were performed on a Micromeritics Autochem II 2920 instrument interfaced with a thermal conductivity detector (TCD) and a Micromeritics MicroStar^{TM} mass spectrometer (MS) with the results normalised to the sample loadings. For TPR experiments, each sample (50 mg) was pre-treated at 120 °C under He (50 ml min^{-1}) for 1 h and cooled to ambient temperature. TPR was then performed under 5 % H_2/He (50 ml min^{-1}) at a ramp rate of 10 °C min^{-1} from 100 °C to 1000 °C with the reacted gas analysed by a TCD.

Spent catalysts were subjected to TPO analysis. During TPO, the catalyst bed was ramped to 600 °C at 10 °C min^{-1} under 5%O_2/He (50 mL min^{-1}). Previous work [18] showed that CO_2 would evolved when the carbonaceous species on the surface of the catalyst were oxidised. The MicroStar^{TM} MS was used to detect the presence of CO_2.

The dispersion and average sizes of the Pt deposits was determined by CO pulse chemisorption using a Micromeritics Autochem II 2920 instrument. The Pt/oxide samples were first reduced in 50 ml/min of 5 % H_2/He for 60 min at 300 °C followed by flushing with 50 ml/min of He at 310 °C for 60 min. Pulse injections of 0.5 ml 10 % CO in He were introduced at -80 °C by immersing the sample cell in an isopropanol and liquid nitrogen mixture. This was to ensure that the CeO_2 did not interfere with chemisorption [19]. By assuming a Pt:CO stoichiometric ratio of 1:1 [20], the dispersion of the Pt deposits was defined as the ratio of the atoms accessible to the CO relative to the total number of Pt atoms in the system.

3.2.4 Catalyst activity

CH_4 reforming with CO_2 reaction was performed using a 6 mm I.D. quartz tube packed bed reactor with the as-prepared catalyst sample (300 mg) pelletized, ground, and sieved to diameter in the range of 250 μm to 300 μm. Prior to each activity test, catalysts were reduced under a total flow of diluted hydrogen (10 % H_2/N_2, 100 ml min^{-1}) for 1 h at 400 °C followed by N_2 purging at 700 °C. A ramping rate of 10 °C min^{-1} was employed in both heating steps. After N_2 purging, the reactant gas stream which contained 20 % CH_4, 20 % CO_2 and N_2 as balance was brought into contact with the catalyst bed at a flow rate of 100 ml min^{-1} under atmospheric pressure. The operating temperature was maintained at 700 °C with 20 h of time on stream was used per catalyst. The product stream, after passage through an ice trap to remove water, was analysed using an online gas chromatograph (Varian 3800) fitted with thermal conductivity detectors. The gas chromatograph was operated with argon as the carrier gas through two columns in series. The first column was a 2 m molecular sieve 13X column (Varian) used for H_2, CH_4 and CO analysis followed by a Hayesep N column (Varian) for CO_2 analysis.

3.3 Results and discussion

3.3.1 Structural characterization of catalysts

The XRD patterns of the Pt/CeO_2, Pt/WO_3 and $Pt/xCeO_2$-yWO_3 samples calcined at 700 °C are presented in Fig. 3.1. Due to the low Pt loadings, no detectable diffraction of Pt crystallites could be identified. Instead the Pt-based catalysts showed XRD spectra of

their respective oxide supports. The diffraction lines of a typical fluorite structure of CeO_2 [21] in Fig. 3.1 indicated that this structure was maintained even in the presence of 1 wt% Pt. XRD spectra of as prepared Pt promoted WO_3 showed the monoclinic crystal structure of the WO_3 oxide support [22]. The characteristic XRD spectral lines of CeO_2 remain unchanged up to 20 mol% loading with WO_3. However, at a loading of 30 mol% WO_3, additional peaks other than CeO_2 or WO_3 as indicated by (▲) were observed. These peaks at $2\theta = 25.7°$ and 31.4° can be assigned to a new phase formed by Ce_2O_3 and WO_3 as defined by Yoshimura et al. [23]. The new phase specifically occurs when Ce to W mole ratio of 2:1 respectively is incurred. The crystallite size of the UCG-prepared catalysts was evaluated from XRD using the Scherrer formula (Table 3.1). A general trend of increasing bulk crystallite size was correlated to the addition of WO_3 into the CeO_2 support. This alluded to the idea that the presence of WO_3 enhanced the crystal growth of CeO_2 during UCG synthesis and vice versa. The increase of crystallite size was also reflected by the decrease in BET specific surface area (Table 3.1). The concentration of Pt ranged from 0.95 to 1.05 wt% based on ICP analysis. The Pt/CeO_2 sample showed the highest SSA (7.54 $m^2\ g^{-1}$) while Pt/WO_3 displayed the lowest SSA (1.45 $m^2\ g^{-1}$). The CO chemisorption data indicated the Pt dispersion was lowered by the introduction of WO_3.

Raman analysis of the catalyst surface confirmed whether a solid solution was formed between CeO_2 and WO_3 support during UCG synthesis (Fig. 3.2). The Raman spectra of a typical WO_3 monoclinic phase [24] was detected for the Pt/WO_3 and $Pt/30CeO_2$-$70WO_3$ samples calcined at 700 °C. Raman spectra of Pt/CeO_2, $Pt/90CeO_2$-$10WO_3$ and $Pt/80CeO_2$-$20WO_3$ sample exhibited a characteristic sharp narrow peak of pure CeO_2 with vibration of the CeO_2 lattice at 465 cm^{-1} [21]. No evidence of solid solution was

observed for the samples mentioned earlier, however evidence of the presence of CeO_2/WO_3 solid solution was confirmed by the emergence of new Raman peaks (indicated by '■' in Fig. 3.2) for Pt/70CeO_2-30WO_3 sample. The additional peaks attributed to to the unique Ce_2O_3/WO_3 phase appeared at 766 cm^{-1} with three overlapping peaks occurring between 920 cm^{-1} to 950 cm^{-1}. The Raman results agreed with the XRD analysis.

XPS spectra of Pt 4f, Ce 3d and W 4f core electrons for as-prepared Pt/CeO_2, Pt/WO_3 and Pt/$x$$CeO_2$-$y$$WO_3$ catalysts are shown in Table 3.2. The binding energies (BE) of the Pt $4f_{7/2}$ component were around 72.5 eV, typical of PtO specie [25, 26]. The binding energy of the Ce $3d_{5/2}$ (882.4 eV) corresponded to CeO_2 [6], while the binding energy of W 4f7/2 (35.5 eV) corresponded to WO_3 [27]. Binding energy of O1s was not considered due to complications with the overlapping contribution of oxygen from PtO, CeO_2 and WO_3. No obvious shift in Pt 4f binding energies was observed. The shift in BEs when comparing Pt/CeO_2, Pt/WO_3 and the Pt/composite material provided the evidence of interactions between the Ce^{4+} and W^{6+} species. Inclusion of WO_3 into the Pt/CeO_2 system shifted the BE maxima of Ce $3d_{5/2}$ from 882.6 eV at 10 mol% WO_3 loadings to 883.9 eV at 70 mol% WO_3 loadings, accompanied by a decrease in W $4f_{7/2}$ BE maxima from 36.2 eV to 35.6 eV demonstrating interactions between CeO_2 and WO_3. The simultaneous yet opposite changes of Ce $3d_{5/2}$ and W$4f_{7/2}$ BEs infered a decrease in electron density in the Ce nucleus by increasing WO_3 loading. On the other hand, WO_3 inclusion had no influence on the Pt $4f_{7/2}$ BE maxima.

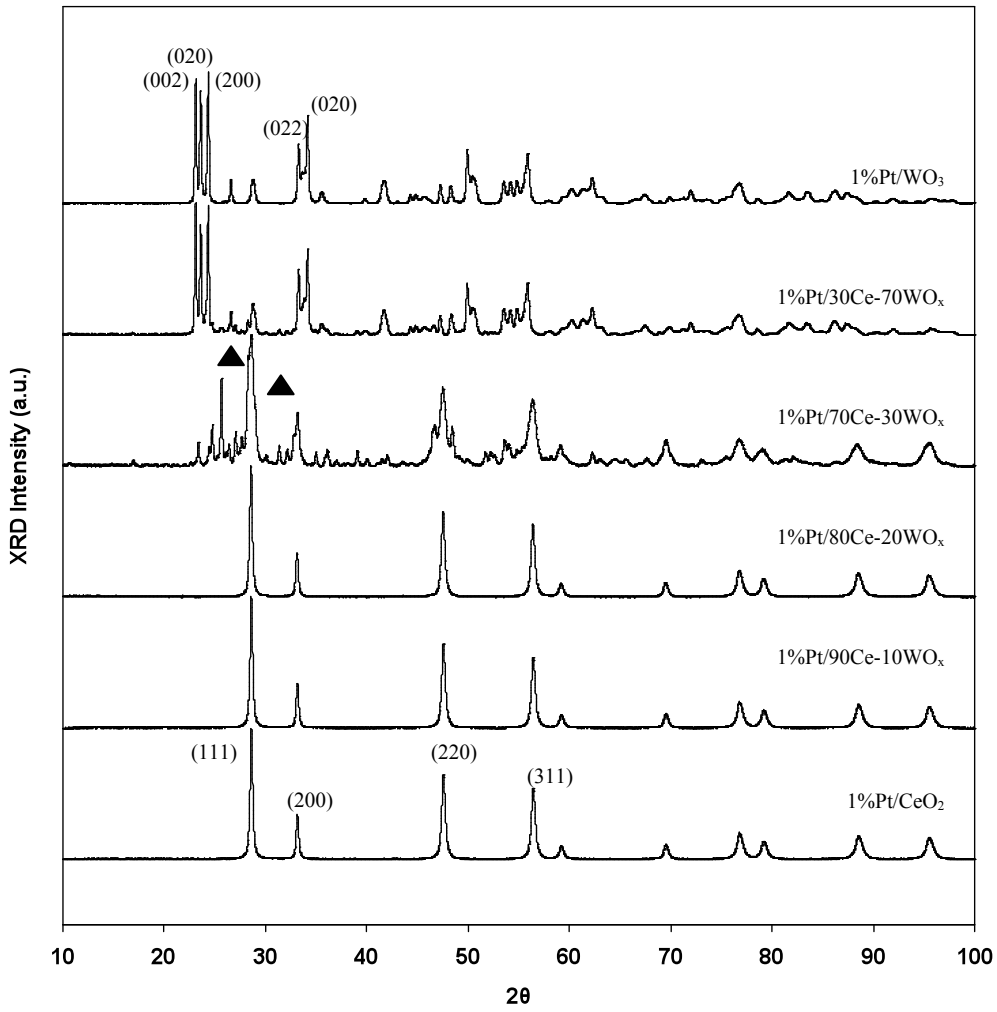

Fig. 3.1: XRD spectra of Pt/CeO_2, Pt/WO_3 and $Pt/xCeO_2$-yWO_3 samples calcined at 700°C. Separate phase of Ce_2O_3/WO_3 are indicated with (▲).

Table 3.1: Physicochemical properties of Pt/CeO_2, Pt/WO_3 and $Pt/xCeO_2$-yWO_3 catalysts calcined at 700°C.

Catalyst	BET surface area ($m^2 g^{-1}$), SSA	Pt loading (wt%)[a]	Pt metal dispersion (%)[b]	Primary oxide support crystallite size (nm)[c]	
				d_{CeO2}	d_{WO3}
$1\%Pt/CeO_2$	7.54	1.01	5.3	40	-
$1\%Pt/90CeO_2$-$10WO_3$	6.99	0.95	3.2	44	-
$1\%Pt/80CeO_2$-$20WO_3$	6.85	0.96	2.1	46	-
$1\%Pt/70CeO_2$-$30WO_3$	6.10	0.97	1.9	51	
$1\%Pt/30CeO_2$-$70WO_3$	1.98	1.03	1.5	-	55
$1\%Pt/WO_3$	1.45	1.05	1.2	-	63

[a] Determined by ICP analysis.

[b] Determined by CO chemisorption.

[c] Determined by XRD and Scherrer formula from averaging diffraction lines (111), (200), (220), and (311) for CeO_2; (002), (020), (200), (022) and (020) for WO_3.

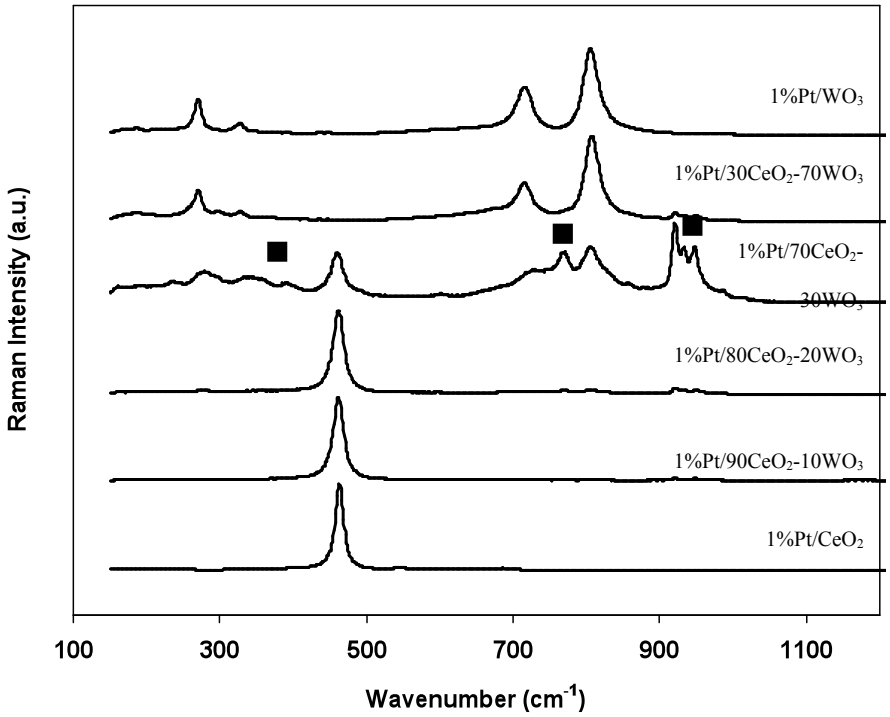

Fig. 3.2: Raman spectra of Pt/CeO_2, Pt/WO_3 and $Pt/xCeO_2$-yWO_3 samples calcined at 700°C. '■' indicates additional peaks that evolved from a unique phase of Ce_2O_3/WO_3 when the mole ratio of 2:1 is achieved for Ce:W, respectively.

3.3.2 Temperature programmed reduction analysis

The TPR profiles of fresh Pt/CeO_2, $Pt/xCeO_2$-yWO_3, Pt/WO_3 samples are shown in Fig. 3.3. A commercial Ni catalyst was included for comparison. In accordance to previously reported data [28], the first peak corresponded to the reduction of PtO_x species as indicated by '▲', occurring at 170 °C when supported on CeO_2 and $70CeO_2$-$30WO_3$; 250 °C for $90CeO_2$-$10WO_3$, $80CeO_2$-$20WO_3$ and $30CeO_2$-$70WO_3$; and 200 °C for the WO_3 oxide support. For the commercial nickel catalyst, the nickel species was reduced to their metallic state at around 400 °C. The Pt/CeO_2 sample displayed two additional broad and asymmetrical peaks 380 °C and 775 °C, typical of a neat CeO_2 [29]. These have been assigned by others as due to the surface and bulk reduction of CeO_2 to Ce_2O_3,

respectively (indicated by '■' and '□' in Fig. 3.3) [30, 31]. The oxide support for Pt/WO_3 was reduced in a multi-step process, with peaks at 680 °C, 790 °C and 900 °C (Fig. 3.3). The observation of multiple intermediate oxidation phases of tungsten during reduction of WO_3 has been previously reported [32, 33], resulting in a reduction process dominated by (although not limited to) $WO_3 \rightarrow WO_{2.72}$ at 680 °C, $WO_{2.72} \rightarrow WO_2$ at 790 °C and finally from WO_2 to tungsten metal (W) at 900 °C.

The TPR profiles showed the complex nature and the effects of WO_3 on the reduction of CeO_2 and vice versa Fig. 3.3. Salient features of increasing WO_3 loading from 10% to 20% mole fraction in the CeO_2 oxide support included the disappearance of the initial peak at 380°C corresponding to surface reduction of CeO_2. At higher WO_3 loadings (30 mol% and 70 mol%), a broad peak was observed at 400 °C. At this instance, the peak was ascribed to the delay in reduction of CeO_2 to Ce_2O_3 which occurred at 380 °C for the Pt/CeO_2 catalyst. This was followed by two obvious reduction peaks at 700 °C and around 900 °C due to the sequential bulk reduction of $WO_{2.72}$ to WO_2, and then finally to W. Qualitatively, it was possible to rank the Pt catalysts' oxide supports in terms of their oxygen capacity by examining the area under the H_2 consumption curve. The order from highest to lowest H_2 consumed was as follows: WO3 > $30CeO_2$-$70WO_3$ > $70CeO_2$-$30WO_3$ > $80CeO_2$-$20WO_3$ > $90CeO_2$-$10WO_3$ > CeO_2.

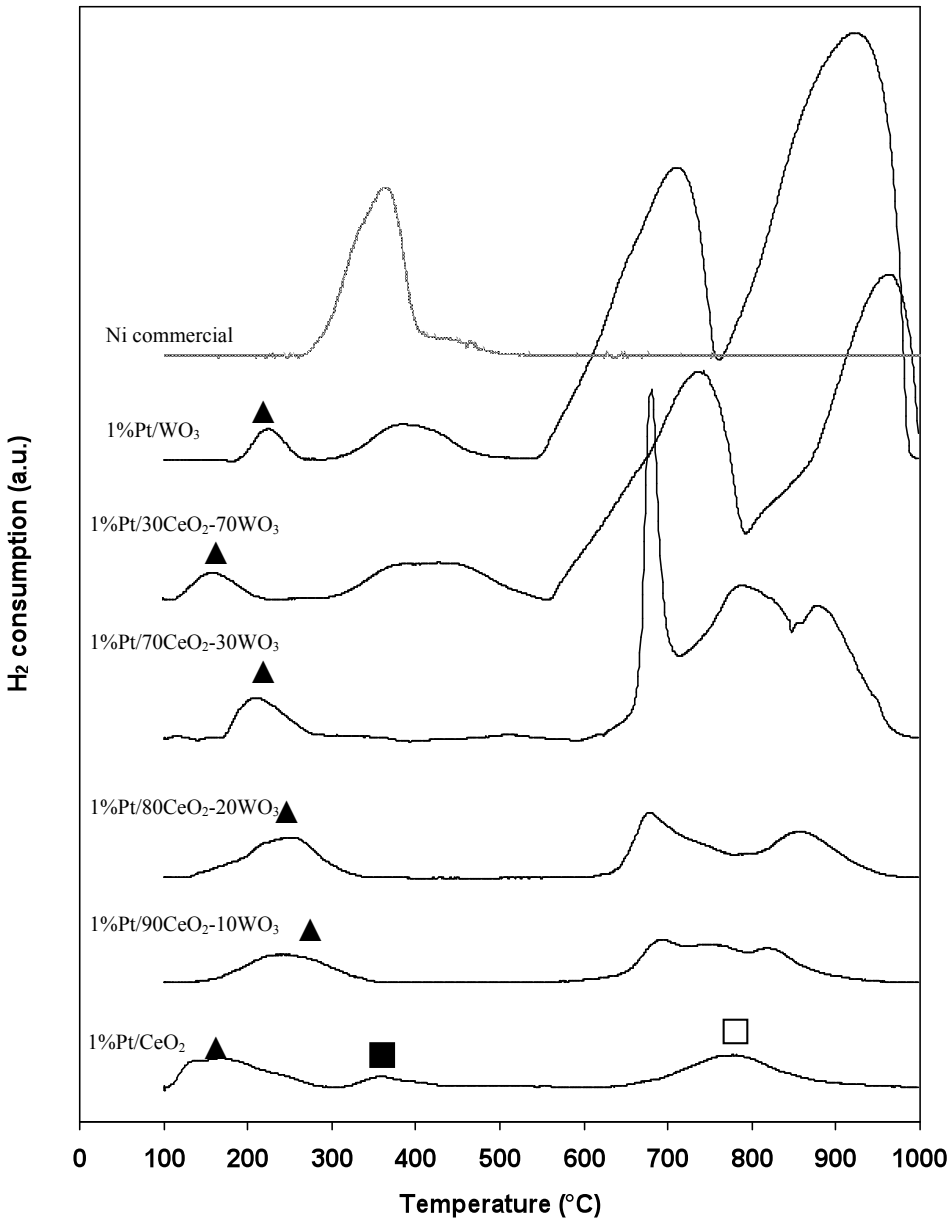

Fig. 3.3: H_2-TPR profiles of UCG-prepared Pt/CeO_2, $Pt/xCeO_2$-yWO_3, Pt/WO_3 and a commercial Ni catalysts. All samples are calcined at 700°C before TPR experiments. '▲' indicates reduction peaks of PtO_x to Pt. '■' and '□' indicates surface and bulk reduction of CeO_2 to Ce_2O_3, respectively.

3.3.3 XPS analysis

In this work, XPS demonstrated a diminishing electron density in the Ce^{4+} nucleus manifested as a gradual shift in the Ce $3d_{5/2}$ spectra (Table 3.2) to higher binding energies with increasing WO_3 loading. The decreasing Ce^{4+} electron density implied the Ce^{4+} and O^{2-} bond was strengthened by WO_3 addition. This would cause Ce^{4+} to be more difficult to reduce, and therefore the reduction that originally occurred at 380 °C would require a higher temperature. This was reflected in the H_2-TPR profiles (Fig. 3.3) as the reduction peak of CeO_2 to Ce_2O_3 at 380 °C observed for Pt/CeO_2 sample was observed at 400 °C when WO_3 was added into the Pt/CeO_2 system, because the surface oxygen has become difficult to remove from the CeO_2 surface.

Table 3.2: XPS analysis on Pt/CeO_2, Pt/WO_3 and $Pt/xCeO_2$-yWO_3 catalysts calcined at 700 °C.

Catalyst	Binding energies (eV)[a]		
	Pt $4f_{7/2}$	Ce $3d_{5/2}$	W $4f_{7/2}$
$1\%Pt/CeO_2$	72.7	882.4	-
$1\%Pt/90CeO_2$-$10WO_3$	72.4	882.6	36.2
$1\%Pt/80CeO_2$-$20WO_3$	72.5	883.3	36.1
$1\%Pt/70CeO_2$-$30WO_3$	72.6	883.7	35.7
$1\%Pt/30CeO_2$-$70WO_3$	72.6	883.9	35.6
$1\%Pt/WO_3$	72.5	-	35.5

[a] Values are indicative of the binding energy maxima of the core electrons

3.3.4 Catalyst activity and stability

All catalysts were tested for activity in the dry reforming of methane reaction using a 1:1 (v/v) mixture of CH_4 and CO_2 and the results are shown in Fig 3.4 (a-c). Commercial Ni catalyst was very active for dry reforming of methane, achieving 95% conversion for both CH_4 and CO_2 with H_2/CO ratio close to unity. However, the reaction had to be terminated after 1 h of time on stream because of tremendous pressure drop across the reactor due to blockage from severe coking. The growth of carbon filaments is known to occur on a Ni metal surface where the Ni metal is carried at the tip of the carbon filament [34] and, as a consequence, the catalytic activity remains constant as shown within the 1 h of DRM time on stream (Fig 3.4a) since the active Ni metal is still accessible to the reactants. TPO characterisation indicated that a large amount of CO_2 evolved at 550°C from the spent commercial Ni catalysts (Fig. 3.5). In comparison, Pt/CeO_2 catalyst showed the highest activity among the Pt-catalysts: 70% CH_4 and 75% CO_2 conversion, while the H_2 to CO ratio was maintained at 0.95, with no sign of deactivation over the 20 h of time on stream.

The activity profiles indicated the propensity of WO_3 especially at higher loadings to be detrimental to the performance of Pt/CeO_2 during CO_2 reforming of CH_4, as the addition of WO_3 into Pt/CeO_2 catalyst caused a marked decrease in activity. This would be connected with the differences in the number of accessible active metal surface sites on the catalyst surface. CO chemisorption showed the dispersion of metallic Pt decreases by increasing WO_3 content (Table 3.1), the number of accessible metallic active sites is decreased. Therefore, there is a relation between accessible metal Pt area and the activity of the catalysts. Damyanova et al. [6] showed similar results as the

DRM activity worsened for a Pt/ZrO_2 catalyst because the increasing CeO_2 content decreases the Pt dispersion.

$Pt/90CeO_2$-$10WO_3$ and $Pt/80CeO_2$-$20WO_3$ catalysts could maintain CH_4 and CO_2 conversion at around 20% and H_2/CO ratio at 0.40 throughout the experiment. $Pt/70CeO_2$-$30WO_3$ slowly deactivated over time from 20% to 15% in terms of CH_4 conversion and 20% to 10% for CO_2 conversion. No observable activity was detected for $Pt/30CeO_2$-$70WO_3$ and Pt/WO_3. TPO characterisation (Fig. 3.5) indicated that the catalyst inactivity was due to the rapid build-up of carbonaceous species on the surface of the $Pt/30CeO_2$-$70WO_3$ and Pt/WO_3. The TPR analysis showed that the co-existence of WO_3 (especially >70 mol% loading) and CeO_2 has enhanced the reduction of material by increasing the oxygen capacity particularly at 700 °C (Fig. 3.3). One would expect that the improved redox would be beneficial in enhancing the catalyst activity during CO_2 and CH_4 reforming. However, this was not to be the case here, suggesting that the redox property of WO_3 did not play an important role in the reaction and preventing carbon formation, nor enhanced the performance of Pt/CeO_2 catalyst.

It was apparent that the H_2/CO ratio in the product stream was lower than unity because of the consequential involvement of the reverse water-gas shift (RWGS) reaction (Eq. 3.5). The simultaneous occurrence of the RWGS reaction during the experiment increased the CO concentration in the product stream, causing the H_2/CO ratio to be unequal to one, which was also observed by Damyanova et al. [6] on Pt/CeO_2-ZrO_2 catalysts during dry reforming of CH_4.

$$CO_2 + H_2 \rightarrow CO + H_2O \qquad \Delta H°_{298} = +41.1 \text{ kJ mol}^{-1} \qquad \text{(Eq. 3.5)}$$

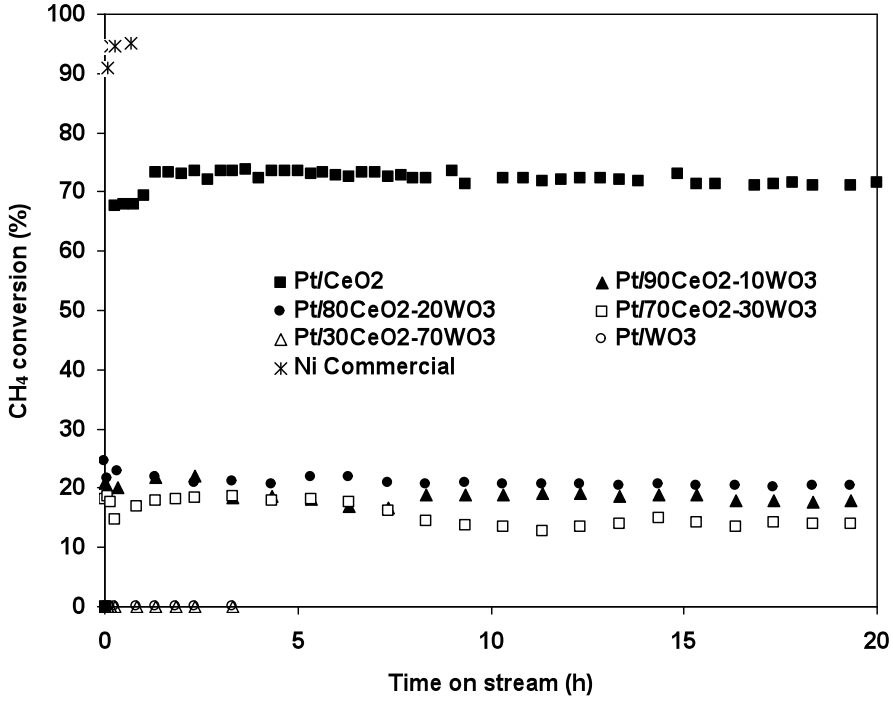
CH4 conversion (%)
Time on stream (h)
Pt/CeO2
Pt/90CeO2-10WO3
Pt/80CeO2-20WO3
Pt/70CeO2-30WO3
Pt/30CeO2-70WO3
Pt/WO3
Ni Commercial

(a)

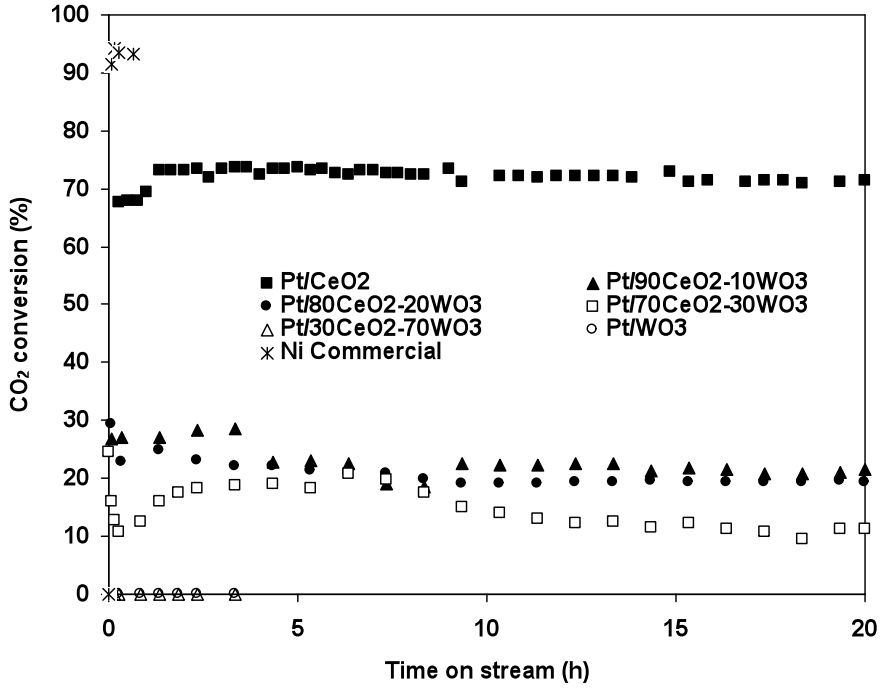
CO2 conversion (%)
Time on stream (h)
Pt/CeO2
Pt/90CeO2-10WO3
Pt/80CeO2-20WO3
Pt/70CeO2-30WO3
Pt/30CeO2-70WO3
Pt/WO3
Ni Commercial

(b)

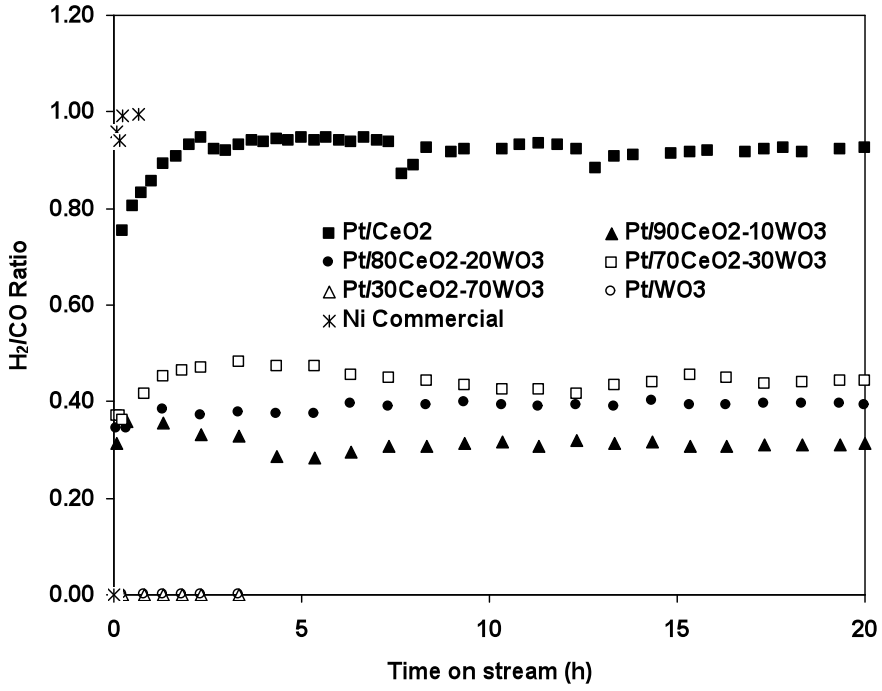

(c)

Fig. 3.4: (a) CH_4 conversion for Pt/CeO_2, $Pt/xCeO_2$-yWO_3, Pt/WO_3 and commercial Ni catalysts; (b) CO_2 conversion for the same set of catalysts (c) H_2/CO ratio of the product gas during CO_2 reforming of CH_4 operation. Reaction conditions: operating temperature 700°C, operating time = 20 h, total flow = 100 ml min^{-1} (20%CH_4, 20%CO_2 and 60%N_2); catalysts loading 0.50 g; pressure = 1 atm.

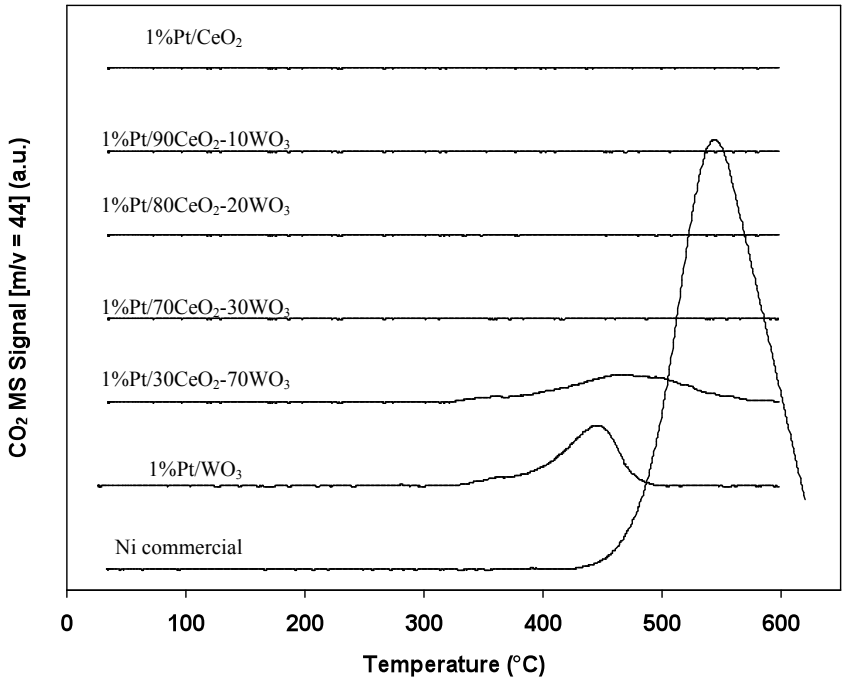

Fig. 3.5: TPO curves for spent Pt/CeO_2-WO_3 catalysts after CO_2 reforming of methane reaction. Spent Ni commercial catalyst was included for comparison.

3.4 Conclusions

XPS characterisation revealed the electron interactions between Ce and W components, corroborating the increase of Ce^{4+} binding energy to O^{2-} from increased concentration of WO_3 loadings. This caused a delay in surface reduction of CeO_2 to Ce_2O_3 from 380 °C to 400 °C, suggesting that WO_3 had the ability to control the mobility of oxygen in the ceria lattice. TPR analysis showed that the presence WO_3 (>30 mol% loading) induced a major improvement in the oxygen capacity of Pt/CeO_2 catalyst by producing large H_2 consumption peaks above 700 °C. Even though the co-existence of WO_3 in CeO_2 improved the redox ability, the activity of the Pt/CeO_2 catalyst was not enhanced during the dry reforming of CH_4 suggesting the redox property of WO_3 did not play an important role in the dry reforming of methane reaction. The presence of WO_3 (10

mol% to 30 mol%) lowered the conversion of CH_4 from 70 mol% to 20 mol% of the Pt/CeO_2 catalysts. However, $Pt/90CeO_2$-$10WO_3$ and $Pt/80CeO_2$-$20WO_3$ catalysts were very stable under the dry reforming reaction, showing no sign of catalyst deactivation over 20h of time on stream. In comparison, the commercial Ni catalyst was very active during the dry reforming reaction, but succumbed to severe coking after 1 hour of operation. Further increase in WO_3 loading (>70 mol%) appeared to promote carbon formation on the surface of the catalyst, suggesting that the mixed oxide support was not able to prevent catalyst coking. Tungsten trioxide may be suitable for the two-step cyclic steam reforming of methane but from this study, WO_3 as a promoter did not improve the catalytic activity of the Pt/CeO_2 catalyst during dry reforming of methane.

3.5 References

1. J.R.H. Ross, A.N.J. van Keulen, M.E.S. Hegarty, and K. Seshan, 'The catalytic conversion of natural gas to useful products', *Catalysis Today* 30(1-3) (**1996**) 193-199.
2. M.C.J. Bradford and M.A. Vannice, 'CO_2 reforming of CH_4', *Catalysis Reviews: Science and Engineering* 41(1) (**1999**) 1-42.
3. J.R. Rostrup-Nielsen and J.H.B. Hansen, 'CO_2-Reforming of Methane over Transition Metals', *Journal of Catalysis* 144 (**1993**) 38-49.
4. D.L. Trimm, 'The Formation and Removal of Coke from Nickel Catalyst', *Catalysis Reviews: Science and Engineering* 16(1) (**1977**) 155-189.
5. I.M. Bodrov and L.O. Apel'baum, 'Kinetics of the reaction of methane with carbon dioxide on a nickel surface', *Kinetics and Catalysis* 8 (**1967**) 326-329.

6. S. Damyanova, B. Pawelec, K. Arishtirova, M.V.M. Huerta, and J.L.G. Fierro, 'The effect of CeO_2 on the surface and catalyric properties of Pt/CeO_2-ZrO_2 catalysts for methane dry reforming', *Applied Catalysis B: Environmental* 89 (**2009**) 149-159.

7. E. Aneggi, M. Boaro, C. Leitenburg, G. Dolcetti, and A. Trovarelli, 'Insights into the redox properties of ceria-based oxides and their implications in catalysts', *Journal of Alloys and Compounds* 408-412 (**2006**) 1096-1102.

8. Y. Nagai, T. Hirabayashi, K. Dohmae, N. Takagi, T. Minami, H. Shinjoh, and S.i. Matsumoto, 'Sintering inhibition mechanism of platinum supported on ceria-based oxide and Pt-oxide–support interaction', *Journal of Catalysis* 242 (**2006**) 103–109.

9. E. Aneggi, C.d. Leitenburg, G. Dolcetti, and A. Trovarelli, 'Promotional effect of rare earths and transition metals in the combustion of diesel soot over CeO_2 and CeO_2–ZrO_2', *Catalysis Today* 114 (**2006**) 40-47.

10. E.C. Su and W.G. Rothschild, 'Dynamic Behavior of Three-Way Catalysts', *Journal of Catalysis* 99 (**1986**) 506-510.

11. S. Ricote, G. Jacobs, M. Milling, Y. Ji, P.M. Patterson, and B.H. Davis, 'Low temperature water–gas shift: Characterization and testing of binary mixed oxides of ceria and zirconia promoted with Pt', *Applied Catalysis A: General* 303 (**2006**) 35-47.

12. D.C. Vermaire and P.C. van Berge, 'The preparation of WO_3/TiO_2 and WO_3/Al_2O_3 and characterization by temperature-programmed reduction', *Journal of Catalysis* 116(2) (**1989**) 309-317.

13. T. Kodama, H. Ohtake, S. Matsumoto, A. Aoki, T. Shimizu, and Y. Kitayama, 'Thermochemical methane reforming using a reactive WO_3/W redox system', *Energy* 25 (**2000**) 411-425.

14. T. Kodama, T. Shimizu, T. Satoh, and K.I. Shimizu, 'Stepwise production of CO-rich syngas and hydrogen via methane reforming by a WO_3-redox catalyst', *Energy* 28 (**2003**) 1055-1068.

15. C. Perego and P. Villa, 'Catalyst preparation methods', *Catalysis Today* 34 (**1997**) 281-305.

16. Y. Li, Q. Fu, and M. Flytzani-Stephanopoulos, 'Low-temperature water-gas shift reaction over Cu- and Ni-loaded cerium oxide catalysts', *Applied Catalysis B: Environmental* 27 (**2000**) 179-191.

17. J.-D. Lin and J.-G. Duh, 'Coprecipitation and Hydrothermal Synthesis of Ultrafine 5.5 mol% CeO_2–2 mol% $YO_{1.5}$–ZrO_2 Powders', *Journal of the American Ceramic Society* 80(1) (**1997**) 92-98.

18. X. Liu, W. Ruettinger, X. Xu, and R. Farrauto, 'Deactivation of Pt/CeO_2 water-gas shift catalysts due to shutdown/startup modes for fuel cell applications', *Applied Catalysis B: Environmental* 56 (**2005**) 69–75.

19. T. Tanabe, Y. Nagai, T. Hirabayashi, N. Takagi, K. Dohmae, N. Takahashi, S.i. Matsumoto, H. Shinjoh, J.N. Kondo, J.C. Schouten, and H.H. Brongersma, 'Low temperature CO pulse adsorption for the determination of Pt particle size in a Pt/cerium-based oxide catalyst', *Applied Catalysis A: General* 370 (**2009**) 108–113.

20. R. Strobel, W.J. Stark, L. Mädler, S.E. Pratsinis, and A. Baiker, 'Flame-made platinum/alumina: structural properties and catalytic behaviour in enantioselective hydrogenation', *Journal of Catalysis* 213 (**2003**) 296–304.

21. R. Kydd, W.Y. Teoh, K. Wong, Y. Wang, Jason Scott, Q.-H. Zeng, A.-B. Yu, J. Zou, and R. Amal, 'Flame-Synthesized Ceria-Supported Copper Dimers for Preferential Oxidation of CO', *Advanced Functional Materials* 19 (**2009**) 369-377.

22. M. Ashokkumar and P. Maruthamuthu, 'Preparation and characterization of doped WO_3 photocatalyst powders', *Journal of Materials Science Letters* 24 (**1989**) 2135-2139.

23. M. Yoshimura, F. Sibieude, A. Rouanet, and M. Foex, 'Identification of binary compounds in the system Ce_2O_3-WO_3', *Journal of Solid State Chemistry* 16 (**1976**) 219-232.

24. J. Gabrusenoks, A. Veispals, A. von-Czarnowski, and K.-H. Meiwes-Broer, 'Infrared and Raman spectroscopy of WO_3 and $CdWO_4$', *Electrochimica Acta* 46 (**2001**) 2229-2231.

25. W. Yang, Y. Ma, J. Tang, and X. Yang, '"Green synthesis" of monodisperse Pt nanoparticles and their catalytic properties', *Colloids and Surfaces A: Physicochemical and Engineering Aspects* 302 (**2007**) 628–633.

26. Z. Yi, W. Wei, S. Lee, and G. Jianhua, 'Photocatalytic performance of plasma sprayed Pt-modified TiO_2 coatings under visible light irradiation', *Catalysis Communications* 8 (**2007**) 906–912.

27. X. Xia, R. Jin, Y. He, J.-F. Deng, and H. Li, 'Surface properties and catalytic behaviors of WO_3/SiO_2 in selective oxidation of cyclopentene to glutaraldehyde', *Applied Surface Science* 165 (**2000**) 255-259.

28. P. Panagiotopoulou and D.I. Kondarides, 'Effect of the nature of the support on the catalytic performance of noble metal catalysts for the water–gas shift reaction', *Catalysis Today* 112 (**2006**) 49–52.

29. P. Panagiotopoulou, J. Papavasiliou, G. Avgouropoulos, T. Ioannides, and D.I. Kondarides, 'Water-gas shift activity of doped Pt/CeO_2 catalysts', *Chemical Engineering Journal* 134 (**2007**) 16-22.

30. A.M.D.d. Farias, P. Bargiela, M.d.G.C. Rocha, and M.A. Fraga, 'Vanadium-promoted Pt/CeO_2 catalyst for water-gas shift reaction', *Journal of Catalysis* 260(1) (**2008**) 93-102.

31. S. Letichevsky, C.A. Tellez, R.R.d. Avillez, M.I.P.d. Silva, M.A. Fraga, and L.G. Appel, 'Obtaining CeO_2–ZrO_2 mixed oxides by coprecipitation: role of preparation conditions', *Applied Catalysis B: Environmental* 58 (**2005**) 203–210.

32. I.M. Szilágyi, J. Madarász, F. Hange, and G. Pokol, 'Partial thermal reduction of ammonium paratungstate tetrahydrate', *Journal of Thermal Analysis and Calorimetry* 88 (**2008**) 139-144

33. N.E. Fouad, K.M.E. Attyia, and M.I. Zaki, 'Therrnogravimetry of WO_3 reduction in hydrogen: kinetic characterization of autocatalytic effects', *Powder Technology* 74 (**1993**) 31-37.

34. A.E.C. Luna and M.E. Iriarte, 'Carbon dioxide reforming of methane over a metal modified $Ni-Al_2O_3$ catalyst', *Applied Catalysis A: General* 343 (**2008**) 10–15.

CHAPTER FOUR

The role of metal oxides in promoting Cu as a catalyst for the low temperature water-gas shift reaction

4.1 Introduction

The water-gas shift (WGS) reaction is a reversible, exothermic, catalyst-assisted, chemical reaction, whereby steam is reacted with carbon monoxide to produce carbon dioxide and hydrogen gas (Eq. 4.1):

$$CO_{(g)} + H_2O_{(g)} \leftrightarrow CO_{2(g)} + H_{2(g)} \qquad \Delta H = -41.1 \text{ kJ mol}^{-1} \qquad \text{(Eq. 4.1)}$$

The WGS reaction is of particular interest due to its importance in many industrial applications such as methanol, ammonia, and Fisher-Tropsch synthesis, fuel cell technologies and hydrogen production. The demand for hydrogen, a product of the reaction, is increasing on the basis of it being a “clean” energy. Since carbon monoxide can deactivate the catalyst in ammonia synthesis and Pt electrodes in a fuel cell, the WGS reaction is crucial for reducing CO levels and producing additional hydrogen in the overall process.

Supported copper catalysts are widely used for the low temperature WGS (LT-WGS) reaction due to their cost-effectiveness to deliver high activity and selectivity as compared to other metals [1, 2]. It is believed both the metal and support have an influence on the catalyst performance [3, 4]. Uncertainties concerning the reaction

mechanism, active sites and structure-sensitivity remain due to the different preparation methods, operating conditions and feed gas compositions in testing these catalysts [3, 5-7]. In most cases, pure carbon monoxide and water feed compositions have been used to test the LT-WGS activity of catalysts, although such an ideal situation is highly unlikely in practice. The reaction products of hydrogen and carbon dioxide have been found to have an inhibiting effect on the reaction rate [8]. Although some Cu-based catalysts other than the commercial $Cu/ZnO/Al_2O_3$ have been assessed for LT-WGS, including Cu/ZrO_2 [9], Cu/TiO_2 [10] and Cu/CeO_2 [11, 12], comparing their performances is difficult due to the different conditions when they were being assessed. Screening of different copper catalyst supports for the LT-WGS reaction have been conducted in the past [1, 13, 14]. Thinon et al. [1] found that Cu/CeO_2 exhibited the highest WGS activity although no comparison was made to the more commonly used Cu/ZnO catalyst or Cu/MgO system. Yahiro et al. [13] observed that Cu/ZnO with another oxide support (Al_2O_3, MgO, or CeO_2) incorporated into the system showed high WGS activity when compared to Cu catalysts supported on SiO_2/Al_2O_3, SiO_2/MgO and zeolite support. However, the cause of enhanced LT-WGS activity still remained unclear.

In this study, Cu/metal oxide catalysts, synthesized by flame spray pyrolysis were evaluated under practical feed conditions with typical composition of a reformate stream for LT-WGS activity. Physicochemical properties of the materials were assessed to identify parameters important for LT-WGS activity. Oxide supports investigated were CeO_2, ZnO, TiO_2, SiO_2, Al_2O_3, ZrO_2, MgO and SnO_2, with the selection designed to provide a range of characteristics including surface area, reducibility, and acid/base strength.

4.2 Material and methods

4.2.1 Catalyst preparation

A flame spray pyrolysis (FSP) reactor [15] was used to synthesize binary copper oxide and metal oxide (M_xO_y) nanoparticles. In all cases the Cu loading was maintained at between 3 to 4 wt%. Precursor solutions of single metal oxides (M_xO_y) with a total molar concentration of 0.5 M were prepared by mixing respectively; titanium isopropoxide (TTIP, Aldrich, purity > 97%), cerium 2-ethylhexanoate (Strem, 49% solution in 2-ethylhexanoic acid), zinc 2-ethylhexanoate (Alfa, purity > 99%), tetraethyl orthosilicate (TEOS, Aldrich, purity >98%), aluminium s-butoxide (Strem, purity > 98%), zirconium(IV) propoxide (Alrich, 70 wt.% solution in 1-propanol), magnesium methoxide (Aldrich, 6-10 wt.% in methanol), tin(II) 2-ethylhexanoate (Aldrich), with a predetermined amount of copper 2-ethylhexanoate (Aldrich, purity > 99.9%) in xylene (Riedel de Haen, 96%). During FSP synthesis, the liquid precursor was fed (rate: 5 ml min^{-1}) to the flame by a syringe pump (Inotech R232) and dispersed with O_2 (5 L min^{-1}, BOC Gases, >99.95%) forming fine spray droplets. The pressure drop at the nozzle tip was maintained at 1.5 bar (1 bar = 10^5 Pa) by adjusting the orifice gap opening. The spray flame was surrounded and ignited by a premixed CH_4:O_2 ratio (1.5 L min^{-1}:3.2 L min^{-1}, respectively) supporting flame. A sintered metal plate ring provided an additional 5 L min^{-1} of sheath O_2. The product particles were collected on a glass fiber filter (Whatmann GF/D) with the aid of a vacuum pump (Alcatel).

4.2.2 Catalyst characterisation

X-ray diffraction (XRD) spectra were collected on a Philips X'Pert MPD instrument using Cu Kα (λ = 1.542Å) with scan range from 20° to 90° at a scan rate of 0.22° min^{-1} and step size of 0.026°. Surface analysis of the catalysts was performed by X-ray Photoelectron Spectroscopy (XPS) on ESCALab220i-XL (VG Scientific) using a monochromatised Al *K*α radiation at a pass energy of 20 eV and at $P < 2 \times 10^{-9}$ mbar. The energy scale was calibrated and corrected for charging by using the C1s (285.0 eV) line as the binding energy reference. Inductively coupled plasma optical emission spectrometry (ICP-OES) was used to determine the metal content in each synthesized sample. The measurements were performed on a Perkin-Elmer OPTIMA DV3000 apparatus, and the sample was dissolved in nitric acid (3 M) before measurement. Copper metal surface area (CSA) was determined by the N_2O decomposition method at 90 °C using the same experimental methodology reported by Jensen et al. [16], assuming a reaction stoichiometry of two Cu atoms per N_2 atom and a Cu surface density of 1.46 x 10^{19} atom m^{-2} [17]. Prior to the measurement, 50 mg of sample was reduced at 230 °C for 30 min and flushed with He (50 mL min^{-1}) for a further 30 min with the exception of Cu/MgO catalyst, where a 300 °C reduction was used. The specific surface areas (SSA) of the prepared catalysts were analysed by nitrogen adsorption at 77 K, on the Micromeritics Tristar 3000, using the BET model. Raman spectra were collected using a Renishaw inVia microscope at an excitation wavelength of 514 nm. Sampling time was 30 s at an incident energy of 5.0 mW. Spectra were normalised to the maximum intensity of each individual run.

4.2.3 Temperature-programmed reduction and desorption experiments

Temperature-programmed reduction (TPR) and desorption (TPD) experiments were designed to investigate interaction between the catalyst and CO, H_2O, H_2 and CO_2. TPR and TPD were performed on a Micromeritics Autochem 2920 II instrument interfaced with a thermal conductivity detector (TCD). An isopropanol cooling trap was placed between the sample and the TCD to retain water formed during the reduction process. Downstream to the TCD, gases were analysed with an online mass spectrometer (Balzers Thermostar Quadrupole). For TPR experiments, each sample (50 mg) was pre-treated at 120°C under He (50 ml min^{-1}) for 1 h then cooled to ambient temperature. TPR was then performed under 5%H_2/He (50 ml min^{-1}) at a ramp rate of 5 °C min^{-1} to 400 °C.

Before each H_2O-TPD experiment the catalyst (50 mg) was reduced with 10%H_2/He (50 ml min^{-1}) at 230 °C for 1 h. The catalyst was then flushed for 1 h in He (50 ml min^{-1}) for the remainder of the TPD experiment. Deionised water (1.0 μL) was injected into the sample cell using a micro-syringe. Pulses were repeated five times with a one minute interval between each injection and the catalyst bed was then flushed with He for a further 30 min. Finally, the catalyst bed was ramped to 600 °C at a rate of 10 °C min^{-1}. The outlet gas was monitored by mass spectrometry (Balzers Thermostar) when H_2O was pulsed into the sample cell housing the reduced sample. No hydrogen was generated during this period.

During CO-TPD, the catalyst was reduced with 5%CO/He (50 ml min^{-1}) at 230 °C for 1 h followed by flushing under He (50 ml min^{-1}) for 1 h to remove physisorbed CO before

returning to ambient temperature. The CO-TPD proceeded by ramping to 600 °C at a rate of 10 °C min^{-1}. In all TPD experiments, oxidative pre-treatment of catalysts to remove residue carbonaceous species derived during FSP synthesis was not employed. The temperature requirement to oxidize these species was too high (400-450 °C) [18] which would likely have invoked catalyst sintering and influenced the results. Hydrogen TPD was carried out in similar fashion except a 5%H_2/He gas feed was used instead.

To examine the amount and strength of basic sites on the surface of the catalysts, CO_2 temperature-programmed desorption (CO_2-TPD) was performed. The catalyst (50 mg) was oxidised in a flow of 50 mL min^{-1} (5 vol.% O_2/He) at a heating rate of 10°C min^{-1} from ambient temperature to 450 °C to remove any surface carbonaceous species, followed by cooling to ambient temperature. Afterwards, the catalyst was reduced in 5%H_2/He at 230 °C. The catalyst bed was cooled and flushed with 10%CO_2/He (50 mL min^{-1}) to room temperature and then flushed for a further 30 min in He (50 mL min^{-1}) before it was ramped to 700 °C at a heating rate of 10°C min^{-1}.

4.2.4 Catalyst activity

Activity testing was performed using a 6 mm I.D. stainless steel packed bed reactor with the as-prepared catalyst sample (100 mg) diluted with α-Al_2O_3 (70 μm, 500 mg). Prior to each activity test, catalysts were reduced under a total flow of 100 ml min^{-1} (10% H_2/N_2) for 1 h at 230 °C (ramp rate of 5 °C min^{-1}), except for Cu/MgO catalyst where the reduction temperature was 300 °C. The Cu/MgO TPR profile indicated that a higher temperature was required to reduce the CuO component. After reduction, the sample was flushed with N_2 for 30 min before being returned to ambient temperature. The H_2

concentration and temperature ramping rate were selected to avoid thermal sintering of the catalyst due to the exothermic nature of the CuO reduction to Cu metal (Eq. 4.2) [19].

$CuO + H_2 \rightarrow Cu^0 + H_2O$ $\Delta H = -80.8$ kJ mol^{-1} (Eq. 4.2)

The reactant gas stream typically comprised 7% CO, 8.5% CO_2, 23% H_2O, 37.5% H_2 and 25% N_2 (Coregas) at a flow rate of 100 ml min^{-1} and was discharged at atmospheric pressure. Deionised water was added via a vaporizer fed by a high precision syringe pump (ISCO Inst., model 260D). Operating temperatures ranged from 150-300 °C with 50 °C increments ramped at 10 °C min^{-1}. The product stream, after passage through an ice trap to remove water, was analysed using two gas chromatographs (Shimadzu GC8A) fitted with thermal conductivity detectors. One chromatograph was operated with helium as the carrier gas through a 1.8 m CTR I column (Alltech Associates, Inc) for CO_2, CO, N_2, O_2 and CH_4 analysis. The second chromatograph employed argon as the carrier gas through a 2 m molecular sieve 13X column (Alltech Associates, Inc) for H_2 analysis. The CO conversion was far from thermodynamic equilibrium [20] due to design of the experimental setup which induced low residence times to avoid mass transfer limitations on the results.

4.3 Results and discussion

4.3.1 Structural characteristics

The XRD patterns of the Cu-supported catalysts are presented in Fig. 4.1. Due to the low copper loadings, no detectable diffraction of copper oxide crystallites could be distinguished. Instead the Cu-based catalysts showed XRD spectra of their respective

oxide supports. The XRD patterns of pure FSP-prepared CuO and TiO_2 are also provided for comparison as the XRD spectra for TiO_2 and Cu/TiO_2 differed. This difference derived from the change in rutile weight fraction of TiO_2 support with and without Cu. The presence of Cu increased the intensity of the main rutile reflection (Fig. 4.1: $2\theta = 27.8°$), which was consistent with the findings from Teleki et al. [21] who showed the rutile weight fraction in TiO_2 increased with Cu content in their FSP-prepared Cu/TiO_2 particles. In the case of the SiO_2 support, the wide hump in the range of 2θ from 15° to 30° is typical for amorphous SiO_2 [22].

Specific surface area (SSA) and copper metal loadings of all the Cu-based catalysts are shown in Table 4.1. The concentration of Cu ranged between 3.0 to 4.1 wt % from ICP-OES analysis. The 3.03 wt%Cu/ZnO showed the lowest SSA (53 $m^2\ g^{-1}$) while 3.54 wt%Cu/SiO_2 displayed the highest SSA (402 $m^2\ g^{-1}$). The mole ratio of Cu to oxide cation (Me^{X+}) in the bulk of the catalyst was calculated based on ICP analysis.

XPS spectra of CuO regions for the samples showed Cu $2p_{3/2}$ peaks ranging from 934.07 eV to 935.7 eV (Table 4.1), pure FSP-prepared CuO is also included for comparison. The binding energy of supported Cu $2p_{3/2}$ differed significantly among the oxide supports suggesting an interaction between each support and the Cu^{2+} species (Fig. 4.2). All Cu $2p_{3/2}$ peaks from different oxide supports demonstrated the characteristics of CuO with a satellite peak at 944-945 eV, in accordance with the literature [23, 24]. This connotes the Cu species existed as Cu^{2+} after FSP synthesis. The lack of a peak at 932 eV indicated negligible Cu^0 or Cu^+ was present on the catalyst surface [25]. The surface elemental ratio of Cu relative to the Me^{X+} of the support was calculated from the intensity ratios normalized by an atomic sensitivity factor [26]. These ratios are listed in

Table 1. The distribution of Cu diverges from uniformity in a number of cases, as illustrated by the difference in relative surface elemental ratio compared to the bulk ICP Cu/Me^{x+} ratio. When the XPS elemental ratio is lower than the ICP ratio, namely for Cu supported on ZnO, Al_2O_3 and SiO_2, most of the Cu^{2+} is likely to be incorporated into the support's lattice, forming a solid solution during FSP synthesis. The possibility of synthesizing material as a solid solution has been reported before [27, 28]. Conversely, when the surface elemental ratio is higher than the bulk ratio, such as for Cu supported on CeO_2, TiO_2, ZrO_2, MgO and SnO_2, the Cu component is likely to reside predominantly on the surface of the support, with little or no solid solution formation [21, 29].

Raman analysis of the catalyst surface confirmed whether a solid solution was formed between CuO and the oxide support during FSP synthesis (Fig. 4.3). No support modification was observed when CuO was supported on CeO_2, TiO_2, ZrO_2, MgO and SnO_2 as no extra peaks were detected to indicate a solid solution was present, confirming the XPS analysis (Table 4.1). Evidence of a solid solution for the ZnO, SiO_2, and Al_2O_3 was confirmed by the additional Raman peaks (indicated by '■' in Fig. 4.3) which were not present in pure CuO or their respective pure oxides. In the case of Cu/ZnO, an additional peak appeared at 575 cm^{-1}. Two further peaks at 1310 cm^{-1} and 1580 cm^{-1} were evident for Cu/SiO_2. One distinct peak was observed at 2925 cm^{-1} for Cu/Al_2O_3.

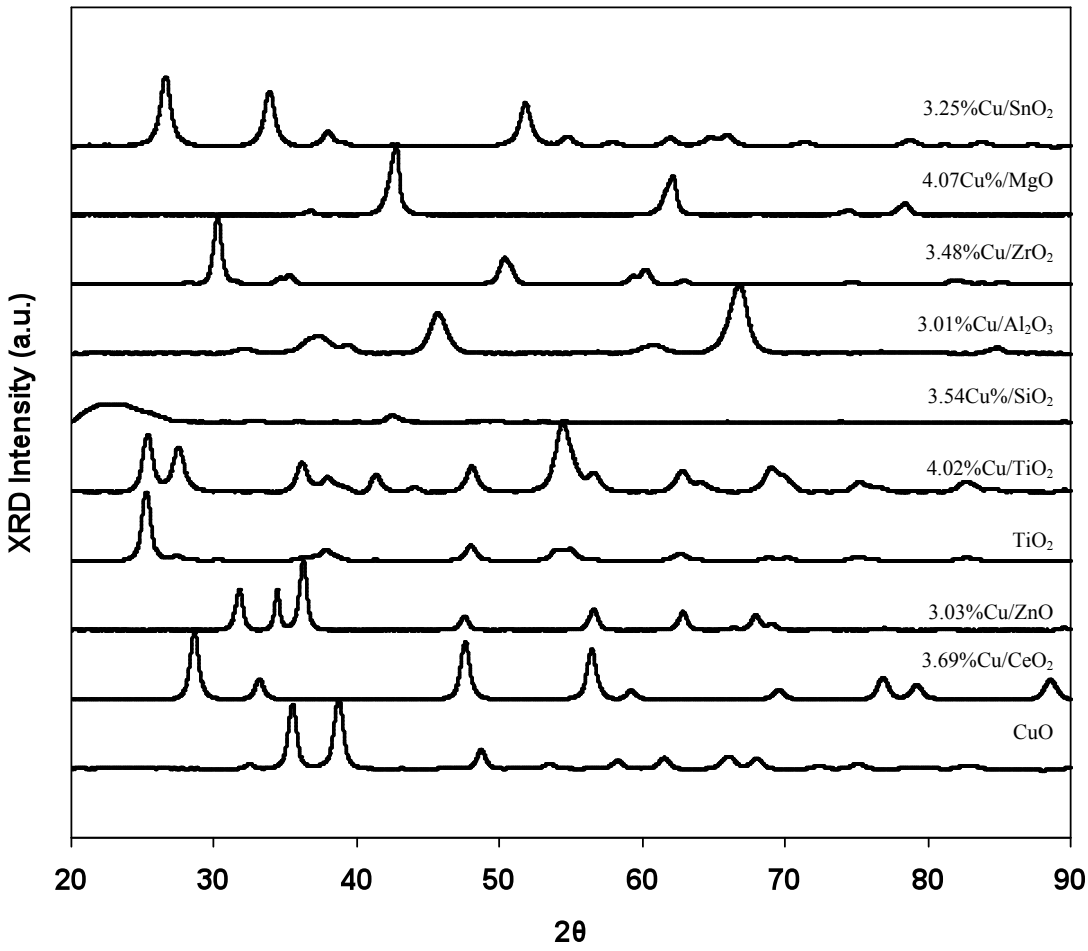

Fig. 4.1: Powder X-ray diffraction patterns for CuO (3 - 4 wt% Cu loading) on various metal oxide supports as catalysts for LT-WGS reaction.

Table 4.1: Characteristics of Cu-based catalysts for LT-WGS reaction.

Catalyst support	BET surface area ($m^2 g^{-1}$), SSA	ICP-OES analysis		XPS analysis	
		Cu conc. (wt %)	Bulk elemental Cu/Me^{x+} ratio (%)	Binding energies (eV) of Cu $2p_{3/2}$	Surface elemental Cu/Me^{x+} ratio (%)
CeO_2	75	3.69	10.48	934.24	35.29
ZnO	53	3.03	4.03	934.31	3.78
TiO_2	110	4.02	5.32	934.07	29.25
SiO_2	402	3.54	3.50	934.81	2.25
Al_2O_3	129	3.01	2.51	934.78	2.20
ZrO_2	68	3.48	7.05	934.23	12.67
MgO	111	4.07	2.72	935.70	4.53
SnO_2	90	3.25	8.03	934.20	14.65

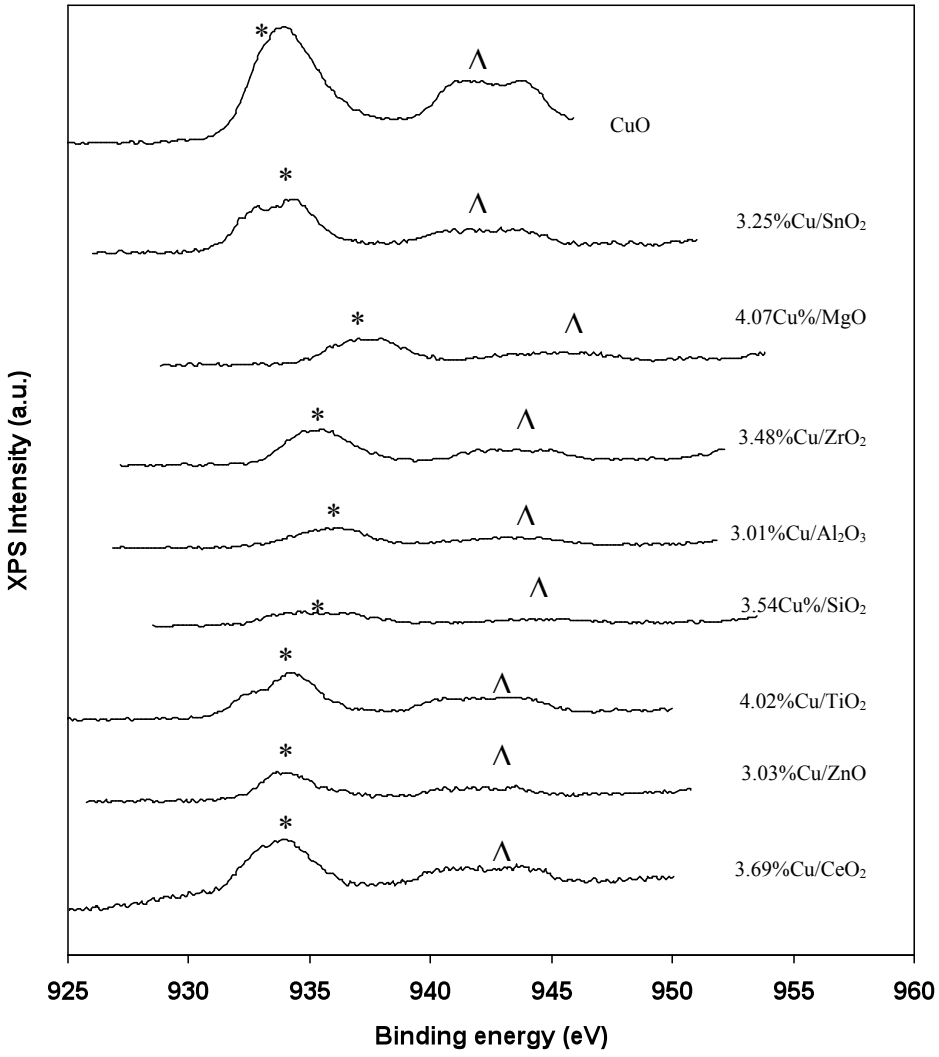

Fig. 4.2: Cu $2p_{3/2}$ XPS photoemission peaks (*) for CuO (3 – 4 wt% Cu loading) on various metal oxide supports as catalysts for LT-WGS reaction. $Cu2p_{3/2}$ satellite peaks (Δ) illustrating presence of Cu^{2+} species.

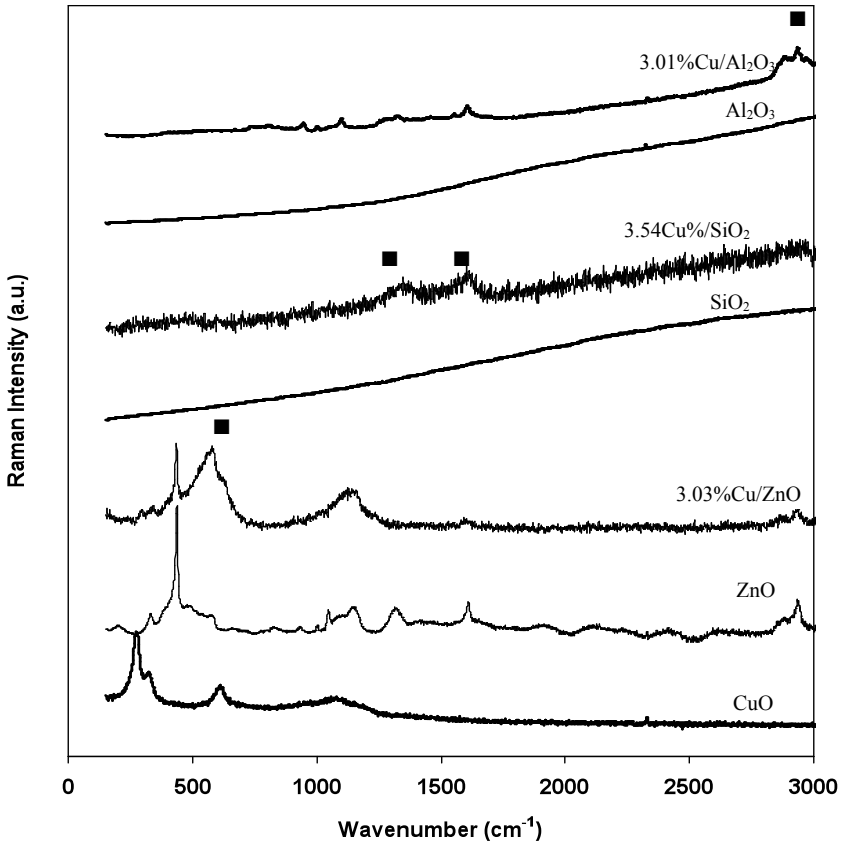

Fig. 4.3: Raman spectra of CuO (3 – 4 wt% Cu loading) on selected metal oxide supports and their corresponding pure oxides. '■' indicates additional peak that evolved from solid solution formation.

4.3.2 TPR studies of Cu catalysts supported on various oxides

The H_2-TPR behaviour of supported Cu-based catalysts from this study is displayed in Fig. 4.4. The CuO reduction peak temperature varied with each support, suggesting specific interactions between the Cu^{2+} species with each particular oxide. This observation agrees with the variations in binding energies of the Cu $2p_{3/2}$ peak from XPS analysis (Table 4.1). Comparing Table 4.1 with Fig. 4.4, it is generally apparent a low Cu $2p_{3/2}$ binding energy correlates to a lower reduction temperature. In this study, Cu $2p_{3/2}$ on TiO_2 showed a binding energy of 934.07 eV corresponding to a reduction

peak around 150°C. The highest Cu $2p_{3/2}$ binding energy (935.70 eV) occurred for MgO where the temperature of the reduction peak was 290°C. The differences in the intensity of the reduction peaks were attributed to the amount of Cu^{2+} species present on the surface, which correlated with the XPS elemental ratios (Table 4.1). Reduction peak intensity was particularly strong for TiO_2, CeO_2, ZrO_2 and SnO_2 as Cu was likely to be situated on the surface of these oxides as confirmed by the XPS results. This was also reinforced by Raman spectra (Fig. 4.3) due to the inability of CuO to form a solid solution with these oxide matrixes. In the case of Cu/ZrO_2, two overlapping peaks are clearly seen, with maxima at approximately 180°C and 200°C. A similar pattern was reported by Liu et al. [30] and Aguila et al. [31] for CuO reduction on tetragonal zirconia. According to these reports, the peaks corresponded to the reduction of highly dispersed Cu^{2+} species, which were first reduced to Cu^{1+} (α) and then to Cu^0 (β), giving rise to the dual TPR peaks. A similar phenomenon has been reported in the case of Cu/CeO_2 [32]. The twin reduction peaks were also present for Cu/TiO_2 and Cu/SnO_2 in this work, suggesting an analogous effect is present.

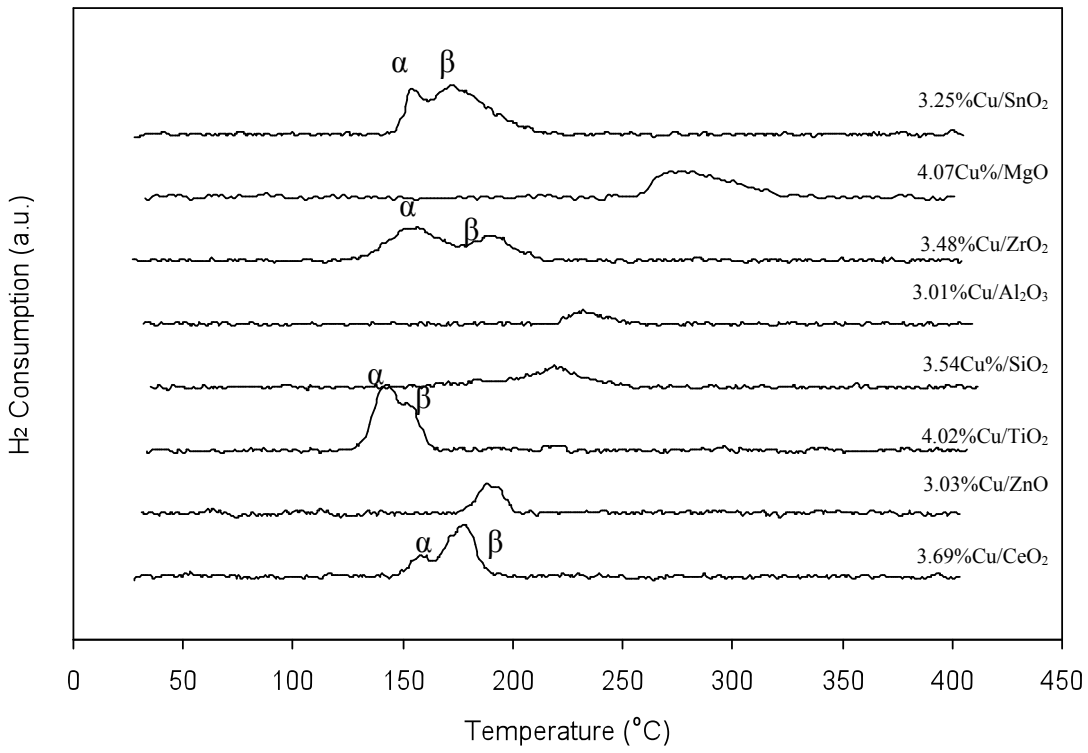

Fig. 4.4: H_2-TPR profiles of Cu-based catalysts on various metal oxide supports. Reduction from Cu^{2+} to Cu^{1+} is indicated by 'α' and Cu^{1+} to Cu^0 by 'β'. In all cases, CuO in the catalysts was reduced to metallic Cu.

4.3.3 LT-WGS activity of CuO catalysts supported on various oxides

The catalysts were assessed for water-gas shift activity using a gas mixture simulating the typical composition of a reformate stream. The comparison of CO conversion achieved in the LT-WGS reaction over Cu catalyst supported on various metal oxides is shown in Fig. 4.5. Significant differences in LT-WGS activity were observed for Cu catalysts depending on the oxide support. Copper catalysts supported on ZnO and MgO were substantially more active than the other oxide supports in this study indicating a cooperative effect on activity by Cu and the support. Activity of the remaining oxide supports was poor and could not be effectively ranked as conversion was within experimental error of the system (±0.5 vol. % CO conversion).

It is generally considered that the LT-WGS reaction occurs solely on metallic Cu sites on the catalyst [2, 6, 33]. However, the results from present study suggested otherwise, since despite the presence of metallic Cu on the surface of CeO_2, TiO_2, SiO_2, Al_2O_3, ZrO_2 and SnO_2 (Table 4.2), none exhibited any LT-WGS activity. The low activity of these samples meant their apparent activation energies and turnover frequencies (TOF) could not be obtained. The uptake of N_2O to measure Cu surface area was not suitable for CeO_2 and ZrO_2 as both oxides were slightly reduced during H_2 pre-treatment. The reduced states of these oxides make them prone to reacting with N_2O to form N_2, resulting in unrealistically high values as also found by Koryabkina et al. [2] for Cu/CeO_2. In this study, no clear relationship between metallic surface areas to WGS activity was apparent as the TOF values for Cu supported on ZnO and MgO were not constant. . If metallic Cu sites were responsible for LT-WGS activity then the TOF values for these materials should be equal. This finding suggested that (Cu) species

other than metallic Cu could be responsible for LT-WGS activity. The most active LT-WGS catalyst was Cu/ZnO followed by Cu/MgO coinciding with apparent activation energies of 58.9 and 73.8 kJ mol^{-1}, respectively (Table 4.2*)*.

Similarly, no correlation was observed between LT-WGS activity and SSA or LT-WGS activity at H_2-TPR peak temperature. These findings indicate LT-WGS performance of the Cu-loaded metal oxides was predominantly governed by an alternate property of the catalyst.

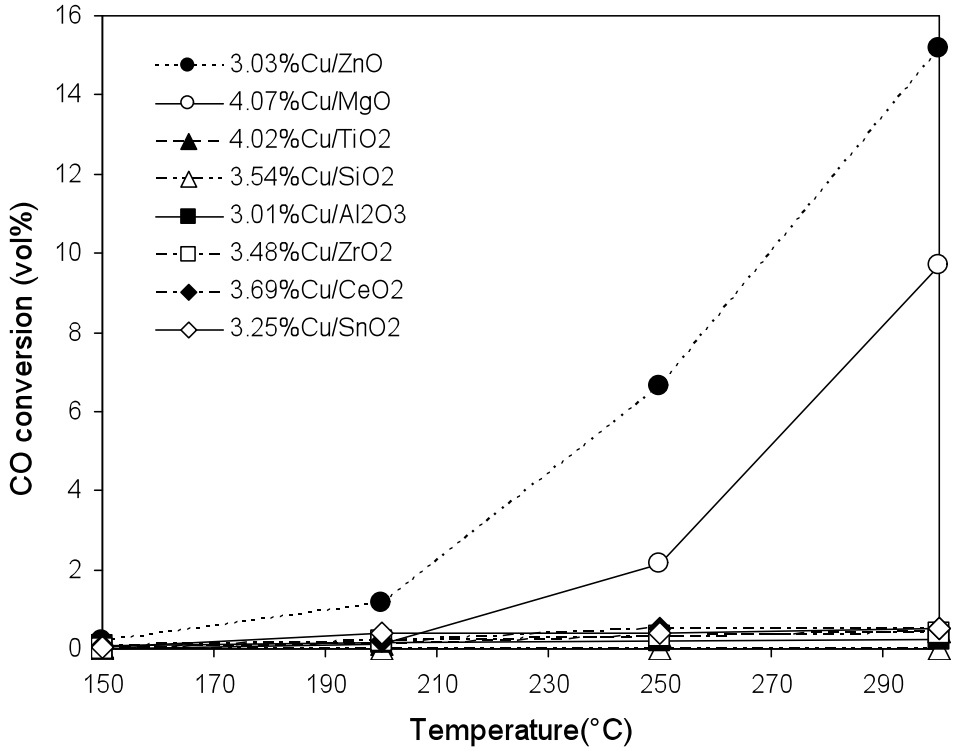

Fig. 4.5: Activity of Cu catalysts on various metal oxide supports for LT-WGS reaction. Reaction conditions: operating temperature 150-300°C, total flow = 100 mL min^{-1} (7% CO, 8.5% CO_2, 23% H_2O, 37.5% H_2 and 25% N_2); catalyst loading = 0.10 g catalyst; pressure = 1 atm.

Table 4.2: Apparent activation energy and turnover frequency for the forward LT-WGS reaction on Cu-based catalysts.

Catalyst s	Cu metal dispersion (%)	Cu surface area (m^2 g^{-1})[a], CSA	Ea (kJ mol^{-1})	TOF (s^{-1})[b]
CeO_2	n.a.	n.a.	n.a.	n.a.
ZnO	45.7	8.92	58.9	0.011
TiO_2	28.8	7.44	n.a.	n.m.
SiO_2	31.8	7.21	n.a.	n.m.
Al_2O_3	53.0	8.65	n.a.	n.m.
ZrO_2	n.a.	n.a.	n.a.	n.m.
MgO	48.1	12.58	73.8	0.0033
SnO_2	35.8	7.48	n.a.	n.m.

[a] Determined by N_2O decomposition and the calculation of the copper surface area, it is assumed a reduced copper surface has a surface density of 1.46×10^{19} copper atoms m^{-2}

[b] TOF for the WGS reaction on Cu-based catalysts at 300°C, 1 atm total pressure, 7% CO, 8.5% CO_2, 23% H_2O, 37.5% H_2 and 25% N_2. Calculation based on mole of CO converted per mole of metallic Cu.

4.3.4 TPD studies of Cu catalysts supported on various oxides

H_2O, CO, H_2 and CO_2 TPD studies were performed to probe the interaction of these molecules with the catalyst surface. The objective of this comparative study was to determine the desorption behaviour of the molecules inherent in each sample. The ability of each Cu-oxide catalyst to adsorb water and their subsequent H_2O- TPD profiles are shown in Fig. 4.6. The results indicated all samples were able to adsorb water with Cu/MgO adsorbing the greatest amount followed by Cu/ZnO. The first H_2O desorption peak appeared at 300°C for Cu/MgO, while the second occured at 520°C. In the case of Cu/ZnO, a strong peak at 420°C was evident. Qualitatively, it was possible to rank the Cu-oxides in terms of their ability to chemisorb H_2O by examining the area

under their corresponding H_2O-TPD curve. The order from highest to lowest H_2O adsorbed was as follows: $MgO > ZnO > TiO_2 > Al_2O_3 \approx SnO_2 \approx SiO_2 > CeO_2 \approx ZrO_2$.

The CO-TPD profiles on the reduced Cu-loaded catalysts are shown in Fig. 4.7. Weakly chemisorbed CO was evident for all samples as indicated by the small CO signals at around 60 to 80°C. The 3.69%Cu/CeO_2 catalyst adsorbed the highest amount of CO, evident from its large CO peak at 410°C. In terms of CO desorption strength, the order from the strongest to the weakest in terms of oxide support was as follows: $Al_2O_3 > CeO_2 > ZnO \approx ZrO_2 > MgO$. No CO desorption peaks were observed for TiO_2, SiO_2 and SnO_2 beyond 100°C, indicating these oxides had no interaction with the CO molecule. CO-TPD experiments were performed on reduced pure CuO and pure oxide supports, with no CO desorption peaks observed for any material. H_2-TPD indicated that H_2 did not adsorb on the surface of the samples, with no H_2 desorption peak observed over the range 25°C to 500 °C.

The surface alkali properties of the catalysts were elucidated by CO_2 TPD as shown in Fig. 4.8. Basic site concentration is reflected in the intensity of the CO_2-TPD peak, while the strength of basic site is indicated by the temperature where the CO_2 desorption peak occurred. With the exception of Cu/SiO_2, all supports displayed some CO_2 chemisorption at around 90-100°C. As acidic CO_2 desorbed at a higher temperature from stronger basic sites [34], the base strength of catalysts was in the order of: CeO_2, ZnO, ZrO_2, MgO, TiO_2, SnO_2, Al_2O_3 and SiO_2. Results from this study suggest Cu/CeO_2 was the most alkaline sample through the presence of a small CO_2 desorption peak at 600°C. The next most alkaline material was Cu/ZnO which possessed a CO_2 desorption peak at 450°C. Cu/MgO featured the greatest number of alkaline sites as

illustrated by its two large CO_2 desorption peaks at 150°C and 250°C. The CO_2-TPD results implied no direct of a relationship between the alkali properties of the catalyst and its LT-WGS activity.

The characterisation and TPD studies indicated the intrinsic properties of Cu/MgO and Cu/ZnO to adsorb both water (Fig. 4.6) and CO (Fig. 4.5) coincided with high LT-WGS activity (Fig. 4.4). Other factors such as Cu surface area, Cu inclusion in the metal oxide matrix, Cu surface area or Cu reducibility and the different oxide support structure did not correlate to catalyst activity. This finding suggested that the ability of the material to adsorb both H_2O and CO molecules could be the key to LT-WGS activity. Previous work has shown the possibility of a bifunctional synergistic effect whereby the copper component adsorbs the CO molecule [35, 36] and the oxide support is responsible for activating the H_2O molecule [37, 38]. The TPD results indicated that the Cu and its oxide support play an important role in interacting with the CO and H_2O molecules, respectively. The lack of H_2 production during H_2O-TPD inferred that the associative LT-WGS mechanism [3, 39] was favoured as opposed to the regenerative route [2, 5]. The primary difference between the two mechanisms concerns the formation of formate-type (HCOO*) and/or carboxyl-type (OCOH*) intermediates for the associative mechanism. These species subsequently decompose into the reaction products (Eq. 4.3) during the associative route.

$$CO + H_2O \leftrightarrow (HCOO^* \text{ or } OCOH^*) + H^* \leftrightarrow CO_2 + H_2 \qquad \text{(Eq. 4.3)}$$

The regenerative route consists of surface oxidation of a oxygen vacancy site (*) by water vapour (Eq. 4.4) followed with surface reduction by carbon monoxide (Eq. 4.5) [2, 5].

$$H_2O + * \rightarrow H_2 + O^* \qquad \text{(Eq. 4.4)}$$

$CO + O^* \rightarrow CO_2 + *$ (Eq. 4.5)

Fig. 4.9 provides the schematic of the associative LT-WGS mechanism on a Cu-loaded metal oxide catalyst surface.

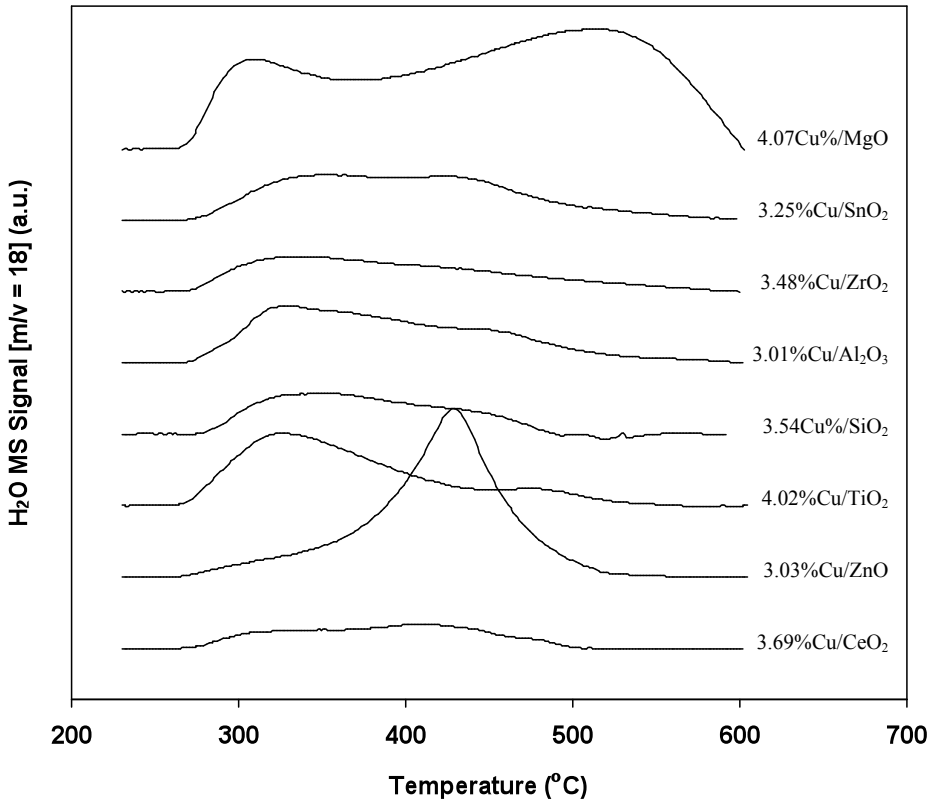

Fig. 4.6: H_2O-TPD profiles of Cu-based catalysts on various metal oxide supports.

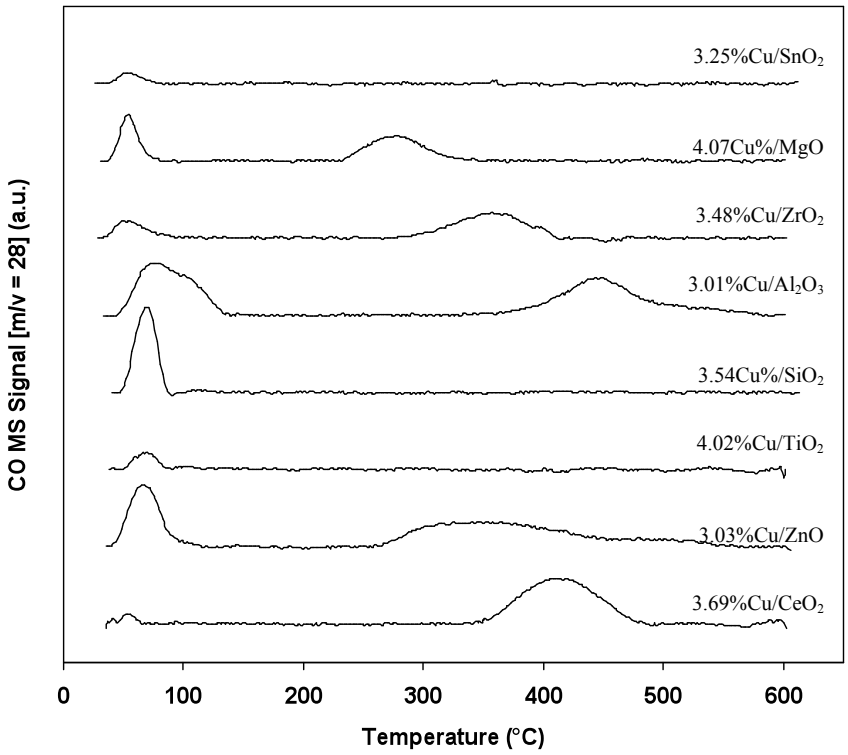

Fig. 4.7: CO-TPD profiles of Cu-based catalysts on various metal oxide supports.

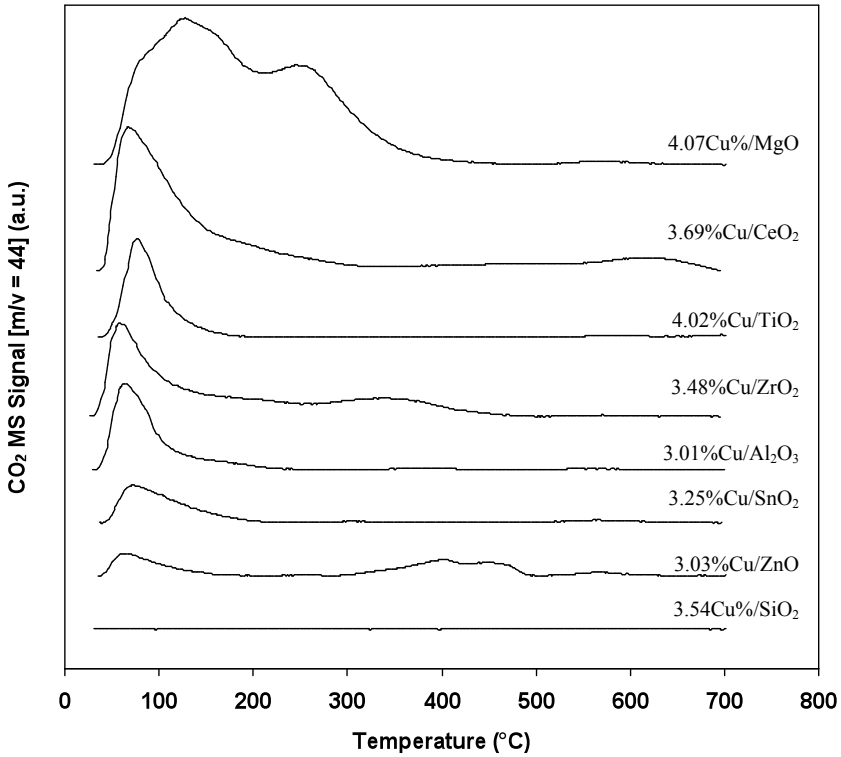

Fig. 4.8: CO_2-TPD profiles of of Cu-based catalysts on various metal oxide supports.

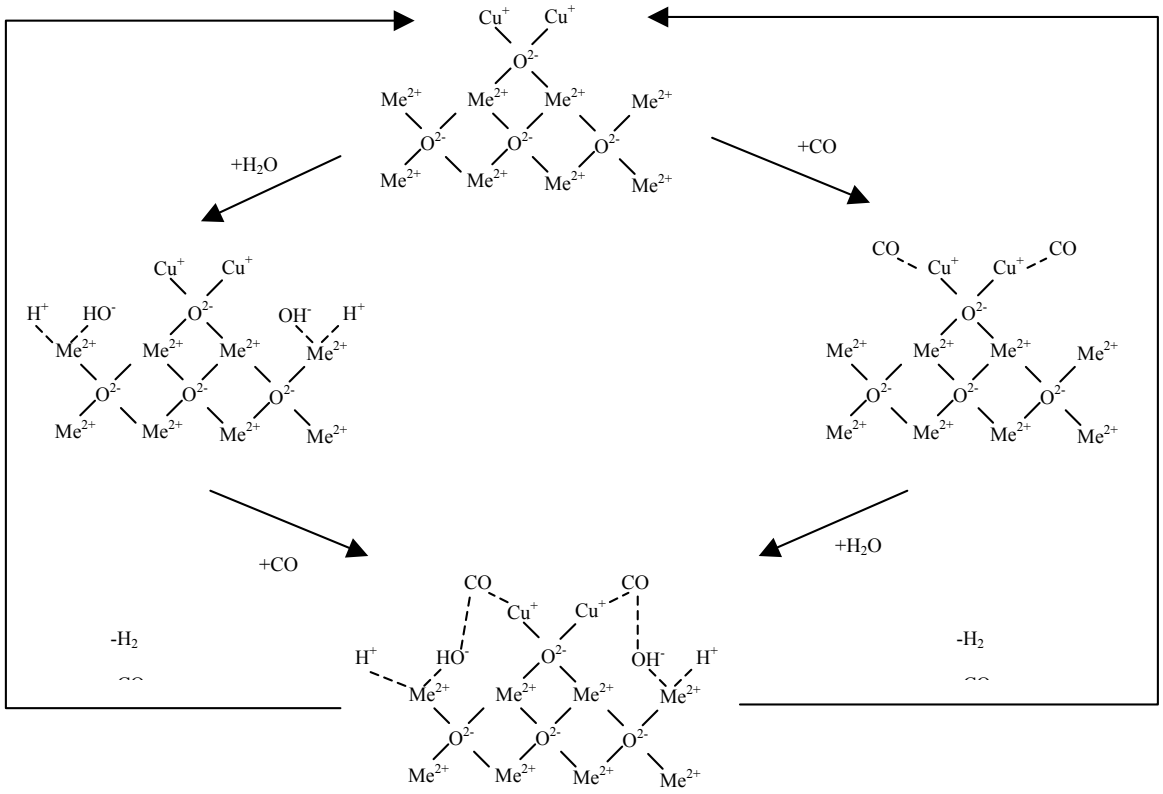

Fig. 4.9: Schematic of the associative LT-WGS mechanism on Cu/metal oxide catalyst showing the role of copper species and metal oxide support (Me^{2+} = metal cation of the oxide support e.g. Zn^{2+}, Mg^{2+}, etc).

4.4 Conclusions

The choice of oxide support has been demonstrated to affect LT-WGS activity of Cu-based catalysts under realistic feed conditions. Cu/ZnO and Cu/MgO ascertained the highest LT-WGS activity compared to the other catalysts in this study. No evidence was found relating metal oxide support acid/base properties to LT-WGS performance. Similarly, metallic copper sites were not found to be responsible for LT-WGS activity. XPS characterisation revealed evidence of electronic interactions between the Cu and metal oxide support and confirmed that the Cu^{2+} to O^{2-} binding energy dictated the

reduction temperature of CuO. H_2O-TPD and CO-TPD experiments indicated the propensity of Cu/ZnO and Cu/MgO to adsorb comparatively higher levels of both H_2O and CO, suggesting the significance of this property for LT-WGS activity. The lack of H_2 generation during H_2O-TPD furthermore implied that associative LT-WGS mechanism was favoured by these Cu-based catalysts.

4.5 References

1. O. Thinon, F. Diehl, P. Avenier, and Y. Schuurman, 'Screening of bifunctional water-gas shift catalysts', *Catalysis Today* 137 (**2008**) 29-35.
2. N.A. Koryabkina, A.A. Phatak, W.F. Ruettinger, R.J. Farrauto, and F.H. Ribeiro, 'Determination of kinetic parameters for the water-gas shift reaction on copper catalysts under realistic conditions for fuel cell applications', *Journal of Catalysis* 217 (**2003**) 233-239.
3. D.C. Grenoble, M.M. Estadt, and D.F. Ollis, 'The Chemistry and Catalysis of the Water Gas Shift Reaction', *Journal of Catalysis* 67 (**1981**) 90-102.
4. P. Panagiotopoulou and D.I. Kondarides, 'Effect of the nature of the support on the catalytic performance of noble metal catalysts for the water–gas shift reaction', *Catalysis Today* 112 (**2006**) 49–52.
5. T. Shishido, M. Yamamoto, D. Li, Y. Tian, H. Morioka, M. Honda, T. Sano, and K. Takehira, 'Water-gas shift reaction over Cu/ZnO and Cu/ZnO/Al_2O_3 catalysts prepared by homogeneous precipitation', *Applied Catalysis A: General* 303 (**2006**) 62-71.

6. M.J.L. Gines, N. Amadeo, M. Laborde, and C.R. Apesteguia, 'Activity and structure-sensitivity of the water-gas shift reaction over Cu-Zn-Al mixed oxide catalysts', *Applied Catalysis A: General* 131 (**1995**) 283-296.

7. G.C. Chinchen and M.S. Spencer, 'Sensitive and insensitive reactions on copper catalysts: the water-gas shift reaction and methanol synthesis from carbon dioxide', *Catalysis Today* 10 (**1991**) 293-301.

8. Y. Denkwitz, A. Karpenko, V. Plzak, R. Leppelt, B. Schumacher, and R.J. Behm, 'Influence of CO_2 and H_2 on the low-temperature water-gas shift reaction on Au/CeO2 catalysts in idealized and realistic reformate', *Journal of Catalysis* 246 (**2007**) 74-90.

9. J.B. Ko, C.M. Bae, Y.S. Jung, and D.H. Kim, 'Cu-ZrO_2 catalysts for water-gas-shift reaction at low temperatures', *Catalysis Letters* 105 (**2005**) 157-161.

10. F. Boccuzzi, A. Chiorino, M. Manzoli, D. Andreeva, T. Tabakova, L. Ilieva, and V. Iadakiev, 'Gold, Silver and copper catalysts supported on TiO2 for pure hydrogen production', *Catalysis Today* 75 (**2002**) 169-175.

11. H. Kusˇar, S. Hocˇevar, and J. Levec, 'Kinetics of the water–gas shift reaction over nanostructured copper–ceria catalysts', *Applied Catalysis B: Environmental* 63 (**2006**) 194–200.

12. A.S. Quiney and Y. Schuurman, 'Kinetic modelling of COconversion over a Cu/ceria catalyst', *Chemical Engineering Science* 62 (**2007**) 5026 – 5032.

13. H. Yahiro, K. Murawaki, K. Saiki, T. Yamamoto, and H. Yamaura, 'Study on the supported Cu-based catalysts for the low-temperature water–gas shift reaction', *Catalysis Today* 126 (**2007**) 436-440.

14. T. Utaka, K. Sekizawa, and K. Eguchi, 'CO removal by oxygen-assisted water gas shift reaction over supported Cu catalysts', *Applied Catalysis A: General* 194-195 (**2000**) 21–26.

15. L. Mädler, H.K. Kammler, R. Mueller, and S.E. Pratsinis, 'Controlled synthesis of nanostructured particles by flame spray pyrolysis', *Journal of Aerosol Science* 33 (**2002**) 369-389.

16. J.R. Jensen, T. Johannessen, and H. Livbjerg, 'An improved N_2O-method for measuring Cu-dispersion', *Applied Catalysis A: General* 266 (**2004**) 117-122.

17. J.W. Evans, M.S. Wainwright, A.J. Bridgewater, and D.J. Young, 'On the determination of copper surface area by reaction with nitrous oxide', *Applied Catalysis* 7 (**1983**) 75-83.

18. X. Liu, W. Ruettinger, X. Xu, and R. Farrauto, 'Deactivation of Pt/CeO_2 water-gas shift catalysts due to shutdown/startup modes for fuel cell applications', *Applied Catalysis B: Environmental* 56 (**2005**) 69–75.

19. C. Rhodes, G.J. Hutchings, and A.M. Ward, 'Water-gas shift reaction: finding the mechanistic boundary', *Catalysis Today* 23(1) (**1995**) 43-58.

20. G.C. Chinchen, P.J. Denny, J.R. Jennings, M.S. Spencer, and K.C. Waugh, 'Synthesis of Methanol Part 1. Catalysts and Kinetics', *Applied Catalysis* 36 (**1988**) 1-65.

21. A. Teleki, N. Bjelobrk, and S.E. Pratsinis, 'Flame-made Nb- and Cu-doped TiO_2 sensors for CO and ethanol', *Sensors and Actuators B: Chemical* 130 (**2008**) 449–457.

22. N. Bogdanchikova, A. Pestryakov, M.H. Farias, J.A. Diaz, M. Avalos, and J. Navarrete, 'Formation of TEM- and XRD-undetectable gold clusters

accompanying big gold particles on TiO_2-SiO_2 supports', *Solid State Sciences* 10 (**2008**) 908-914.

23. F. Garbassi and G. Petrini, 'XPS Study on the Low-Temperature CO Shift Reaction Catalyst', *Journal of Catalysis* 90 (**1984**) 106-112.

24. C.C. Chusuei, M.A. Brookshier, and D.W. Goodman, 'Correlation of Relative X-ray Photoelectron Spectroscopy Shake-up Intensity with CuO Particle Size', *Langmuir* 15 (**1999**) 2806-2808.

25. W.-L. Dai, Q. Sun, J.-F. Deng, D. Wu, and Y.-H. Sun, 'XPS studies of $Cu/ZnO/Al_2O_3$ ultra-fine catalysts derived by novel gel oxalate co-precipitation for methanol synthesis by $CO_2 + H_2$', *Applied Surface Science* 177 (**2001**) 172-179.

26. M. Daturi, C. Binet, J.-C. Lavalley, A. Galtayries, and R. Sporkenb\, 'Suface investigation on $Ce_xZr_{1-x}O_2$ compounds', *Physical Chemistry Chemical Physics* 1 (**1999**) 5717-5724.

27. B. Weidenhof, M. Reiser, K. Stowe, W.F. Maier, M. Kim, J. Azurdia, E. Gulari, E. Seker, A. Barks, and R.M. Laine, 'High-Throughput Screening of Nanoparticle Catalysts Made by Flame Spray Pyrolysis as Hydrocarbon/NO Oxidation Catalysts', *Journal of the American Chemical Society* 131 (**2009**) 9207–9219.

28. D.J. Seo, K.O. Ryu, S.B. Park, K.Y. Kim, and R.-H. Song, 'Synthesis and properties of $Ce_{1-x}Gd_xO_{2-x/2}$ solid solution prepared by flame spray pyrolysis', *Materials Research Bulletin* 41 (**2006**) 359-366.

29. R. Kydd, W.Y. Teoh, K. Wong, Y. Wang, Jason Scott, Q.-H. Zeng, A.-B. Yu, J. Zou, and R. Amal, 'Flame-Synthesized Ceria-Supported Copper Dimers for

Preferential Oxidation of CO', *Advance Functional Materials* 19 (**2009**) 369-377.

30. Z. Liu, M.D. Amiridis, and Y. Chen, 'Characterization of CuO Supported on Tetragonal ZrO_2 Catalysts for N_2O Decomposition to N_2', *Journal of Physical Chemistry B* 109 (**2005**) 1251-1255.

31. G. Águila, S. Guerrero, and P. Araya, 'Influence of the crystalline structure of ZrO_2 on the activity of Cu/ZrO_2 catalysts on the water gas shift reaction', *Catalysis Communications* 9 (**2008**) 2550–2554.

32. P. Djinovic, J. Batista, and A. Pintar, 'Calcination temperature and CuO loading dependence on $CuO\text{-}CeO_2$ catalyst activity for water-gas shift reaction', *Applied Catalysis A: General* 347 (**2008**) 23–33.

33. F. Nishida, I. Atake, D. Li, T. Shishido, Y. Oumi, T. Sano, and K. Takehira, 'Effects of noble metal-doping on Cu/ZnO/Al2O3 catalysts for water–gas shift reaction Catalyst preparation by adopting “memory effect” of hydrotalcite', *Applied Catalysis A: General* 337 (**2008**) 48-57.

34. Y. Fukuda and K. Tanabe, 'Infrared Study of Carbon Dioxide Adsorbed on Magnesium and Calcium Oxides', *Bulletin of the Chemical Society of Japan* 46 (**1973**) 1616-1619.

35. R. Burch, R.J. Chappell, and S.E. Golunski, 'Synergy at a distance in the synthsis of methanol over copper catalysts', *Catalysis Letters* 1 (**1988**) 439-444.

36. Y. Okamoto, K. Fukino, T. Imanaka, and S. Teranishi, 'Synergy between Cu and ZnO for methanol conversionsover Cu-ZnO catalysts', *Chemistry Letters* (**1984**) 71-74.

37. T. Shido and Y. Iwasawa, 'Reactant-Promoted Reaction Mechanism for Water-Gas Shift Reaction on ZnO, as the Genesis of Surface Catalysis', *Journal of Catalysis* 129 (**1991**) 343-355.

38. G. Ghiotti and F. Bocuzzi, 'Chemical and Physical Properties of Copper-Based Catalysts for CO shift Reaction and Methanol Synthesis', *Catalysis Reviews: Science and Engineering* 29(2 & 3) (**1987**) 151-182.

39. J.L.C. Fajin, M.N.D.S. Cordeiro, Francesc Illas, and J.R.B. Gomes, 'Influence of step sites in the molecular mechanism of the water gas shift reaction catalyzed by copper', *Journal of Catalysis* 268 (**2009**) 131-141.

CHAPTER FIVE

The influence of La doping on the activity and stability of Cu/ZnO catalyst for the low temperature water-gas shift reaction

5.1 Introduction

The water-gas shift (WGS) is a reversible, exothermic chemical reaction for conditioning product streams from the steam reforming of hydrocarbons for industrial hydrogen production. It describes the reaction between carbon monoxide and water vapour to produce carbon dioxide and hydrogen (Eq. 5.1).

$$CO + H_2O \leftrightarrow CO_2 + H_2 \qquad \Delta H = -41.1 \text{ kJ mol}^{-1} \qquad \text{(Eq. 5.1)}$$

Commercially, the WGS reaction is performed in two stages to overcome the thermodynamic and kinetic limitations of the reaction. The two steps involve a high-temperature (350-500°C) shift (HT-WGS) reaction typically over Fe_2O_3/Cr_2O_3 catalysts [1, 2], at which the favourable kinetics can be exploited and the volume of the catalyst minimised, followed by a low temperature (200-250°C) shift (LT-WGS) reaction over a Cu/ZnO-based catalyst which takes advantage of the thermodynamic equilibrium at low temperature [1, 3]. Currently, the LT-WGS typically requires a large reactor volume due to its slow reaction kinetics [1]. The LT-WGS has also been observed to occur in small reactors at low temperatures [4] although under these conditions the reverse reaction (i.e. CO generation) was favoured. Hence, it remains desirable to develop catalysts with

higher activity to reduce steam production requirements [5], reduce the LT-WGS catalyst volume and ultimately reduce the costs associated with reactor size. Improving catalyst stability is also a major challenge for the Cu/ZnO system for LT-WGS reactions. It is well documented that Cu/ZnO is susceptible to sintering during reaction [6, 7], resulting in a loss of active sites. Cu/ZnO deactivation has been reported to derive from carbonate build-up on the surface which acts as a reaction-inhibiting spectator specie [8].

Improved LT-WGS catalyst performance may be achieved by doping the Cu/ZnO with additional metal cations. This is the case for commercial $Cu/ZnO/Al_2O_3$ catalyst where alumina is employed to stabilise the ZnO and prolong catalyst life [1, 2, 5, 9]. Alkaline-type cations have also been reported to improve Cu/ZnO LT-WGS activity. Shishido et al. [6] found doping Cu/ZnO with alkaline-earth metals (Mg, Ca, Sr and Ba) increased catalyst activity but did not improve stability. Lanthanum (La) is an alkaline-type metal that has been demonstrated by Schaper et al. [10] to provide structural stability for a methanation catalyst support (γ-Al_2O_3).

Even though Cu/ZnO catalysts are well studied, uncertainties still remain regarding the precise nature of the WGS mechanism. These mechanisms are generally believed to be either associative [11, 12] or regenerative [6, 13, 14]. Salient features of the proposed WGS mechanisms involve the adsorption of CO and H_2O onto the catalyst surface [15]. Some hold the view that during the WGS reaction, a bifunctional synergistic effect exists between the copper and zinc oxide [16, 17] where the copper species activates the CO molecule while the ZnO activates the water molecule [11, 18]. The main difference between the two mechanisms concerns the formation of formate-type ($HCOO^*$) and/or

carboxyl-type ($OCOH^*$) intermediates that subsequently decompose into the reaction products (Eq. 5.2) during the associative route [12, 15, 19].

$$CO + H_2O \leftrightarrow (HCOO^* \text{ or } OCOH^*) + H^* \leftrightarrow CO_2 + H_2 \quad \text{(Eq. 5.2)}$$

The regenerative route consists of surface oxidation of a oxygen vacancy site (*) by water vapour (Eq. 5.3) followed with surface reduction by carbon monoxide (Eq. 5.4) [7, 13].

$$H_2O + * \rightarrow H_2 + O* \quad \text{(Eq. 5.3)}$$

$$CO + O* \rightarrow CO_2 + * \quad \text{(Eq. 5.4)}$$

The objective of this study is to explore the effect of lanthanum (La) as a promoter in the Cu/ZnO catalytic system during WGS reaction. In particular, the influence of La on Cu/ZnO catalyst activity and stability were investigated to gain greater insights on the mechanisms governing catalyst performance of La promoted Cu/ZnO catalyst. The catalysts were bench-marked against a commercial $Cu/ZnO/Al_2O_3$ formulation for the LT-WGS reaction.

5.2 Experimental

5.2.1 Catalyst preparation

A flame spray pyrolysis (FSP) reactor [20] was used to synthesise CuO, ZnO, Cu/ZnO, $Cu/ZnO/La_2O_3$ and $Cu/ZnO/Al_2O_3$ particles. In all cases the Cu loading was maintained at approximately 37 wt% while the Zn and La loadings were varied. The $Cu/ZnO/Al_2O_3$ catalyst (F-COM) was fabricated based on a typical commercial catalyst composition (weight ratio 37:55:8, respectively [21]). Precursor solutions containing predetermined

amounts of metal oxides with a total molar concentration of 0.5 M were prepared by mixing zinc 2-ethylhexanoate (Alfa, purity > 99%), lanthanum (III) 2-ethylhexanoate (10 wt% in hexane solution, Aesar), aluminium s-butoxide (Strem, purity > 98%), and copper 2-ethylhexanoate (Aldrich, purity > 99.9%) in xylene (Riedel de Haen, 96%). During FSP synthesis, the liquid precursor was fed (rate: 5 ml min^{-1}) to the flame by a syringe pump (Inotech R232). The generated particles were collected on a glass fibre filter (Whatmann GF/D) with the aid of a vacuum pump (Alcatel). Detailed descriptions on other operating conditions can be found elsewhere [20]. La_2O_3 (Aldrich, 99.9%) was used as the La reference in this study.

5.2.2 Catalyst characterization

X-ray diffraction (XRD) spectra were collected on a Philips X'Pert MPD instrument using Cu Kα (λ = 1.542Å) with scan range from 20° to 90° at a scan rate of 0.22° min^{-1} and step size of 0.026°. Surface analysis of the catalysts was performed by X-ray Photoelectron Spectroscopy (XPS) on ESCALab220i-XL (VG Scientific) using a monochromatised Al *K*α radiation at a pass energy of 20 eV and at $P < 2 \times 10^{-9}$ mbar. The energy scale was calibrated and corrected for charging by using the C1s (285.0 eV) line as the binding energy reference. Transmission electron microscope (TEM) imaging of the catalysts was performed using a Phillips CM-200 to observe size and morphology. Inductively coupled plasma optical emission spectrometry (ICP-OES) was used to determine the metal content in each synthesised sample. The measurements were performed on a Perkin-Elmer OPTIMA DV3000 apparatus, and the sample was dissolved in nitric acid (3 M) before measurement. Copper metal surface area (CSA) was determined by the N_2O decomposition method at 90°C using the same experimental

methodology reported by Jensen et al. [22], assuming a reaction stoichiometry of two Cu atoms per N_2 atom and a Cu surface density of 1.46 x 10^{19} atom m^{-2} [23]. Prior to the measurement, 30 mg of sample was reduced at 230°C for 30 min and flushed with He (50 ml min^{-1}) for a further 30 min. The specific surface areas (SSA) of the prepared catalysts were analysed by nitrogen adsorption at 77 K, on the Micromeritics Tristar 3000, using the BET model.

5.2.3 Temperature-programmed reduction, desorption and oxidation

Temperature-programmed reduction (TPR), H_2O and CO desorption (TPD) and oxidation (TPO) experiments were performed on a Micromeritics Autochem 2920 instrument interfaced with a thermal conductivity detector (TCD) with the results normalised to the mass of the sample used in the experiments. An isopropanol cooling trap was placed between the sample and the TCD to retain the water formed during the reduction process. Downstream to the TCD, gases were analysed with an online mass spectrometer (Balzers Thermostar Quadrupole). For TPR experiments, each sample (50 mg) was pre-treated at 120°C under He (50 ml min^{-1}) for 1 h then cooled to ambient temperature. TPR was then performed under 5%H_2/He (50 ml min^{-1}) at a ramp rate of 5°C min^{-1} to 400°C with the results recorded by the TCD.

Before each H_2O-TPD experiment the catalyst (50 mg) was reduced with 10%H_2/He (50 ml min^{-1}) at 230°C for 1 h. The catalyst was then flushed for 1 h in He (50 ml min^{-1}) for the remainder of the TPD experiment. Deionised water (1.0 μL) was injected into the sample cell using a micro-syringe. Pulses were repeated five times with a one minute interval between each injection and the catalyst bed was then flushed with He for a

further 30 min. Finally, the catalyst bed was ramped to 600°C at a rate of 10°C min^{-1}. The outlet gas was monitored by mass spectrometry (Balzers Thermostar) when H_2O was pulsed into the sample cell housing the reduced sample. No hydrogen was generated during this period.

During CO-TPD, the catalyst was reduced with 5%CO/He (50 ml min^{-1}) at 230°C for 1 h followed by flushing under He (50 ml min^{-1}) for 1 h to remove physisorbed CO before returning to ambient temperature. The CO-TPD proceeded by ramping to 600°C at a rate of 10°C min^{-1}. In all TPD experiments, oxidative pre-treatment of catalysts to remove residue carbonaceous species derived during FSP synthesis was not employed. The temperature requirement to oxidize these species was too high (400-450°C) [24] which would likely have invoked catalyst sintering and influenced the results. During TPO the catalyst bed was ramped to 500°C at 10°C min^{-1} under 5%O_2/He (50 mL min^{-1}). No catalyst pretreatment was conducted prior to TPO experiments.

5.2.4 Catalyst activity

Activity testing was performed using a 6 mm I.D. stainless steel packed bed reactor with the as-prepared catalyst sample (100 mg) diluted with α-Al_2O_3 (70 μm, 500 mg). Prior to each activity test, catalysts were reduced under a total flow of 100 ml min^{-1} (10% H_2/N_2) for 1 h at 230°C (ramp rate of 5°C min^{-1}) and flushed with N_2 for 30 min before being returned to ambient temperature. The H_2 concentration and temperature ramping rate were selected to avoid thermal sintering of the catalyst due to the exothermic nature of the reduction from CuO to Cu metal reaction (Eq. 5.5) [3].

$CuO + H_2 \rightarrow Cu^0 + H_2O$ $\Delta H = -80.8$ kJ mol^{-1} (Eq. 5.5)

The reactant gas stream typically comprised 7% CO, 8.5% CO_2, 23% H_2O, 37.5% H_2 and 25% N_2 (Coregas) at a flow rate of 100 ml min^{-1} and was discharged at atmospheric pressure. Deionised water was added via a vaporizer fed by a high precision syringe pump (ISCO Inst., model 260D). Operating temperatures ranged from 150-300 with 50°C increments ramped at 10°C min^{-1}. The product stream, after passage through an ice trap to remove water, was analysed using two gas chromatographs (Shimadzu GC8A) fitted with thermal conductivity detectors. One chromatograph was operated with helium as the carrier gas through a 1.8 m CTR I column (Alltech Associates, Inc) for CO_2, CO, N_2, O_2 and CH_4 analysis. The second chromatograph employed argon as the carrier gas through a 2 m molecular sieve 13X column (Alltech Associates, Inc) for H_2 analysis. The CO conversion was far from thermodynamic equilibrium [25] due to design of the experimental setup which induced low residence times to avoid mass transfer limitations on the results.

Catalyst stability was continuously evaluated at an operating temperature of 300°C for 25 h. This temperature is higher than standard LT-WGS conditions (200-250°C) [2, 26] and was selected to accelerate the rate of any deactivation. Catalysts samples were not diluted with α-Al_2O_3 in this series of experiments due to the need for post-reaction characterization. Further details regarding the calculations for CO conversion are provided in **Appendix I**.

5.3 Results

5.3.1 Structural properties of the catalysts

The XRD spectra of nominal 37 wt% Cu loaded ZnO-based nanoparticles synthesised by FSP (Fig. 5.1) showed the hexagonal structure of ZnO [27] was maintained over the range of La doping concentrations. The elevated Cu loading was also detectable by XRD and gave a weak Bragg reflection at $2\theta = 38°$, belonging to the monoclinic CuO (111) phase [28]. There was no detectable XRD reflection from La_2O_3 crystallites and no shift in Bragg positions of ZnO with increasing La loading. Evaluation of the ZnO crystallite size from XRD using the Scherrer formula (Table 5.1) indicated Cu addition reduced the crystal size from 20nm to 17nm. The CuO (111) XRD reflection, indicated by (○) in Fig. 5.1, was too small for accurate crystallite size determination, hence CuO crystallite size could not be determined. Increasing La addition promoted further ZnO crystal size reduction to 13nm at 11wt% La. The decrease in crystallite size is reflected in the TEM images of neat, Cu-loaded and Cu/La loaded ZnO (Figure 5.2(a-d)). The TEM micrographs also indicated a shift in ZnO morphology moving from a rod-like shape for neat ZnO (Fig. 5.2a) to spherical particles upon Cu incorporation (Figure 5.2b). Likewise, the decreasing crystal size influenced the specific surface areas of the neat and composite materials (Table 5.1) with a corresponding increase in this characteristic with increasing La loading. Although not depicted here, all the prepared samples exhibited Type II N_2 adsorption-desorption isotherms, suggesting the particles are nonporous, as frequently observed for flame-made particles [29].

The bulk weight ratio of Cu, Zn and La determined by ICP-OES (Table 5.1) indicated actual cation loadings were close to the nominal values. Cu^0 surface area increased from 7.6 m^2/g for the neat material to 27.4 m^2/g when mixed with Zn however, the presence

of La served to decrease the Cu^0 surface area. This is reflected by a drop in the Cu metal dispersion from 12.4% for Cu/ZnO to between 5.4 - 8.4% depending on La loading (Table 5.1). A similar influence was observed when 8 wt% Al_2O_3 was included in the Cu/ZnO, with Cu dispersion decreasing from 12.4% to 3.9%.

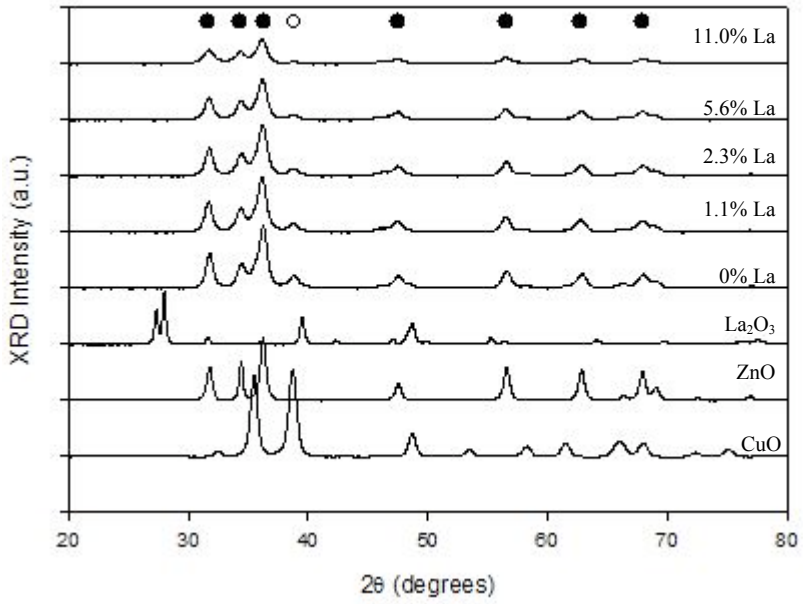

Fig. 5.1: XRD spectra (Cu Kα, λ = 1.542) of FSP-made nominal 37 wt% Cu/ZnO doped with varying La loadings. Pure CuO, ZnO and La_2O_3 are included for comparison. The solid circles (•) represent characteristic peaks of ZnO hexagonal wurzite-phase. The open circle (○) denotes peaks of monoclinic CuO (111) phase.

Table 5.1: Physicochemical properties, apparent activation energy and turnover frequency of neat, La-doped and Al-doped Cu/ZnO catalysts

Catalyst (nominal weight ratio)	BET surface area ($m^2 g^{-1}$), SSA	Bulk composition in weight ratio[a] (mole ratio), %			Crystallite Size (nm)[b]		Cu metal dispersion (%)	Cu surface area ($m^2 g^{-1}$)[c], CSA	Ea (kJ mol^{-1})	TOF (s^{-1})[d]
		Cu	Zn	La	d_{CuO}	d_{ZnO}				
CuO	35.8	100	0	0	25	-	1.4	7.6	0	0
ZnO	42.8	0	100	0	-	20	0	0	0	0
37%Cu/ZnO	67.5	37.3 (38.0)	62.7 (62.0)	0	-	17	12.4	27.4	42.9 ± 3	0.008
Cu/ZnO/La (37:62:1)	72.0	38.4 (39.3)	60.5 (60.2)	1.1 (0.5)	-	16	7.6	17.2	43.1	0.012
Cu/ZnO/La (37:61:2)	72.8	38.3 (39.4)	59.4 (59.5)	2.3 (1.1)	-	15	5.4	12.3	33.6	0.018
Cu/ZnO/La (37:58:6)	75.2	37.5 (39.7)	55.9 (57.6)	5.6 (2.7)	-	14	8.4	18.8	31.6	0.009
Cu/ZnO/La (37:50:11)	80.4	37.1 (40.1)	51.9 (54.5)	11.0 (5.4)	-	13	6.5	14.4	32.6	0.004
F-COM Cu/ZnO/Al_2O_3 (37:55:8)	80.3	37.0 (38.8)	54.9 (55.9)	8.1[e] (5.3)	-	14	3.9	8.6	60.9	0.063

[a] Determined by ICP analysis.
[b] Determined by XRD and Scherrer formula from averaging ZnO(1 0 0), ZnO(0 0 2) and ZnO(1 0 1) diffraction lines.
[c] Determined by N_2O decomposition and the calculation of the copper surface area, it is assumed that a reduced copper surface has a surface density of 1.46×10^{19} copper atoms m^{-2}.
[d] TOF for the overall WGS reaction on Cu/ZnO-based catalysts at 230°C, 1 atm total pressure, 7% CO, 8.5% CO_2, 23% H_2O, 37.5% H_2 and 25% N_2.
[e] Weight ratio of Al_2O_3 component.

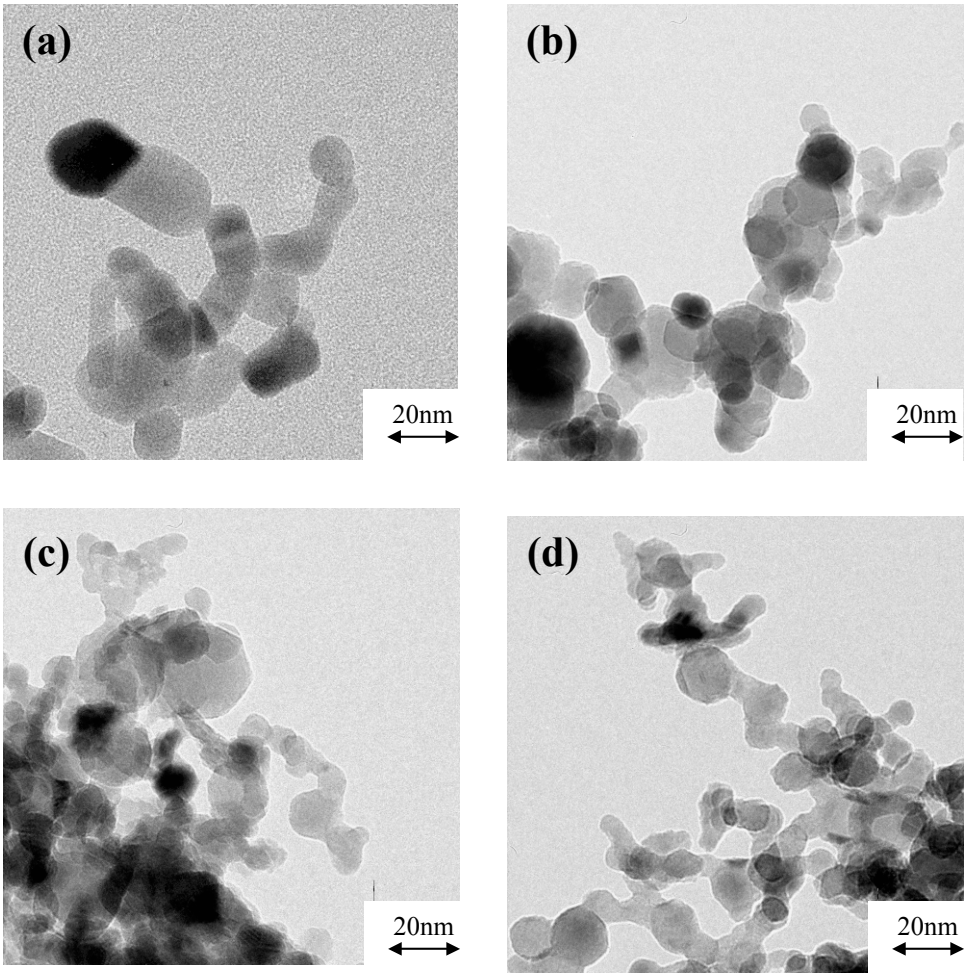

Fig. 5.2: TEM images of FSP-prepared (a) ZnO; (b) 37.3 wt% Cu/ZnO; (c) 5.6 wt% La-doped 37.5 wt% Cu/ZnO and (d) 11.0 wt% La-doped 37.1 wt% Cu/ZnO.

5.3.2 XPS analysis

Changes to surface bonding with increasing La dopant concentration were monitored by measuring the binding energies (BE) of Cu 2p3, Zn 2p3 and La 3d5 core electrons. BEs and surface atomic Cu/Zn and La/Cu ratios for La doped Cu/ZnO catalysts are summarised in Table 5.2. Binding energy of O1s was not considered due to complications with the overlapping contribution of oxygen from CuO, La_2O_3 and the ZnO support.

The BEs of Cu $2p_{3/2}$ and Zn $2p_{3/2}$ gave values of 933.9 eV and 1020.9 eV, respectively corresponding to CuO and ZnO (Table 5.2). These values differ slightly to those of Garbassi et al. [30] who reported values of 933.4 eV and 1022.2 eV respectively. This may arise from the different synthesis routes during catalyst preparation as Garbassi et al. [30] used co-precipitation. The shift in BEs when comparing the neat ZnO, CuO and the composite material (Table 5.2) provides evidence of an interaction between the Cu^{2+} and Zn^{2+} species. The presence of Cu^{2+} species can be readily identified by a strong satellite peak at 944-945 eV [30, 31] as seen in Fig. 5.3. This satellite peak, implies copper species on the catalyst exist in the Cu^{2+} oxidation state following FSP synthesis [31]. The lack of a peak at 932 eV indicates negligible Cu^{0} or Cu^{+} is present on the catalyst surface [32]. Inclusion of La into the system shifted the Cu $2p_{3/2}$ peak maxima (Fig. 5.3) from 933.4 eV at low La loadings (1 wt%) to 933.7 eV at higher La loadings (11 wt%) and was accompanied by a decrease in La $3d_{5/2}$ peak maxima (Table 5.2) from 835.4 to 835.1 eV demonstrating an interaction between CuO and La_2O_3. The simultaneous and opposing changes to Cu 2p and La 3d BEs infers a decrease in electron density in the Cu nucleus by increasing La dopant concentration. La_2O_3 inclusion had no influence on the ZnO peak maxima.

The surface elemental ratios of Cu and Zn relative to La were estimated from intensity ratios normalised by an atomic sensitivity factor [33]. These ratios are listed in Table 5.2. It can be seen that the Cu/Zn ratios are lower than bulk ratios obtained from ICP analysis indicating depletion in the Cu concentration on the particle surface. On comparing the La/Zn and La/Cu ratios an opposite effect was observed, where the surface elemental ratio is higher than the bulk ratio.

Table 5.2: Binding energies of core electrons and XPS atomic ratios of as-prepared FSP catalysts.

Catalyst (nominal weight ratio)	XPS binding energies (eV)			Surface elemental ratio (%)[a]		
	Cu $2p_{3/2}$	Zn $2p_{3/2}$	La $3d_{5/2}$	Cu/Zn	La/Zn	La/Cu
CuO	933.9	-	-	-	-	-
ZnO	-	1020.9	-	-	-	-
37%Cu/ZnO	933.4	1021.5	-	39.47 (61.29)	-	-
Cu/ZnO/La (37:62:1)	933.4	1021.5	835.4	49.98 (65.28)	1.42 (0.83)	2.79 (1.27)
Cu/ZnO/La (37:61:2)	933.5	1021.6	835.3	50.06 (66.22)	2.68 (1.85)	5.36 (2.79)
Cu/ZnO/La (37:58:6)	933.6	1021.5	835.2	51.78 (68.92)	6.50 (4.69)	12.54 (6.80)
Cu/ZnO/La (37:50:11)	933.7	1021.5	835.1	62.59 (73.58)	17.98 (9.91)	28.72 (13.47)

[a] Values in parenthesis are elemental ratio determined by ICP analysis

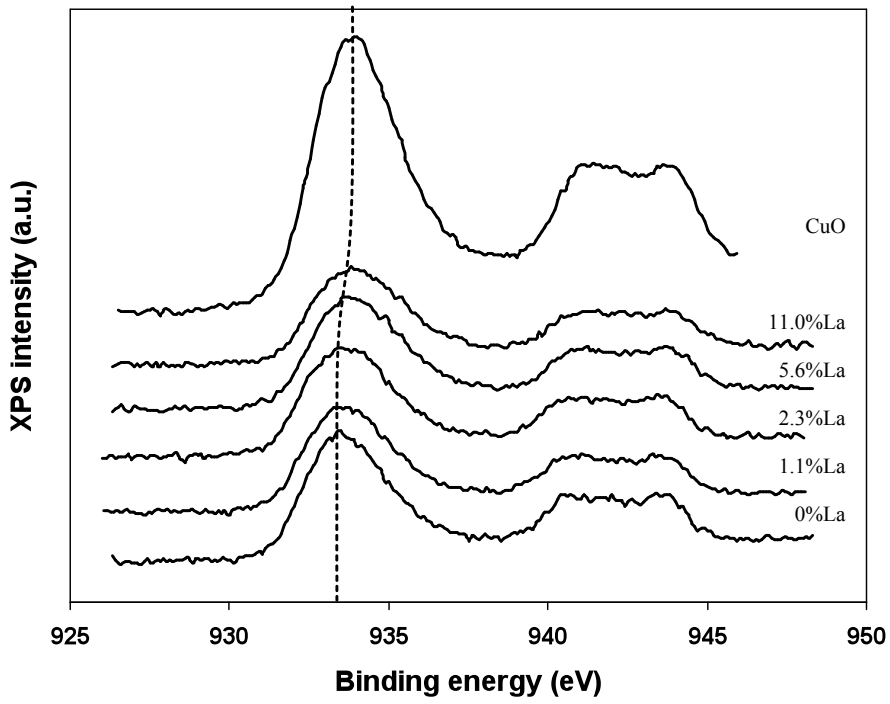

Fig. 5.3: Cu $2p_{3/2}$ XPS photoemission peak for FSP-prepared nominal 37%Cu/ZnO catalysts with varying La loadings. Pure FSP-prepared CuO is included for comparison.

5.3.3 TPR analysis

The TPR profile of pure FSP-prepared CuO (Fig. 5.4) shows a strong reduction peak at 290°C which is assigned to the reduction of CuO to metallic Cu as described by Eq. 5. The lack of any additional peaks agrees with XPS results indicating no Cu^{+} species are present [34, 35]. Peak shoulders appear for the composite material between 170°C to 200°C and are more pronounced for the 11.0 wt% La-doped and F-COM catalysts. Although bulk ZnO reduction is thermodynamically feasible, temperatures as high as 650°C are required to reduce ZnO to metallic zinc [36] with no ZnO reduction peaks observed in this study (up to 400°C). The Cu/ZnO composite material possesses a lower reduction temperature (~210°C) than either of the neat materials, with this peak ascribed

to CuO reduction and the temperature shift ascribed to interaction between the two oxides. The inclusion of La into the particles had minimal effect on the CuO reduction temperature up to a 2.3 wt% loading. Beyond this, La inclusion shifted the reduction temperature to higher values: 220°C for 5.6 wt% and 230°C for 11.0 wt%. The TPR profile of F-COM is included for reference and shows a reduction peak at ~235°C.

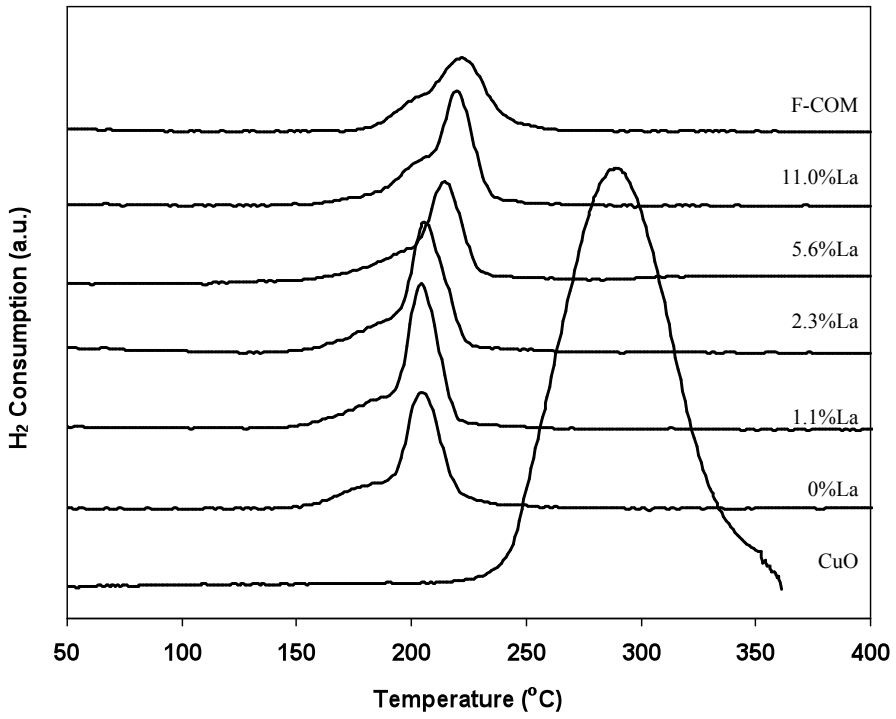

Fig. 5.4: H_2-TPR profiles of FSP-prepared 37%Cu/ZnO catalysts at different La dopant loading. Pure FSP-prepared CuO is included as a reference.

5.3.4 TPD analysis

The TPD spectra of water adsorbed on the reduced catalysts are presented in Fig 5.5. Water is strongly adsorbed on the neat FSP ZnO surface as indicated by its gradual desorption from ~270°C onwards, which accelerates at ~350°C and culminates in a peak maxima at 420°C. Similar chemisorption of H_2O on ZnO has been demonstrated

by others [37, 38]. Introducing Cu into the structure distinctly alters the H_2O-TPD profile with more rapid desorption beginning at ~270°C, where it reaches a broader maxima between 370 and 400°C, and then tapers off to around 600°C. While La addition does not alter the general shape of the Cu/ZnO H_2O desorption profile it does introduce some modifications. As the La loading is increased the initial H_2O desorption front becomes steeper, the peak maxima increases and tapering off of the peak is slower (incomplete by 600°C). In the case of F-COM, Fig. 5.5 indicates that while its desorption profile exhibits similarities to the Cu/ZnO profile, the presence of Al_2O_3 in a Cu/ZnO system does not facilitate H_2O adsorption, as demonstrated by the lower H_2O-TPD maxima. Reduced FSP CuO was not observed to adsorb/desorb water (result not shown).

The findings demonstrate, while H_2O is strongly chemisorbed to ZnO, the inclusion of CuO has a substantial influence on the ZnO adsorption sites, shifting desorption to lower temperatures and broadening the desorption peak. Increasing La addition boosts H_2O desorption, encouraging greater desorption at the lower temperature and further broadening the adsorption site distribution.

The CO-TPD spectra on the reduced La/Cu/ZnO samples are shown in Fig. 5.6. Weakly chemisorbed CO was evident as small CO signals were detected at around 60°C to 80°C for all the samples which agrees with literature [39, 40]. A dominant peak was also observed for all samples, exhibiting a maximum at between 300°C and 320°C. As the La loading increased, the amount of desorbed CO decreased and the peak maxima shifted to slightly higher temperatures. The presence of Al_2O_3 in the structure, as shown by the F-COM profile in Fig. 5.6 was detrimental to CO adsorption. CO-TPD on neat

FSP ZnO and reduced neat FSP CuO did not show evidence of any CO adsorption (results not shown). Robert and Griffin studied a series of Cu/ZnO catalysts [39], prepared by different methods, using CO-TPD coupled with infrared (IR) spectroscopy. They found CO did not chemisorb on ZnO in their Cu-containing catalysts but adsorbed only on the copper component [39]. To confirm the carbonaceous species deposited on the catalyst surface during FSP preparation did not influence CO-TPD results, the accompanying CO_2 signals are provided in Fig. S2 (**Appendix II**).

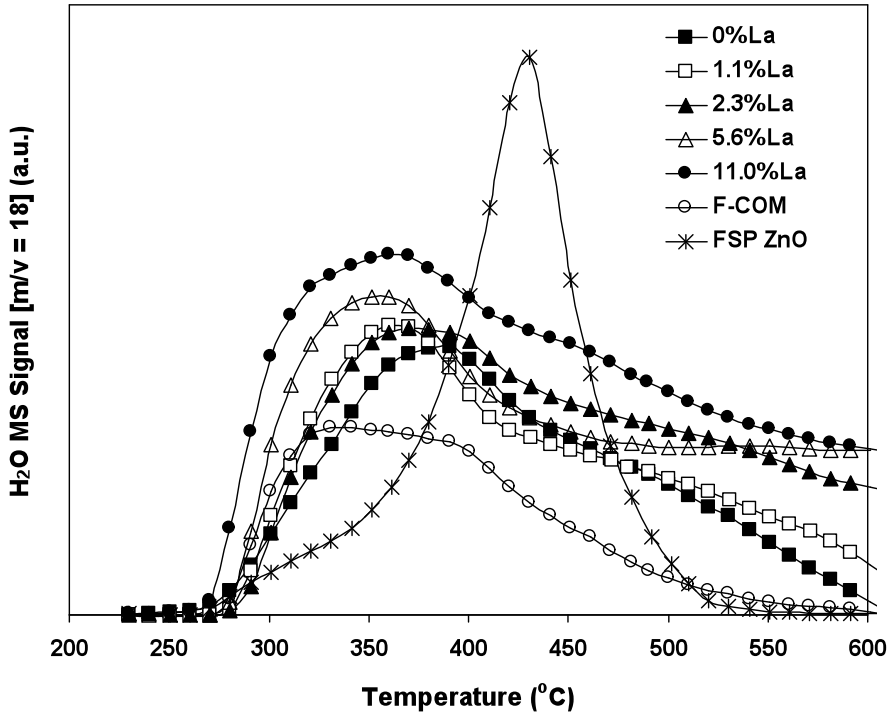

Fig. 5.5: H_2O-TPD profiles of FSP-prepared 37%Cu/ZnO catalysts with increasing La dopant loadings. F-COM represents the Al-doped catalyst and is included for comparison.

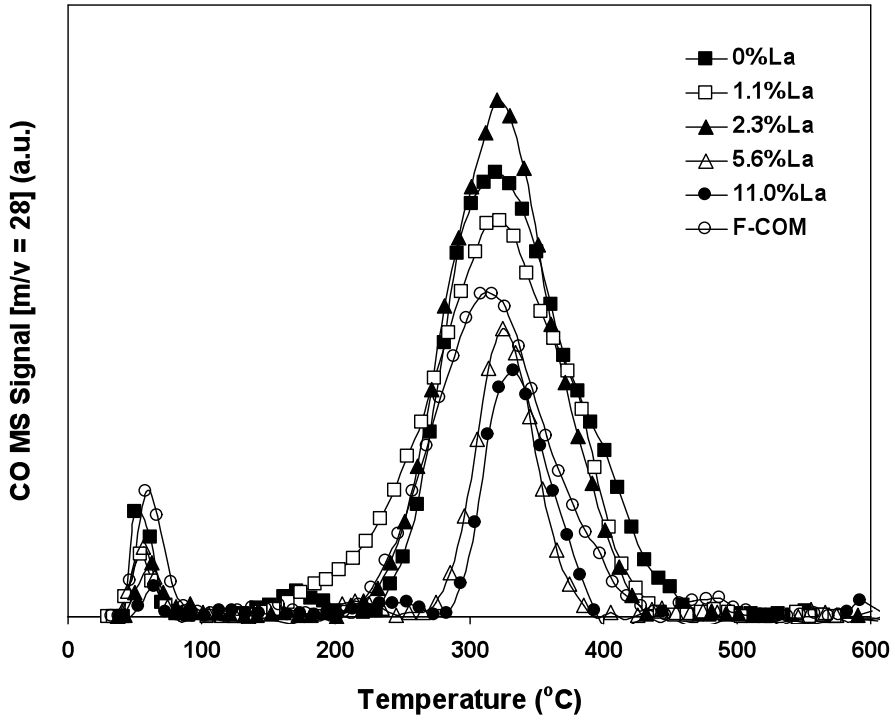

Fig. 5.6: CO-TPD profiles of FSP-prepared 37%Cu/ZnO catalysts at increasing La dopant loadings. F-COM represents the Al-doped catalyst and is included for comparison.

5.3.5 WGS performance of catalysts

The effect of La content on the activity of FSP-prepared La/Cu/ZnO catalysts for the LT-WGS reaction is given in Fig. 5.7. While adding 1.1 wt% La had negligible influence on activity, promotion with 2.3 wt% La increased CO conversion by ~5% (to 44%) over the undoped Cu/ZnO catalyst. Further La addition was detrimental to LT-WGS activity with CO conversion dropping to ~50% (to 23%) of the undoped material for 5.6 wt% La loading. Apparent activation energies (*E*a) were determined (Table 5.1) from the rates of CO consumption over the La/Cu/ZnO catalysts between 150°C and 300°C. The turnover frequencies (TOF) were also evaluated assuming the active sites

were surface copper metal (Table 5.1). Cu/ZnO catalyst loaded with 2.3 wt% La invoked a substantial decrease in *Ea* (10 kJ mol^{-1} difference) implying the forward WGS reaction was promoted. At greater La loadings, despite the decrease in CO conversion, the *Ea* remained relatively constant. No methane was detected in this study suggesting high selectivity of the Cu/ZnO catalysts. The stainless steel reactor did not contribute to LT-WGS activity in this study (see Fig. S3 in **Appendix III**).

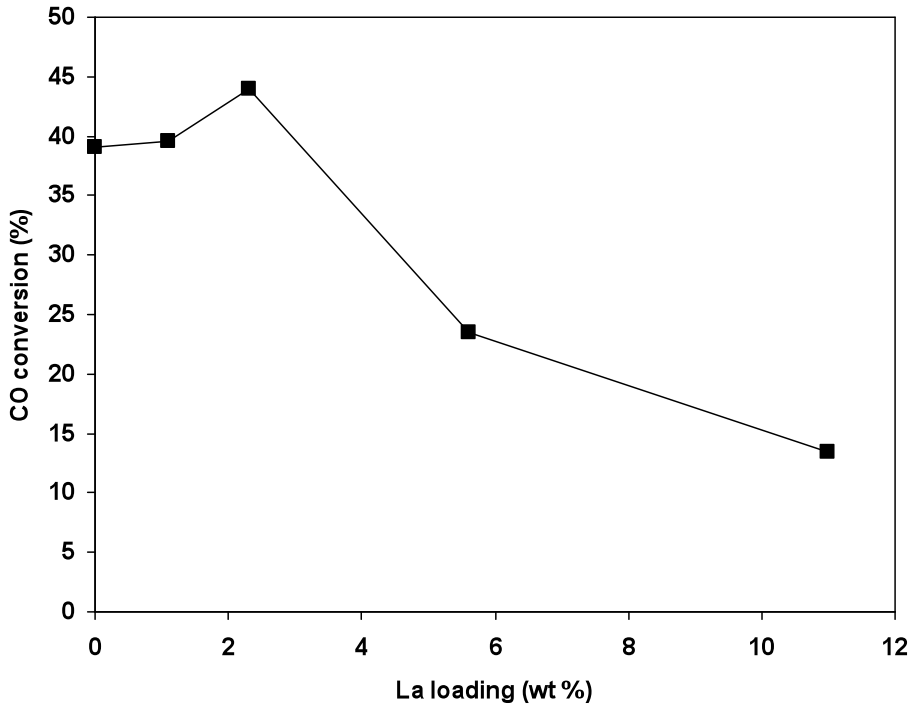

Fig. 5.7: Effect of lanthanum doping on CO conversion by 37 wt% Cu/ZnO (nominal) for the LT-WGS reaction. Reaction conditions: operating temperature = 300°C, total flow = 100 mL min^{-1} (7% CO, 8.5% CO_2, 23% H_2O, 37.5% H_2 and 25% N_2); catalyst loading = 0.10 g; pressure = 1 atm.

5.3.6 Catalyst stability and post reaction characteristics

The stability of three catalyst samples: (i) 37.3 wt% Cu/ZnO; (ii) 2.3 wt% La doped-38.3 wt% Cu/ZnO; and (iii) F-COM, during the WGS reaction (at 300°C) was assessed under 25 h of continuous run-time. CO conversion with operating time is shown in Fig. 5.8. Cu/ZnO, conversion dropped by ~11% over the first 5 h after which it decreased a further 4 % over the next 20 h. The presence of 2.3 wt% La markedly improved active site stability although some deactivation was evident with an observed ~5% decrease in CO conversion over the 25 h period. Initial CO conversion by F-COM was approximately 15% and 20% lower than the un-doped and La-doped catalysts respectively; however, its activity was maintained over the 25 h time frame.

To aid in identifying the sources of catalyst deactivation/stability, surface areas (Fig. 5.9) and TPD profiles (Fig. 5.10) of the post-reaction materials were assessed. Fig. 5.9 indicates the Cu/ZnO catalyst lost 33% and 18% of its initial specific surface area (SSA) and copper surface area (CSA), respectively, during the reaction which may account for the activity loss incurred by this material. While La addition gave a mildly improved resistance to sintering (23% and 25% loss of its initial SSA and CSA, respectively) compared with the undoped Cu/ZnO, the loss of these attributes remained substantial but was not reflected by the catalyst activity. The presence of alumina in the catalyst make-up gave a lower initial activity but imparted increased stability for both the catalyst structure and the CSA. The 25 h reaction presented a small decrease in SSA (~ 8%) and negligible change in CSA. Fig. 5.9 also lends some support to the notion that Cu metal is not solely responsible for LT-WGS activity, as previously reported by Guo

et al. [8]. Comparing the initial CSA's with initial LT-WGS activities indicates no correlation between the two.

Surface characterization of the three catalysts post-reaction by H_2O TPD and CO TPD is shown in Fig. 5.10 (a) and (b), respectively. Fig. 5.10 (a) indicates the 37.3%Cu/ZnO lost almost half its H_2O adsorption sites over the 25 h reaction period. The 2.3% La loaded Cu/ZnO catalyst also lost H_2O adsorption sites however to a lesser extent than the undoped material. In the case of F-COM, the loss of H_2O adsorption sites was small. Similar behaviour was observed for CO-TPD (Fig. 5.10 (b)), with a substantial portion of the CO adsorption sites lost during reaction for the undoped and La-doped Cu/ZnO and a minor number lost for F-COM.

To assess whether a build-up of carbonaceous species contributed to catalyst deactivation, TPO experiments were administered on the fresh and used catalysts. Fig. 5.11 shows no accumulation of carbonaceous species occurred on the catalyst surface during the LT-WGS reaction for the neat and La-doped Cu/ZnO system. In fact, it appears intrinsic carbonaceous species present on the fresh catalyst were removed during the WGS reaction as the CO_2 signal is generally lower for the used material. A strong CO_2 peak at 240°C from the used-F-COM suggests a possible build up of formates or carbonates occurs on the catalyst surface over the 25 h. Given there is no loss in activity for F-COM, it appears they behave only as spectator species.

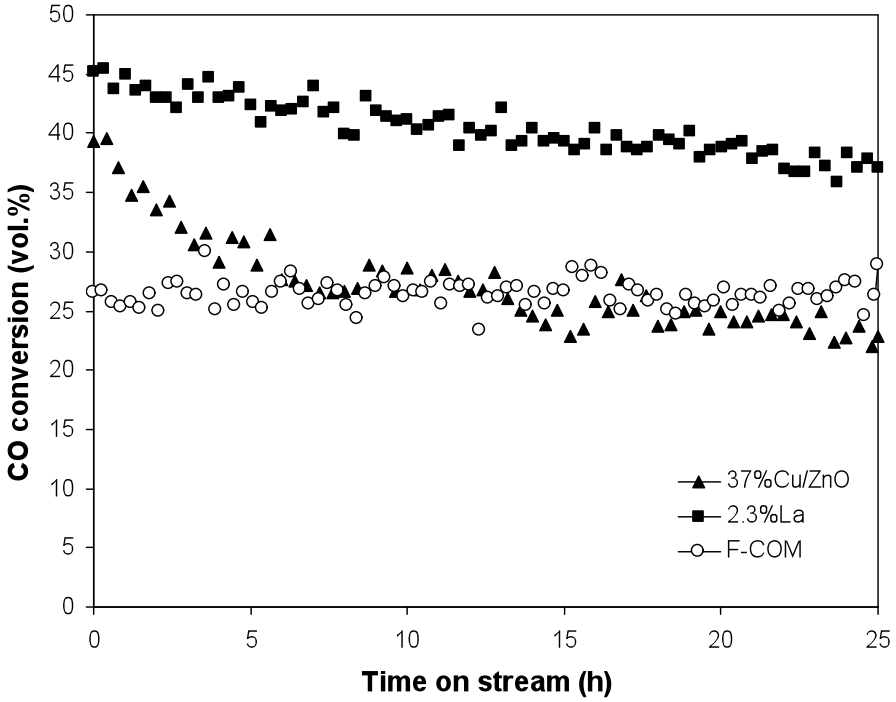

Fig. 5.8: CO conversion with time by 37.3%Cu/62.7%ZnO, 2.3%La/38.3%Cu/59.4%ZnO and F-COM (37%Cu/54.9%ZnO/8.1%Al_2O_3) for the LT-WGS reaction. Reaction conditions: temperature = 300°C; flow rate = 100 mL min^{-1} (7% CO, 8.5% CO_2, 23% H_2O, 37.5% H_2 and 25% N_2); catalyst loading = 0.10 g; pressure = 1 atm.

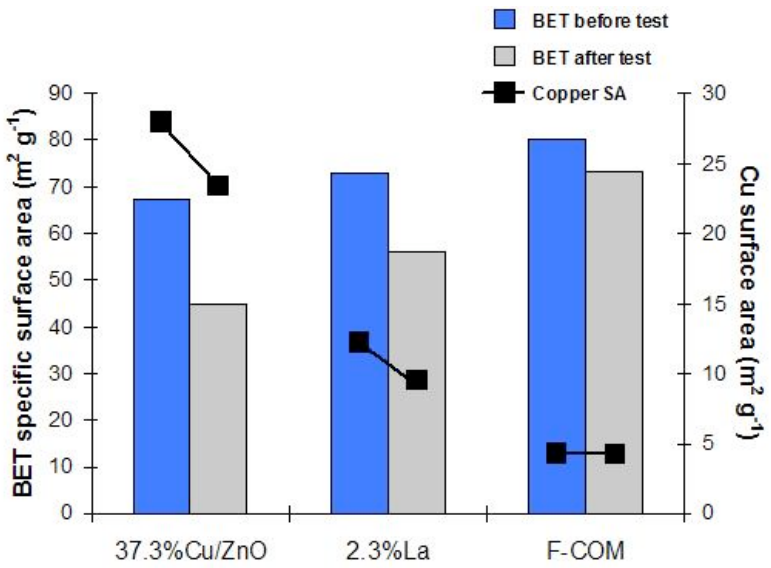

Fig. 5.9: Specific surface area and Cu surface area changes for 37.3%Cu/62.7%ZnO, 2.3%La/38.3%Cu/59.4%ZnO and F-COM (37%Cu/54.9%ZnO/8.1%Al_2O_3) following the LT-WGS reaction for 25 h. Reaction temperature = 300°C.

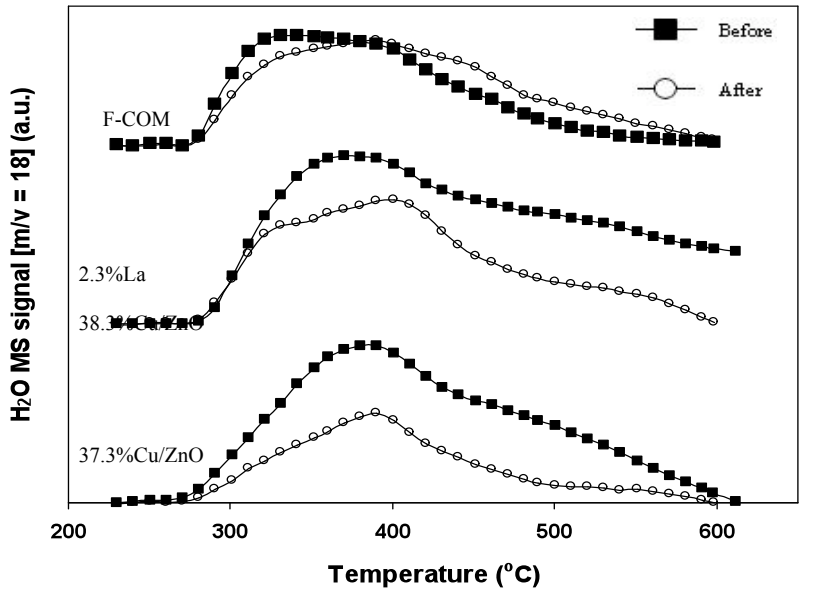

(a)

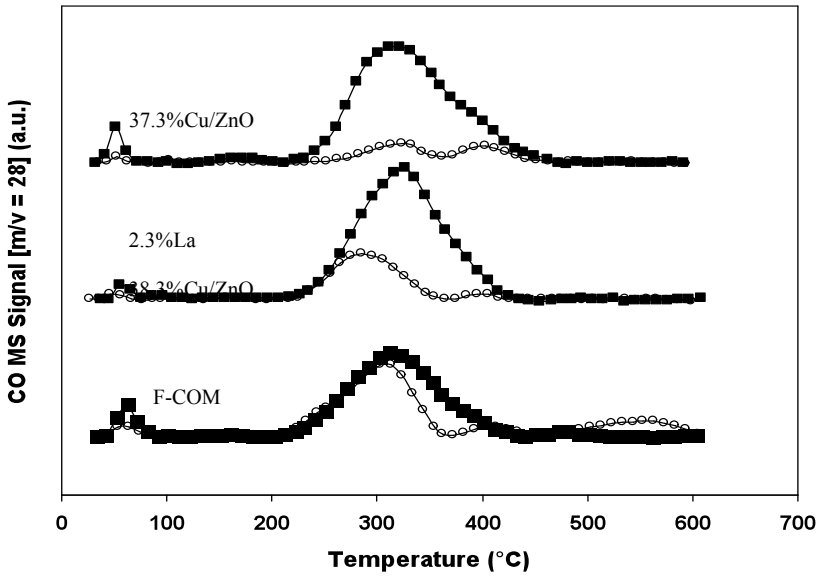

(b)

Fig. 5.10: Comparison of: (a) H_2O-TPD profiles; (b) CO-TPD profiles; for selected catalysts before and after 25 h LT-WGS reaction at 300°C.

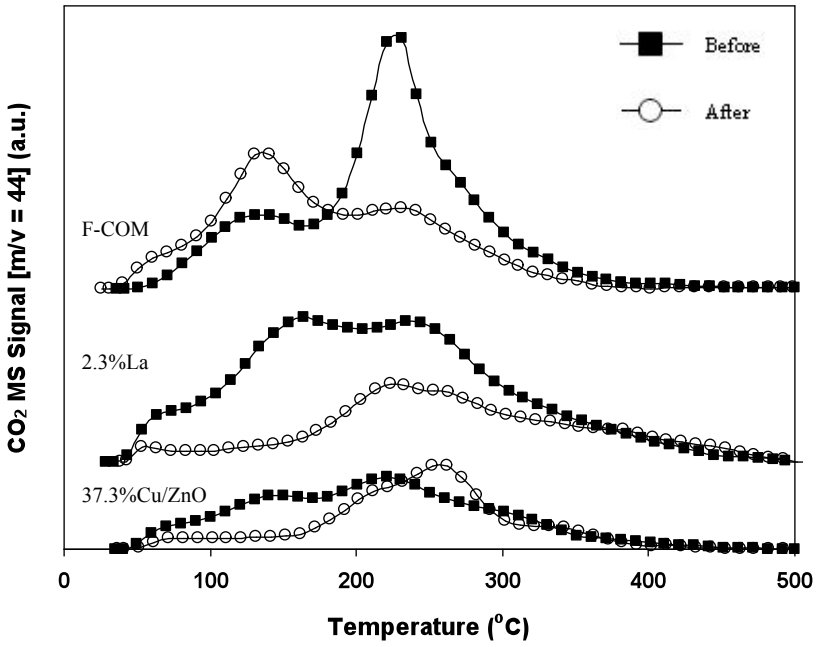

Fig. 5.11: Comparison of TPO curves for selected catalysts before and after the 25 h LT-WGS reaction at 300°C.

5.4 Discussion

5.4.1 Structural and surface features of Cu/ZnO-based catalysts

Transition of the rod-shaped FSP-ZnO crystallites into smaller spherical ZnO crystals, as depicted in the TEM images (Fig 5.2a. and 5.2b.), has been observed by others [41]. Zhu et al. [41] reported the morphology of nanostructured ZnO crystals could be altered by varying the growth temperature and Cu to Zn ratio. Cu plays an important role in confining the lateral growth of ZnO due to competition between Zn and Cu for oxygen [41] which may be evident in the oxidative combustion process during FSP synthesis [42]. Increasing La or Al-dopant loading effectively decreased the Zn content in the catalyst bulk and had the effect of increasing the Cu loading relative to Zn. This is

expected to induce enhanced competition for oxygen by the Cu during synthesis and may be the source of the increasingly smaller ZnO crystallite sizes as demonstrated by XRD (Table 5.1) and TEM (Fig. 5.2 a-d).

The decrease in metallic Cu surface area with increasing La loading may arise from the formation of a solid solution between CuO and La_2O_3 crystals. Jacobs and Jayadevan derived a phase diagram for the Cu-La-O system at 930°C [43] and indicated a solubility limit of 40 mol% CuO in La_2O_3 can be achieved without altering the La_2O_3 structure.

Intensification of the TPR profile shoulder (Fig. 5.4) as La loading was increased in the Cu/ZnO system may be due to a reduction of surface CuO that is kinetically faster and precedes bulk CuO reduction [35]. The shoulder is significant for the 11.0 wt% La-doped and F-COM catalysts possibly due to their high specific surface areas (80.4 and 80.3 m^2/g, respectively). That is the particles possess a lower average size which in turn can affect the kinetics of surface CuO reduction [35].

Pestryakov and Davydov [44] used CO adsorption with IR spectroscopy to show the surface basicity of La_2O_3 to be very high due the strong charge density on La_2O_3 oxygen ions. They were able to observe an electron donor-acceptor interaction between Cu^{x+} ions and La_2O_3 which indicated a loss of electron density in the Cu^{2+} nucleus due to electron scavenging properties of the La_2O_3. We observed from XPS a diminishing electron density in the Cu^{2+} nucleus manifested as a gradual shift in the Cu $2p_{3/2}$ spectra (Table 2) to higher binding energies (Fig. 5.3), with increasing La loading. This agrees well with Pestryakov and Davydov's work [44]. The decreasing Cu^{2+} electron density

implies the Cu^{2+} and O^{2-} bond is strengthened by La addition as the Cu^{2+} becomes more positively charged. This is reflected in the H_2 TPR profiles with the gradual shift in reduction peaks from 205 to 225°C for 2.3 to 11 wt% La/Cu/ZnO (Fig. 5.4) where the oxygen has become increasingly harder to remove from CuO.

The lower Cu/Zn surface ratio from XPS analysis compared with the bulk ratios acquired from ICP implies the CuO is not uniformly distributed throughout the ZnO matrix. The homogeneous solubility limit of Cu in ZnO has been reported as 10 mol% [45] which is considerably lower than the Cu loading used in this FSP catalyst. This alludes to the idea that CuO may exist (in part) as inclusions within the ZnO particles. Additionally, similar transition temperatures from vapour to liquid phase at atmospheric pressure for CuO at 2000°C [46] and vapour to solid phase at 1900°C for ZnO [47] may induce component segregation during the FSP formation process. In the case of La ratio with respect to Cu and Zn, the XPS surface elemental ratio is consistently higher than the bulk ratio (Table 5.2) suggesting an enrichment of La on the catalyst surface due to nucleation of the La_2O_3 component after CuO and ZnO during synthesis.

5.4.2 Catalytic behaviour, active sites and mechanism

The activity results (Fig. 5.7) demonstrated a decrease in CO conversion for La loadings greater than 2.3 wt%. This coincided with the shift to higher CuO reduction temperatures at La loadings greater than 2.3wt% during TPR. The shift may be explained by the XPS findings which indicated increasing La addition decreased Cu core electron density making it more difficult to remove O from the surface CuO.

Coupled with this, CO-TPD results (Fig. 5.6) showed La loadings of 5.6wt% and above promoted a significant loss in CO adsorption capacity of the catalyst. The loss in CO adsorption capacity may derive from the increase in La loading on the surface (with increasing La content) blocking surface active sites or electronic changes it may invoke on the adsorption sites. Given the Cu component of the catalyst is reported to be responsible for CO adsorption [39] it appears that increasing the La content beyond 2.3wt% has a detrimental influence on both its electronic properties and capacity for adsorbing CO, in turn promoting the observed loss in catalyst activity.

Table 5.1 demonstrated that La addition decreased Cu metal dispersion by between 6.5 and 12.4 % over the neat Cu/ZnO. Relating this finding to the activity results in Fig. 5.7 indicates no apparent correlation between the two, implying this characteristic is not responsible for LT-WGS catalyst activity. This notion is supported by the changing TOF values provided in Table 5.1, whereby if the surface Cu metal was responsible for the LT-WGS activity then the TOF would remain constant over all the Cu/ZnO-based catalysts. This finding suggests Cu species other than metallic Cu may be responsible for the LT-WGS activity. Cu has been reported by Okamoto et al. [48] to coexist in various oxidation states on the Cu/ZnO catalyst surface. Using XPS on reduced Cu/ZnO, they revealed for high copper content catalysts (>25 wt% CuO), the predominant Cu metal species was well-dispersed metallic copper (Cu^0) with Cu^+ species also present, originating from CuO dissolved in the ZnO lattice. More recently, Harikumar and Rao [49] confirmed the existence of Cu^0 and Cu^+ species on their reduced Cu/ZnO using Auger spectroscopy analysis. Additionally, surface Cu^+ has a high affinity to bind with CO molecules [49-53]. For instance, Didziulis et al. [54] conducted extensive work on heats of adsorption of CO on different well-defined copper sites and on the ZnO surface.

They associated a high affinity of CO binding site with Cu^{+} centres on ZnO(0001) and ZnO(1010)-dimers [54].

H_2O-TPD studies (Fig. 5.5) indicated the ZnO substrate was responsible for adsorbing water although Cu addition substantially altered the H_2O desorption profile of the support, shifting the peak maxima to a lower temperature. La addition appeared to generally increase the amount of H_2O bound to the catalyst surface compared with neat Cu/ZnO. Lanthanum oxide is known to be highly hygroscopic [55], forming lanthanum hydroxide when exposed to water vapour and then desorbing water under thermal treatment (370°C), to return to its oxide form (Eq. 5.6) [56].

$$La_2O_3 + 3H_2O \leftrightarrow 2La(OH)_3 \qquad \text{(Eq. 5.6)}$$

Notably, increasing La content increased the amount of H_2O desorbed between 280°C and 400 °C. This temperature range overlays the CO desorption temperature range and suggests La may increase the amount of H_2O adsorbed at the expense of CO, particularly at loadings greater than 2.3wt%.

Overall, the TPD results imply the ZnO substrate is primarily responsible for adsorbing the H_2O molecules although the addition of Cu to the system lowers the strength by which they are bound to the surface. Cu on the other hand appears responsible for CO adsorption although this does not derive from its metallic state but some other species, possibly Cu^{+}. This site bifunctionality rules in favour of the associative mechanism during LT-WGS. That is, following H_2O and CO adsorption on the catalyst surface, carbonaceous intermediates are formed which then decompose into the desired products, CO_2 and H_2 [11, 57, 58].

The inclusion of La into the catalyst promotes a mild improvement in activity at 2.3 wt% after which higher loadings are detrimental to catalyst performance. The higher activity at 2.3 wt% is reflected in the lower activation energy at this loading (compared with 1.1 wt% La and neat Cu/ZnO) while further increases in La loading appear to promote H_2O adsorption at the expense of CO. This may provide the source of the observed lower activities. Liu and Rodriguez [59] concluded that dissociation of water is the rate-limiting step in a Cu catalytic system for WGS reaction. Hence, the presence of La increases the water adsorption and provides an initial decrease in activation energy for the water dissociation.

5.4.3 Catalyst stability and deactivation

It is well documented that Cu/ZnO is susceptible to sintering [6, 7] during WGS operation, with a small amount of refractory oxide such as Al_2O_3 or Cr_2O_3 typically added to stabilise the Cu/ZnO structure Post-reaction catalyst characterization showed two effects were evident. Firstly (with the exception of the Al-loaded system), there were losses in catalyst surface area and Cu surface area, the extent depending on the additive. Secondly, there was a loss in CO and H_2O adsorption capacity for the neat and La-loaded catalysts but not for the Al-loaded system. The loss in substrate and Cu surface areas for the neat Cu/ZnO may account for the observed decrease in LT-WGS activity with time; however this is not the case for the La-loaded system with comparative losses in these two characteristics not emulated by the activity decrease. This implies the La acts to preserve the active sites despite the occurrence of thermal sintering. Thermal sintering does appear to govern the relative losses in CO and H_2O adsorption capacity of the catalysts, although the extent of loss in adsorption capacity is

not closely correlated to the activity results. These findings also succinctly demonstrate the capacity of Al for stabilising the Cu/ZnO structure, albeit at the expense of activity.

TPO characterization indicated deactivation did not result from the build-up of carbonaceous species. F-COM was the only catalyst to show carbonaceous species formed and remained on the surface during reaction but there was no corresponding activity decrease. This agrees with the findings by Guo et al. [8] who reported a similar build-up of carbonate species on their $Cu/ZnO/Al_2O_3$ catalyst, however they suggested the presence of these species on the catalyst surface, rather than sintering, coincided with deactivation.

5.5 Conclusions

La addition has been demonstrated to affect the activity and stability of Cu/ZnO catalysts under realistic feed conditions for the LT-WGS reaction. In particular, doping with 2.3 wt% La decreased the apparent activation energy of the Cu/ZnO system and improved the WGS activity compared to un-doped Cu/ZnO. Further increase in La loading appears to promote H_2O adsorption at the expense of CO hence a sharp decrease in WGS activity. Moreover, the La stabilised the active sites over an extended operating period with the rate of deactivation decreased markedly despite a substantial decrease in specific and metallic copper surface area during reaction. These results implied metallic copper sites were not responsible for the LT-WGS activity. XPS characterization revealed electron interaction between Cu and La components which corroborates the increase of Cu^{2+} binding energy to O^{2-} from increased concentration of La-dopant. This is reflected from the increasing temperature required to reduce the CuO to metallic

copper. The CO and H_2O TPD studies seem to point out that the WGS mechanism proceed via associative route on a La doped Cu/ZnO catalytic system. The higher activity at 2.3 wt% is reflected in the lower activation energy at this loading (compared with 1.1 wt% La and neat Cu/ZnO) while further increases in La loading appear to promote H_2O adsorption at the expense of CO. This may provide the source of the observed lower activities.

In comparison to the $Cu/ZnO/Al_2O_3$ system, the La doped Cu/ZnO is more superior in terms of WGS activity even though a loss in activity is apparent over 25 h of WGS operation at 300°C.

5.6 References

1. W. Vielstich, A. Lamm, and H.A. Gasteiger, *Handbook of Fuel Cells – Fundamentals, Technology and Applications, Catalyst development for water-gas shift, J.R. Ladebeck and J. P. Wagner*. Handbook of Fuel Cells – Fundamentals, Technology and Applications. Vol. Volume 3, John Wiley & Sons, Chichester, UK. p. 190, **3 (2003)**.
2. C.H. Bartholomew and R.J. Farrauto, *Fundamentals of Industrial Catalytic Processes*. 2nd Edition ed, John Wiley & Sons, Ltd, Hoboken, NJ, **2006**.
3. C. Rhodes, G.J. Hutchings, and A.M. Ward, 'Water-gas shift reaction: finding the mechanistic boundary', *Catalysis Today* 23(1) (**1995**) 43-58.
4. E. Bogel-Łukasik, R. Bogel-Łukasik, and M.N.d. Ponte, 'Pt- and Pd-catalysed limonene hydrogenation in high-density carbon dioxide', *Monatshefte für Chemie* 140 (**2009**) 1361–1369.

5. D.S. Newsome, 'The Water-Gas Shift Reaction', *Catalysis Reviews: Science and Engineering* 21(2) (**1980**) 275-318.

6. T. Shishido, M. Yamamoto, I. Atake, D. Li, Y. Tian, H. Morioka, M. Hondac, T. Sano, and K. Takehira, 'Cu/Zn-based catalysts improved by adding magnesium for water–gas shift reaction', *Journal of Molecular Catalysis A: Chemical* 253 (**2006**) 270-278.

7. T. Shishido, M. Yamamoto, D. Li, Y. Tian, H. Morioka, M. Honda, T. Sano, and K. Takehira, 'Water-gas shift reaction over Cu/ZnO and Cu/ZnO/Al_2O_3 catalysts prepared by homogeneous precipitation', *Applied Catalysis A: General* 303 (**2006**) 62-71.

8. P.-J. Guo, L.-F. Chen, G.-B. Yu, Y. Zhu, M.-H. Qiao, H.-L. Xu, and K.-N. Fan, 'Cu/ZnO-based water–gas shift catalysts in shut-down/start-up operation', *Catalysis Communications* 10 (**2009**) 1252-1256.

9. M.S. Spencer, 'The role of zinc oxide in Cu/ZnO catalysts for methanol synthesis and the water-gas shift reaction', *Topics in Catalysis* 8 (**1999**) 259-266.

10. H. Schaper, E.B.M. Doesburg, and L.L.v. Reije, 'The influence of lanthanum oxide on the thermal stability of gamma alumina catalyst supports', *Applied Catalysis* 7 (**1983**) 211-220.

11. T. Shido and Y. Iwasawa, 'Reactant-Promoted Reaction Mechanism for Water-Gas Shift Reaction on ZnO, as the Genesis of Surface Catalysis', *Journal of Catalysis* 129 (**1991**) 343-355.

12. D.C. Grenoble, M.M. Estadt, and D.F. Ollis, 'The Chemistry and Catalysis of the Water Gas Shift Reaction', *Journal of Catalysis* 67 (**1981**) 90-102.

13. N.A. Koryabkina, A.A. Phatak, W.F. Ruettinger, R.J. Farrauto, and F.H. Ribeiro, 'Determination of kinetic parameters for the water-gas shift reaction on copper

catalysts under realistic conditions for fuel cell applications', *Journal of Catalysis* 217 (**2003**) 233-239.

14. G.C. Chinchen, M.S. Spencer, K.C. Waught, and D.A. Whan, 'Promotion of Methanol Synthesis and the Water-gas Shift Reactions by Adsorbed Oxygen on Supported Copper Catalysts', *Journal of the Chemical Society, Faraday Transactions 1* 83 (**1987**) 2193-2212.
15. J.L.C. Fajin, M.N.D.S. Cordeiro, Francesc Illas, and J.R.B. Gomes, 'Influence of step sites in the molecular mechanism of the water gas shift reaction catalyzed by copper', *Journal of Catalysis* 268 (**2009**) 131-141.
16. R. Burch, R.J. Chappell, and S.E. Golunski, 'Synergy at a distance in the synthsis of methanol over copper catalysts', *Catalysis Letters* 1 (**1988**) 439-444.
17. Y. Okamoto, K. Fukino, T. Imanaka, and S. Teranishi, 'Synergy between Cu and ZnO for methanol conversionsover Cu-ZnO catalysts', *Chemistry Letters* (**1984**) 71-74.
18. G. Ghiotti and F. Bocuzzi, 'Chemical and Physical Properties of Copper-Based Catalysts for CO shift Reaction and Methanol Synthesis', *Catalysis Reviews: Science and Engineering* 29(2 & 3) (**1987**) 151-182.
19. T.v. Herwijnen and W.A.D. Jon, 'Kinetics and Mechanism of the CO shift on Cu/ZnO', *Journal of Catalysis* 63 (**1980**) 83-93.
20. W.Y. Teoh, L. Mädler, D. Beydoun, S.E. Pratsinis, and R. Amal, 'Direct (one-step) synthesis of TiO_2 and Pt/TiO_2 nanoparticles for photocatalytic mineralisation of sucrose', *Chemical Engineering Science* 60 (**2005**) 5852 – 5861.
21. M.J.L. Gines, N. Amadeo, M. Laborde, and C.R. Apesteguia, 'Activity and structure-sensitivity of the water-gas shift reaction over Cu-Zn-Al mixed oxide catalysts', *Applied Catalysis A: General* 131 (**1995**) 283-296.

22. J.R. Jensen, T. Johannessen, and H. Livbjerg, 'An improved N_2O-method for measuring Cu-dispersion', *Applied Catalysis A: General* 266 (**2004**) 117-122.

23. J.W. Evans, M.S. Wainwright, A.J. Bridgewater, and D.J. Young, 'On the determination of copper surface area by reaction with nitrous oxide', *Applied Catalysis* 7 (**1983**) 75-83.

24. X. Liu, W. Ruettinger, X. Xu, and R. Farrauto, 'Deactivation of Pt/CeO_2 water-gas shift catalysts due to shutdown/startup modes for fuel cell applications', *Applied Catalysis B: Environmental* 56 (**2005**) 69–75.

25. G.C. Chinchen, P.J. Denny, J.R. Jennings, M.S. Spencer, and K.C. Waugh, 'Synthesis of Methanol Part 1. Catalysts and Kinetics', *Applied Catalysis* 36 (**1988**) 1-65.

26. J.R. Ladebeck and J.P. Wagner, 'Catalyst development for water-gas shift', *Handbook of Fuel Cells – Fundamentals, Technology and Applications* Volume 3 Part 2 (**2003**) 190–201.

27. G. Shen, J.H. Cho, J.K. Yoo, G.-C. Yi, and C.J. Lee, 'Synthesis and Optical Properties of S-Doped ZnO Nanostructures: Nanonails and Nanowires', *Journal of Physical Chemistry B* 109 (**2005**) 5491-5496.

28. W. Wang, Y. Zhan, and G. Wang, 'One-step, solid-state reaction to the synthesis of copper oxide nanorods in the presence of a suitable surfactant', *Chemical Communications* (10.1039/b008215p) (**2001**) 727–728.

29. S.E. Pratsinis, 'Flame aerosol synthesis of ceramic powders ', *Progress in Energy and Combustion Science* 24(3) (**1998**) 197-219.

30. F. Garbassi and G. Petrini, 'XPS Study on the Low-Temperature CO Shift Reaction Catalyst', *Journal of Catalysis* 90 (**1984**) 106-112.

31. C.C. Chusuei, M.A. Brookshier, and D.W. Goodman, 'Correlation of Relative X-ray Photoelectron Spectroscopy Shake-up Intensity with CuO Particle Size', *Langmuir* 15 (**1999**) 2806-2808.

32. W.-L. Dai, Q. Sun, J.-F. Deng, D. Wu, and Y.-H. Sun, 'XPS studies of $Cu/ZnO/Al_2O_3$ ultra-fine catalysts derived by novel gel oxalate co-precipitation for methanol synthesis by $CO_2 + H_2$', *Applied Surface Science* 177 (**2001**) 172-179.

33. M. Daturi, C. Binet, J.-C. Lavalley, A. Galtayries, and R. Sporkenb\, 'Suface investigation on $Ce_xZr_{1-x}O_2$ compounds', *Physical Chemistry Chemical Physics* 1 (**1999**) 5717-5724.

34. F. Nishida, I. Atake, D. Li, T. Shishido, Y. Oumi, T. Sano, and K. Takehira, 'Effects of noble metal-doping on Cu/ZnO/Al2O3 catalysts for water–gas shift reaction Catalyst preparation by adopting “memory effect” of hydrotalcite', *Applied Catalysis A: General* 337 (**2008**) 48-57.

35. M. Turco, G. Bagnasco, U. Costantino, F. Marmottini, T. Montanari, G. Ramis, and G. Busca, 'Production of hydrogen from oxidative steam reforming of methanol I. Preparation and characterization of $Cu/ZnO/Al_2O_3$ catalysts from a hydrotalcite-like LDH precursor', *Journal of Catalysis* 228 (**2004**) 43-55.

36. T. Imoto, Y. Harano, Y. Nishi, and S. Masuda, 'The Reduction of Zinc Oxide by Hydrogen. III. The Effect of Nitrogen on the Reduction', *Bulletin of the Chemical Society of Japan* 37(4) (**1964**) 441-444.

37. C. Zwicker and K. Jacobi, 'Site-specific Interaction of H_2O with ZnO Single-crystal Surfaces Studied by Thermal Desorption and UV Photoelectron Spectroscopy', *Surface Science* 131 (**1983**) 179-194.

38. R. Zhang, A. Ludviksson, and C.T. Campbell, 'The chemisorption of H_2O and O_2 on Cu films on ZnO(OOO1)-O', *Surface Science* 289 (**1993**) 1-9.

39. D.L. Roberts and G.L. Griffin, 'Temperature-Programmed Desorption and Infrared Study of CO and H_2 Adsorption on Cu/ZnO Catalysts', *Journal of Catalysis* 110 (**1988**) 117-126.

40. J. Strunk, R.N. d'Alnoncourt, M. Bergmann, S. Litvinov, X. Xia, O. Hinrichsen, and M. Muhler, 'Microkinetic modeling of CO TPD spectra using coverage dependent microcalorimetric heats of adsorption', *Physical Chemistry Chemical Physics* 8 (**2006**) 1556–1565.

41. Y. Zhu, C.-H. Sow, T. Yu, Q. Zhao, P. Li, Z. Shen, D. Yu, and J.T.-L. Thong, 'Co-synthesis of ZnO–CuO Nanostructures by Directly Heating Brass in Air', *Advanced Functional Materials* 16(18) (**2006**) 2415 - 2422.

42. R. Strobel, A. Baiker, and S.E. Pratsinis, 'Aerosol flame synthesis of catalysts', *Advanced Powder Technology* 17(5) (**2006**) 457-480.

43. K.T. Jacob and K.P. Jayadevan, 'Phase relations in the system Cu-La-O and thermodynamic properties of $CuLaO_2$ and $CuLa_2O_4$', *Journal of Materials Science* 37 (**2002**) 1611 – 1620.

44. A.N. Pestryakov and A.A. Davydov, 'The influence of modifying additions of La and Ce oxides on electronic state of surface atoms and ions of supported copper', *Applied Surface Science* 103 (**1996**) 379-483.

45. S.V. Ketchik, T.P. Minyukova, L.I. Kuznetsova, L.M. Plyasova, T.M. Yurieva, and G.K. Boreskov, 'Peculiarities of formation of ZnO and CuO-based solid solution', *Reaction Kinetics and Catalysis Letters* 19 (**1982**) 345-349.

46. E. Mack, G.G. Osterhof, and H.M. Kraner, 'Vapor pressure of copper oxide and of copper', *Journal of the American Chemical Society* 45(3) (**1922**) 617-623.

47. D.F. Anthrop and A.W. Searcy, 'Sublimation and Thermodynamic Properties of Zinc Oxide', *Journal of Physical Chemistry* 68(8) (**1964**) 2335-2342.

48. Y. Okamoto, K. Fukino, T. Imanaka, and S. Teranishi, 'Surface Characterization of CuO-ZnO Methanol-Synthesis Catalysts by X-ray Photoelectron Spectroscopy. 2. Reduced Catalysts', *Journal of Physical Chemistry* 87 (**1983**) 3747.

49. K.R. Harikumar and C.N.R. Rao, 'Interaction of CO with Cu/ZnO catalyst surfaces prepared in situ in the electron spectrometer: evidence for CO_2 and related species relevant to methanol synthesis', *Applied Surface Science* 125 (**1998**) 245-249.

50. E.I. Solomon, P.M. Jones, and J.A. May, 'Electronic Structures of Active Sites on Metal Oxide Surfaces: Definition of the Cu/ZnO Methanol Synthesis Catalyst by Photoelectron Spectroscopy', *Chemical Reviews* 93(8) (**1993**) 2623-2644.

51. D.F. Cox and K.H. Schulz, 'Interaction of CO with Cu^+ cations: CO adsorption on Cu_2O(100)', *Surface Science* 249 (**1991**) 138-148.

52. G.E. Parris and K. Klier, 'The Specific Copper Surface Areas in Cu/ZnO Methanol Synthesis Catalysts by Oxygen and Carbon Monoxide Chemisorption: Evidence for Irreversible CO Chemisorption Induced by the Interaction of the Catalyst Components', *Journal of Catalysis* 97 (**1986**) 374-384.

53. K.-D. Jung and O.-S. Joo, 'Study on CO Adsorption on in-situ Brass Formed Cu/ZnO', *Bulletin of the Korean Chemical Society* 23(12) (**2002**) 1765-1768.

54. S.V. Didziulis, K.D. Butcher, S.L. Cohen, and E.I. Solomon, 'Chemistry of Copper Overlayers on Zinc Oxide Single-Crystal Surfaces: Model Active Sites for Cu/ZnO Methanol Synthesis Catalysts', *Journal of the American Chemical Society* 111 (**1989**) 7110-7123.

55. J. Kwon, M. Dai, M.D. Halls, E. Langereis, Y.J. Chabal, and R.G. Gordon, 'In Situ Infrared Characterization during Atomic Layer Deposition of Lanthanum Oxide', *Journal of Physical Chemistry C* 113 (**2009**) 654-660.

56. A. Neumann and D. Walter, 'The thermal transformation from lanthanum hydroxide to lanthanum hydroxide oxide', *Thermochimica Acta* 445 (**2006**) 200-204.

57. T. Shido and Y. Iwasawa, 'The effect of coadsorbates in reverse-water gas shift reaction on ZnO, in relation to reactant-promoted reaction mechanism', *Journal of Catalysis* 140 (**1993**) 575-584.

58. Y. Amenomiya and G. Pleizier, 'Alkali-Promoted Alumina Catalysts II. Water-Gas Shift Reaction'', *Journal of Catalysis* 76 (**1982**) 345-353.

59. P. Liu and J.A. Rodriguez, 'Water-gas-shift reaction on metal nanoparticles and surfaces', *Journal of Physical Chemistry* 1226(16) (**2007**) 164705.

CHAPTER SIX

Pyrophoricity and stability of copper and platinum based water-gas shift catalysts during oxidative shut-down/start-up operation

6.1 Introduction

The water gas-shift (WGS) reaction ($CO + H_2O \leftrightarrow CO_2 + H_2$) is useful for conditioning hydrocarbon reformed gas for fuel cells because of its ability to remove CO, which is a poison to the Pt electrodes in fuel cells [1, 2], while at the same time generating additional hydrogen [3]. The industrial WGS process is carried out in two stages to overcome the thermodynamic and kinetic limitations of the reaction to achieve high CO conversion [3, 4]. The two steps involve a high-temperature (350-500°C) shift over Fe_2O_3/Cr_2O_3 catalysts followed by a low temperature (200-250°C) shift (LT-WGS) over $Cu/ZnO/Al_2O_3$ catalysts [3]. However, this configuration is not economically feasible for fuel cell type operations [5] encouraging efforts to develop alternate systems which can operate at LT-WGS conditions.

The most intensively studied catalysts for the LT-WGS reaction are Cu/ZnO [6-8], and Pt- [9-11] and Au-loaded [12, 13] metal oxide catalysts. Metal oxide supported Pt and Au catalysts are reported as promising LT-WGS catalysts compared with conventional Cu/ZnO as they are resistant to chlorine and sulphur poisoning, robust and stable in terms of frequent shut-down/start-up type operations common during fuel cell operation

and are not pyrophoric (i.e. temperature rise in the catalyst bed due to spontaneous ignition under an oxidative environment) [14-17].

Precious metals supported on the following oxides are the most effective LT-WGS catalysts [15] and are ranked from descending order in terms of activity: Pt (TiO_2 > CeO_2 > ZrO_2) [14, 15, 18] and Au (CeO_2 > TiO_2 > Fe_2O_3 >ZrO_2) [15, 19, 20]. Unfortunately, they can be prone to thermal instability and rapid deactivation similar to most Cu catalysts. Fu et al. [17] reported the deactivation of Au/CeO_2 during LT-WGS operation was due to both the loss of CeO_2 support area during steady-state reaction and the formation of cerium oxide-hydroxycarbonate (a reaction inhibitor) during shut-down/start-up operation from water condensate. Kim et al. [21] also found the formation of thermally stable carbonate species covering the surface of Au/CeO_2, which blocked the active sites. Denkwit et al. [22] elaborated that the carbonate was of monodentate carbonate species which predominately inhibited the LT-WGS reaction, while their formation was enhanced by CO_2 in the feed gas [22, 23]. Pt/TiO_2 is also unstable as sintering of the active Pt metal sites happens readily during LT-WGS operation [14, 24, 25].

It is well documented that Cu/ZnO-based catalysts are susceptible to sintering, the primary cause of deactivation [6, 26]. Shishido et al. [26] showed that the stability of Cu/ZnO catalysts was dependent on the initial H_2 pretreatment, and the sintering of Cu particles was the main source of catalyst deactivation. Guo et al. [27] reported that the shut-down/start-up cycles during LT-WGS operation did not affect the activity of Cu/ZnO-based systems even when water was condensed on the catalyst during the shut-down period. They argued that deactivation of the Cu/ZnO/Al_2O_3 catalyst was mainly

attributed to the loss of active sites from the formation of carbonate species rather than the sintering of Cu crystallites [27].

This study investigates the activity and stability of Cu/ZnO-based catalysts, including those loaded with refractory oxides such as Al_2O_3 and La_2O_3, and Pt-based catalysts during oxidative shut-down/start-up LT-WGS operating conditions. Cu/ZnO-based catalysts have been previously observed as pyrophoric while Pt-based catalysts are not, however the effect of pyrophoricity on catalyst characteristics and subsequent LT-WGS performance has not been systematically investigated. The knowledge gained here allows for assessment of the suitability of these catalysts for fuel cell application.

6.2 Experimental

6.2.1 Catalyst preparation

A flame spray pyrolysis (FSP) reactor [28] was used to synthesize Cu/ZnO, Cu/ZnO/La_2O_3, Cu/ZnO/Al_2O_3, Pt/TiO_2, Pt/CeO_2 and Pt/ZrO_2 particles. The Cu loading was maintained at approximately 37 wt%, with La loaded at 2.3 wt%. The Cu/ZnO/Al_2O_3 catalyst (F-COM) was fabricated based on a typical commercial catalyst composition with weight ratio of 37:55:8, respectively [29]. Pt loading was maintained at approximately 1 wt% of their respective oxide supports. In the case of copper based catalysts, precursor solutions containing predetermined amounts of metal oxides with a total molar concentration of 0.5 M were prepared by mixing zinc 2-ethylhexanoate (Alfa, purity > 99%), lanthanum (III) 2-ethylhexanoate (10 wt% in hexane solution, Aesar), aluminium s-butoxide (Strem, purity > 98%), and a copper 2-ethylhexanoate

(Aldrich, purity > 99.9%) in xylene (Riedel de Haen, 96%). For platinum based catalysts, precursor solutions of titanium(IV) isopropoxide (TTIP, 97% purity, Aldrich), cerium(III) 2-ethylhexanoate (49 wt% in 2-ethylhexanoic acid, Strem), zirconyl 2-ethylhexanoate (Strem) and platinum(II) acetylacetonate (Aldrich, purity > 97%) were used. During FSP synthesis, the liquid precursor was fed (rate: 5 ml min^{-1}) to the flame by a syringe pump (Inotech R232). The generated particles were collected on a glass fibre filter (Whatmann GF/D) with the aid of a vacuum pump (Alcatel). Detailed descriptions on other operating conditions can be found elsewhere [28]. La_2O_3 (Aldrich, 99.9%) was used as the La reference in this study.

6.2.2 Catalyst characterization

X-ray diffraction (XRD) spectra were collected on a Philips X'Pert MPD instrument using Cu Kα (λ = 1.542 Å) with scan range from 20° to 90° at a scan rate of 0.22° min^{-1} and step size of 0.026°. Inductively coupled plasma optical emission spectrometry (ICP-OES) was used to determine the metal content in each synthesized sample. The measurements for Cu catalysts were performed on a Perkin-Elmer OPTIMA DV3000 apparatus and for Pt catalysts, a Varian Vista-MPX. Cu/ZnO samples were dissolved in nitric acid (3 M) before measurement and Pt samples were dissolved in an acid mixture of nitric, hydrochloric and hydrofluoric with 2:6:5 volume ratios, while being heated at 180°C until solution was near dryness. The resultant solution was then cooled and made to volume with a 5% hydrochloric acid matrix before ICP-OES analysis. Copper metal surface area (CSA) was determined by the N_2O decomposition method at 90°C using the same experimental methodology reported by Jensen et al. [30], assuming a reaction

stoichiometry of two Cu atoms per N_2 molecule and a Cu surface density of 1.46 x 10^{19} atom m^{-2} [31]. Prior to the measurement, 30 mg of sample was reduced at 230°C for 30 min and flushed with He (50 mL min^{-1}) for a further 30 min. The dispersion and sizes of the Pt deposits were determined by CO pulse chemisorption using a Micromeritics Autochem 2920 instrument. The Pt/oxide samples were first reduced in 50 ml/min of 10%H_2/N_2 for 60 min at 300°C followed by flushing with 50 ml/min of He at 310°C for another 60 min. Pulse injections (0.5 ml of 10% CO in He) were introduced at 30°C for Pt/TiO_2 and Pt/ZrO_2 assuming a Pt:CO stoichiometric ratio of 1:1 [32]. For Pt/CeO_2 the CO chemisorption was carried out at -80°C by immersing the sample cell in an isopropanol and liquid nitrogen mixture. This ensured the CeO_2 oxide did not interfere with the chemisorption [33]. Dispersion of the Pt deposits is defined as the ratio of the atoms accessible to the CO relative to the total number of Pt atoms in the system. The specific surface areas (SSA) of the prepared catalysts were analysed by nitrogen adsorption at 77 K, on the Micromeritics Tristar 3000, using the BET model.

6.2.3 Catalyst activity

Activity testing was carried out using a 6 mm I.D. stainless steel packed bed reactor with as-prepared catalyst sample (100 mg) diluted with α-Al_2O_3 (70 μm, 500 mg). Prior to the activity test, catalysts were reduced under a total flow of 100 mL min^{-1} (10% H_2/N_2) for 1 h at 230°C and flushed with N_2 for 30 min before returning to ambient temperature. The standard test stream of 100 mL min^{-1} discharging at atmospheric pressure, comprised 7% CO, 8.5% CO_2, 23% H_2O, 37.5% H_2 and 25% N_2 (Coregas) to which deionised water was added via a vaporizer fed by a high precision syringe pump (ISCO Inst., model 260D). The above conditions corresponded to a gas hourly space

velocity of 11 000 h^{-1}. Operating temperature ranged from 150°C to 300°C with 50°C increments at 10°C min^{-1}. The gases were fed by mass flow controllers (Brooks). The product stream, after passage through an ice trap to remove water, was analysed using two gas chromatographs (Shimadzu GC8A) fitted with thermal conductivity detectors. One chromatograph was operated with helium passing through a 1.8-m CTR I column (Alltech Associates, Inc) for analysis of CO_2, CO, N_2, O_2 and CH_4. The other used argon passing through a 2 m molecule sieve 13X column (Alltech Associates, Inc) for H_2 analysis. CO conversion was removed from thermodynamic equilibrium [34] to induce low residence times and avoid the impact of mass transfer limitations on the results. Further details regarding the calculations for CO conversion are provided in Supporting Information (A).

6.2.4 Cyclic shut-down/start-up operation of catalyst under oxidative environment

This experiment was designed to analyse the pyrophoricity of the catalyst during LT-WGS operation. Cyclic shut-down/start-up operation under an oxidative environment was evaluated after 1 h of LT-WGS steady-state reaction at 230°C; catalysts were not pre-treated with H_2 in this experiment. The reactor was cooled to room temperature under 100 mL min^{-1} of air and then heated to 230°C at a rate of 10°C min^{-1} under reformate gas until steady-state was reached. The cycle was repeated five times. Catalyst samples were not diluted with α-Al_2O_3 in this series of experiments due to the need for post-reaction characterisation.

6.2.3 Temperature-programmed reduction and oxidation

Temperature-programmed reduction (TPR) and temperature-programmed oxidation (TPO) experiments were performed on a Micromeritics Autochem 2920 instrument interfaced with a thermal conductivity detector (TCD). The TCD results were normalised to the mass of the sample used in the experiments. An isopropanol cooling trap was placed between the sample and the TCD to retain water formed during the reduction process. Downstream to the TCD, gases were analysed by an online mass spectrometer (Balzers Thermostar Quadrupole). For TPR experiments, each sample (50 mg) was pretreated at 120°C under He (50 mL min^{-1}) for 1 h then cooled to ambient temperature. TPR was then performed under 5%H_2/He (50 mL min^{-1}) at a ramp rate of 5°C min^{-1} to 400°C with the results recorded by the TCD.

During TPO, the catalyst bed was ramped to 500°C at 10°C min^{-1} under 5%O_2/He (50 mL min^{-1}) with the results analysed by the mass spectrometer. Previous work [35] showed that CO_2 would evolve when the carbonaceous species on the surface of the catalyst were oxidised. No catalyst pre-treatment was conducted prior to TPO experiments.

6.3 Results and discussion

6.3.1 Structural characterization of catalysts

The structural properties of the materials are summarised in Table 6.1. In the case of Cu/ZnO, the additional cations such as La^{3+} and Al^{3+} increased the specific surface area

of the bulk catalyst compared to the neat Cu/ZnO. This was due to the enhanced competition for oxygen between the metallic species that confined the growth of the oxides [36]. The presence of low Pt loading (1 wt%) is known to have very little influence on the surface area of the oxide support compared to bare oxides during FSP synthesis [28, 37] as also demonstrated here. Although not provided, all the prepared samples exhibited Type II N_2 adsorption-desorption isotherms, suggesting the particles were nonporous, as is frequently observed for flame-made particles [38].

The crystallite size of FSP-prepared catalysts was evaluated from XRD using the Scherrer formula, and indicated the particles were all in the nano-size range (Table 6.1). The XRD spectra of nominal 37 wt% Cu loaded on ZnO-based nanoparticles (Fig. 6.1a) showed the hexagonal phase of ZnO [39], indicated by (●), was maintained over the 2.3 wt% La and 8 wt% Al_2O_3 (shown as F-COM) loaded concentrations. The elevated Cu loading was also detectable by XRD and gave a weak Bragg reflection at $2\theta = 38°$, belonging to the monoclinic CuO (111) phase [40]. There was no detectable XRD reflection from La_2O_3 and Al_2O_3 crystallites and no shift in Bragg positions of ZnO for the composite Cu/ZnO catalyst. The CuO (111) XRD reflection, indicated by (○) in Fig. 6.1a, was too small for accurate crystallite size determination. The XRD was unable to detect the presence of Pt, possibly due to the low metal loading in the samples. There was no significant alteration in the oxide support XRD spectra from the addition of 1 wt% Pt loading (Fig. 6.1b). The TiO_2 oxide support contained 85 wt.% anatase and the balance rutile, typical for flame-made 1%Pt/TiO_2 under lean conditions [28, 41]. The fluorite structure of CeO_2 was maintained [42] when loaded with 1 wt% Pt. A pattern typical of monoclinic zirconia in its tetragonal phase [43] was also observed.

The N_2O decomposition data indicated the Cu dispersion was lowered by introducing La or Al compared to the neat Cu/ZnO. The decrease in metallic Cu surface area with increasing La loading may arise from the formation of a solid solution between CuO and La_2O_3 [44] and Al_2O_3 crystals [45]. In this study, Pt dispersion was the highest when loaded on the ZrO_2 support.

Table 6.1: Physicochemical properties and metal dispersion of fresh Cu/ZnO-based and Pt-based catalysts.

Sample	BET surface area ($m^2\ g^{-1}$)	Cu or Pt metal content (wt%)[a]	Crystallite size of oxide support (nm)	Metal dispersion (%)[b]
37%Cu/ZnO	67.5	37.3	17	12.4
Cu/ZnO/La_2O_3 (37:61:2)	72.8	38.3	15	5.4
F-COM Cu/ZnO/Al_2O_3 (37:50:8)	80.3	37.0	14	3.9
TiO_2	121.1	-	14	-
CeO_2	103.9	-	22	-
ZrO_2	75.3	-	24	-
1%Pt/TiO_2	119.7	1.05	14	25.7
1%Pt/CeO_2	106.4	0.99	22	20.2
1%Pt/ZrO_2	74.1	0.95	24	66.8

[a] Determined by ICP-OES analysis.
[b] Cu dispersion was determined by N_2O decomposition and Pt dispersion was determined by CO chemisorption.

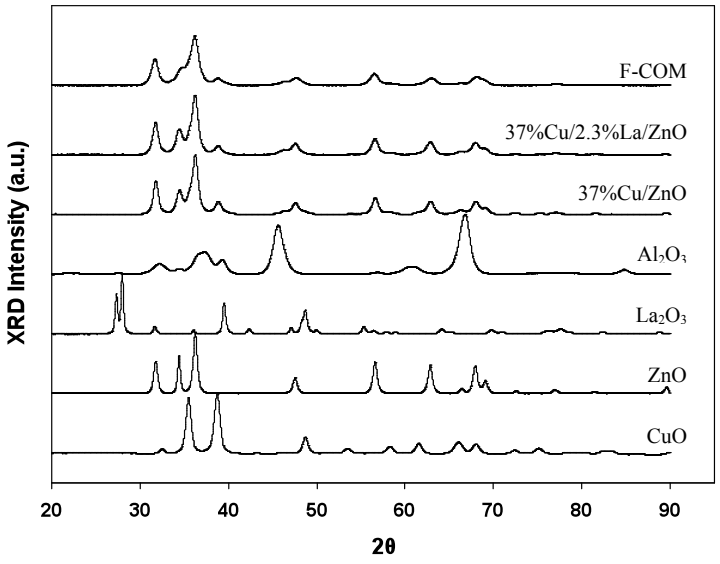

(a)

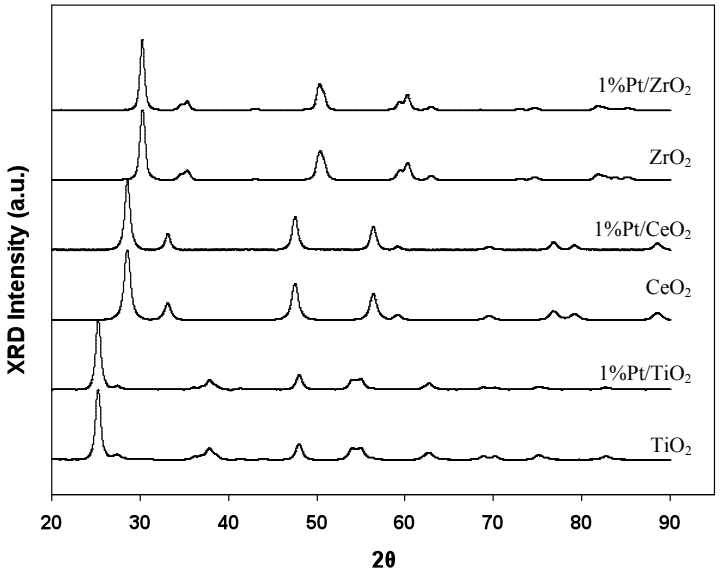

(b)

Fig. 6.1: XRD spectra of FSP-made: (a) 37%Cu/ZnO loaded with cations (Al and La). Pure CuO, ZnO, Al_2O_3 and La_2O_3 are included for comparison. The solid circles (●) represent characteristic peaks of ZnO hexagonal wurzite-phase. The open circle (○) denotes peaks of monoclinic CuO (111) phase; (b) 1%Pt catalyst on TiO_2, CeO_2 and ZrO_2 oxide support. Pure TiO_2, CeO_2 and ZrO_2 are included for comparison.

6.3.2 TPR analysis

The TPR profiles of neat Cu/ZnO, La-loaded Cu/ZnO and F-COM are shown in Fig. 6.2a. The strong reduction peak at 210°C for both neat Cu/ZnO and La-loaded Cu/ZnO and at 235°C for F-COM were attributed to the reduction of CuO to metallic Cu as described by Eq. 6.1 [46].

$$CuO + H_2 \rightarrow Cu^0 + H_2O \qquad \Delta H = -80.8 \text{ kJ mol}^{-1} \qquad \text{(Eq. 6.1)}$$

Although bulk ZnO reduction is thermodynamically feasible, temperatures as high as 650°C are required to reduce ZnO to metallic zinc [47] with no ZnO reduction peaks observed in this study (up to 400°C). The TPR profiles also show the occurrence of shoulder between 170°C to 200°C for the neat and La-loaded Cu/ZnO and between 180°C to 210°C for the F-COM catalyst. This shoulder connotes the possibility of surface CuO reduction which is kinetically faster and precedes the reduction of bulk CuO (within the ZnO matrix) Turco et al. [48] observed a similar phenomenon in their Cu/ZnO/Al_2O_3 system.

Hydrogen-TPR profiles obtained from the FSP synthesized Pt catalysts are shown in Fig 6.2b. In accordance to previously reported data [18], the first peak corresponded to the reduction of PtO_x species, occurring at 305°C when supported on TiO_2, 200°C for CeO_2 and 300°C for the ZrO_2 support. The Pt/CeO_2 sample displayed two additional broad and asymmetrical peaks at ~ 380°C and 900°C, typical of neat CeO_2 [49]. These have been assigned by others as due to the surface and bulk reductions of CeO_2 to Ce_2O_3, respectively [50, 51].

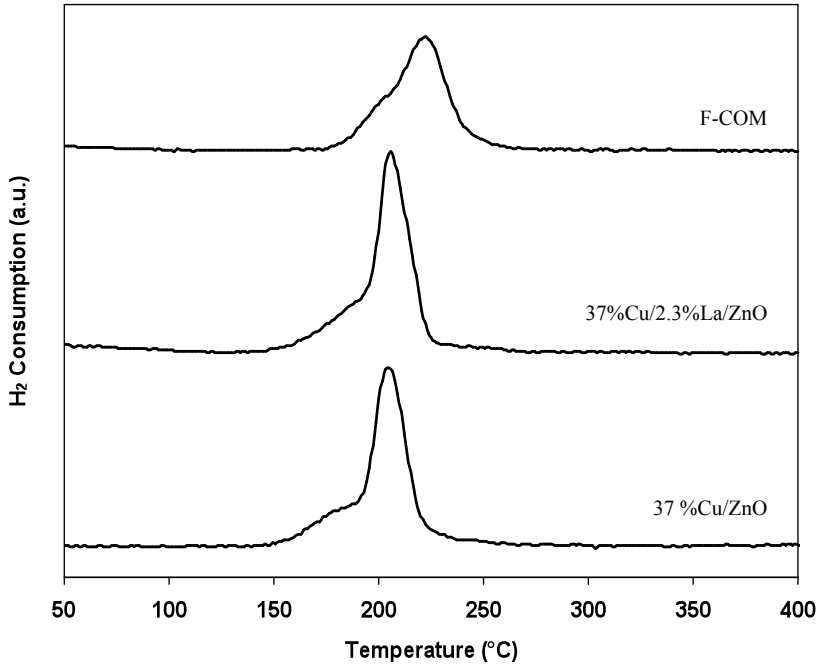

(a)

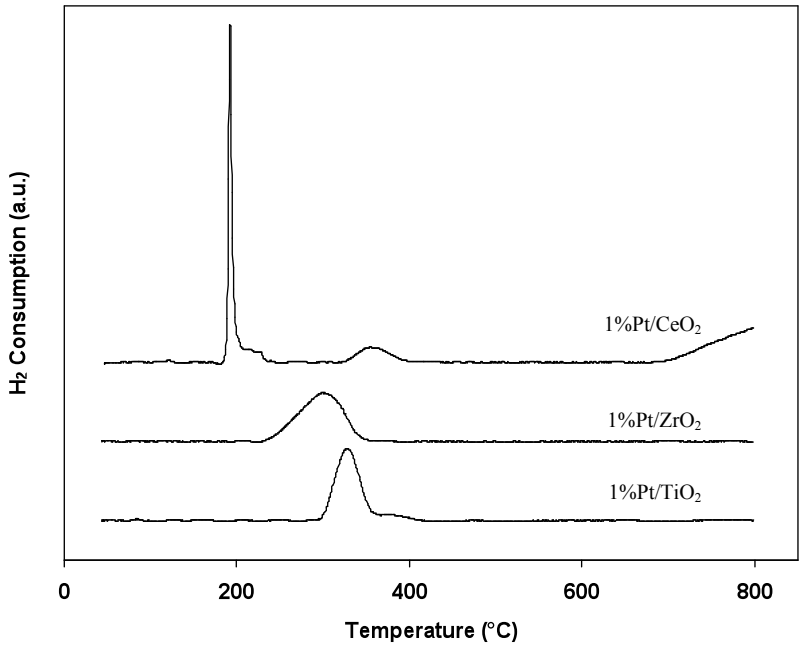

(b)

Fig. 6.2: H_2-TPR profiles of FSP-prepared: (**a**) 37% Cu/ZnO-based catalysts; (**b**) 1%Pt-based catalysts.

6.3.3 Catalyst activity

All catalysts were tested for LT-WGS activity using a gas mixture simulating the typical composition of a reformate stream (Fig 6.3a-b). The LT-WGS activities were evaluated based on the attained CO conversion. In general, Cu/ZnO-based catalysts were more active compared to Pt-based catalysts in the temperature range 150°C to 300°C. The addition of doping agents such as lanthanum and alumina imparted a noticeable effect on the catalyst's LT-WGS performance. While 2.3% La doping was beneficial for the Cu/ZnO LT-WGS performance, alumina promoted a decrease in activity (Fig. 6.3a). Our previous work found that the inclusion of 2.3 wt% La into Cu/ZnO improved catalyst activity compared with neat Cu/ZnO owing to electron density modification of the Cu specie and enhanced adsorption of H_2O due to the presence of La^{3+} [52]. However, the addition of Al^{3+} to Cu/ZnO resulted in a reduction in LT-WGS activity with the explanation given elsewhere [52].

In terms of the Pt-based metal oxides, Pt/TiO_2 was the most active catalyst followed by Pt/CeO_2 and then Pt/ZrO_2 (Fig. 6.3b). These catalyst formulations have been studied by others [9, 14, 15, 18, 53] with the catalyst activity order in this study agreeing with results found in literature. Azzam et al. [9, 14] showed the difference in activity was due to the influence of the oxide supports as they play a significant role in determining the mechanistic reaction sequence for the LT-WGS reaction over Pt-based catalysts. In this work, no apparent correlation can be drawn between the LT-WGS activity of the catalysts and the reducibility of their metals (Cu and Pt) (Fig. 6.2a-b) or their metal dispersion (Table 6.1).

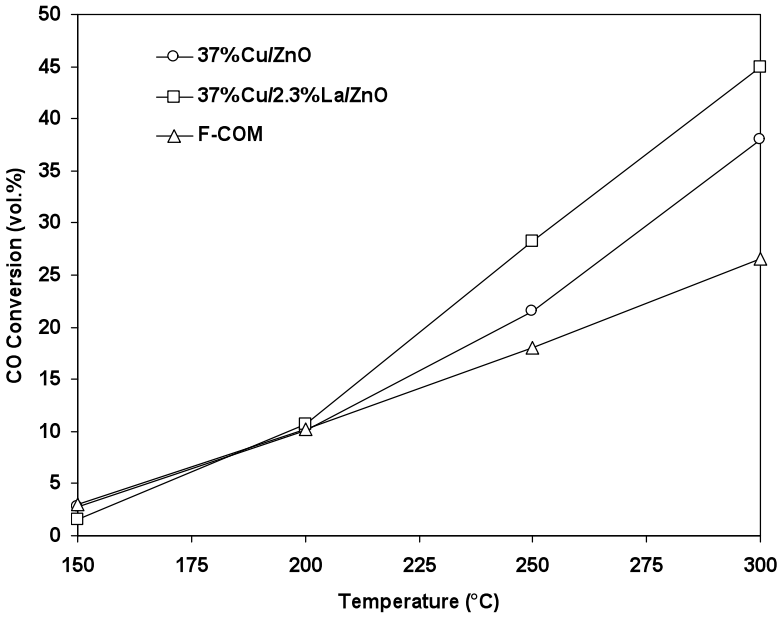

(a)

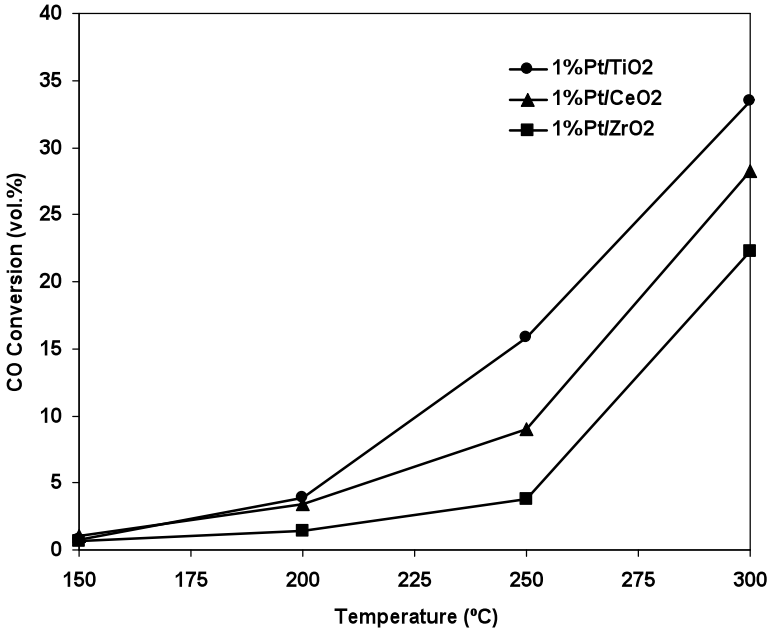

(b)

Fig. 6.3: LT-WGS activity of: (a) 37% Cu/ZnO-based catalysts; (b) 1% Pt-based catalysts. Reaction conditions: operating temperature 150-300°C, total flow = 100 mL min^{-1} (7% CO, 8.5% CO_2, 23% H_2O, 37.5% H_2 and 25% N_2); catalyst loading = 0.10 g; pressure = 1 atm.

6.3.4 Activity and stability of catalysts under oxidative shut-down/start-up operation

All the Cu-based catalysts exhibited signs of deactivation during the shut-down/start-up oxidative operation (Fig. 6.4a). At the fifth cycle, the La-loaded material retained the highest LT-WGS activity even though its CO conversion decreased from 30% to 15%. The neat Cu/ZnO lost almost all its initial LT-WGS activity decreasing from 22% down to 5% CO conversion after five cycles. The extent of deactivation for F-COM was not as profound as the other two but its CO conversion nevertheless decreased from 15% to 10%. To evaluate the catalyst's pyrophoricity, the temperature of the catalyst bed was monitored during the shut-down/start-up operation (Fig. 6.5). Within 30 seconds the temperature of the catalyst bed increased from 230°C to 340°C for the neat Cu/ZnO when the reformate feed was switched to air, while the temperature reached 350°C for La-loaded Cu/ZnO and 360°C for F-COM. This elevated temperature was maintained for 2 to 3 minutes before a gradual return to ambient temperature.

In the case of the Pt series, Pt/TiO_2 lost the greatest proportion of its LT-WGS activity compared with the other two catalysts (Fig. 6.4b) with its CO conversion decreasing from 16% to 7%. A small decrease in CO conversion, from 5% to 2%, was observed for Pt/ZrO_2. Interestingly, Pt/CeO_2 maintained its activity throughout the shut-down/start-up cycles with no observed deactivation. No signs of pyrophoricity were observed for Pt-based catalysts, with no significant changes in the catalyst bed temperature when air was introduced into the system (Fig. 6.5).

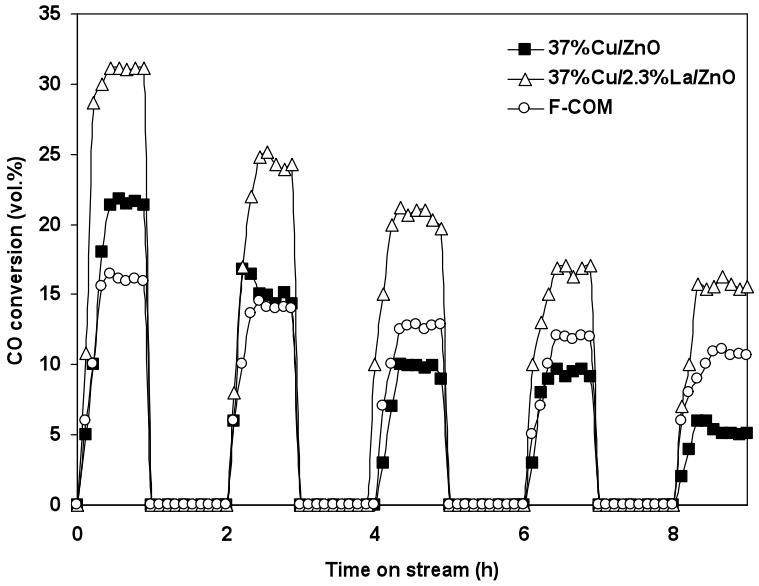

(a)

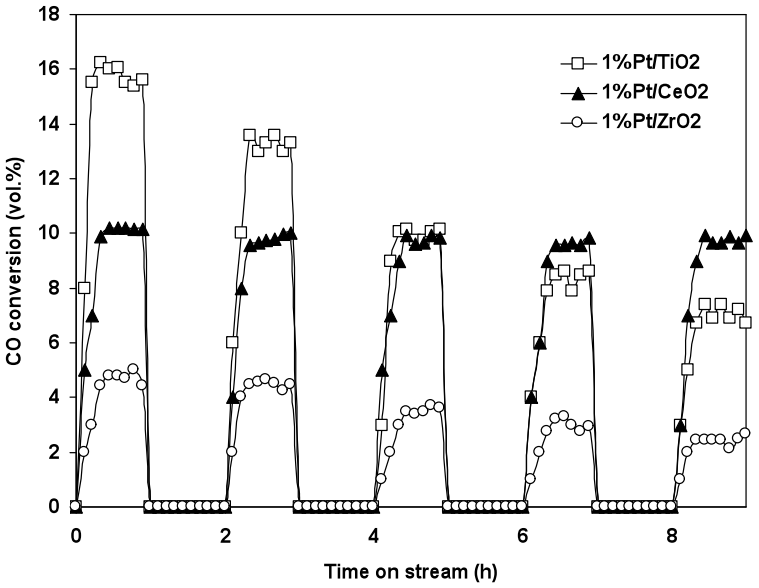

(b)

Fig. 6.4: LT-WGS activity of: (a) 37%Cu/ZnO-based; (b) 1%Pt-based catalysts during oxidative cyclic shut-down/start-up operations. Reaction conditions per cycle: LT-WGS operating temperature 230°C, operating time = 1 h, total flow = 100 ml min^{-1} (7% CO, 8.5% CO_2, 23% H_2O, 37.5% H_2 and 25% N_2); catalyst loading = 0.10 g; pressure = 1 atm; oxidative cooling with air at 100 ml min^{-1} for 1 h.

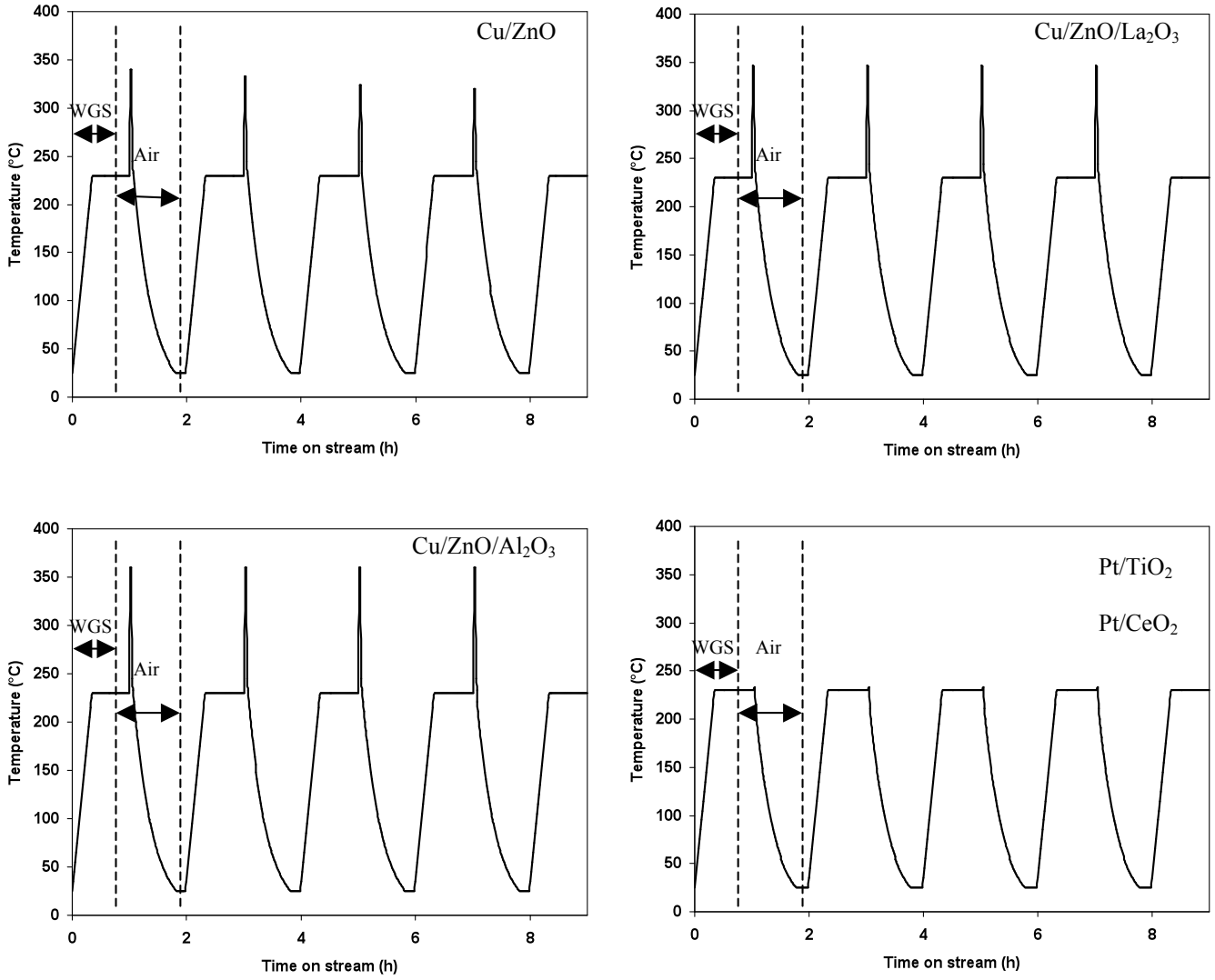

Fig. 6.5: Temperature profile of catalyst beds during 4 cycles of oxidative cyclic shut-down/start-up LT-WGS operations. Reaction conditions per cycle: LT-WGS operating temperature 230°C, operating time = 1 h, total flow = 100 ml min^{-1} (7% CO, 8.5% CO_2, 23% H_2O, 37.5% H_2 and 25% N_2); catalyst loading = 0.10 g; pressure = 1 atm; oxidative cooling with air at 100 ml min^{-1} for 1 h.

6.3.5 Post-cycle catalyst characterization

It is commonly known that Cu/ZnO is susceptible to sintering [6, 26] during LT-WGS operation, with a small amount of refractory oxide such as Al_2O_3 or Cr_2O_3 typically added to stabilize the Cu/ZnO structure [7, 54]. In this work, post-reaction catalyst characterization on Cu/ZnO-based catalysts for the oxidative cyclic operation showed significant sintering of the bulk catalyst and the metallic phases (Fig. 6.6a). The neat Cu/ZnO lost 64% and 89% of its initial SSA and CSA, respectively, while the La-loaded Cu/ZnO lost 55% and 61% of its initial SSA and CSA, respectively. F-COM experienced the lowest relative loss of SSA (31%) and CSA (60%) of the three catalysts. The loss in substrate is closely reflected by the observed decrease in LT-WGS activity. That is, the neat Cu/ZnO displayed the greatest loss in SSA and CSA as well as LT-WGS activity while F-COM displayed the smallest decrease in all these aspects. These findings succinctly demonstrate the capacity of Al_2O_3 for stabilizing the Cu/ZnO structure, albeit at the expense of catalyst activity.

The Pt-loaded catalysts showed some markedly different variations in characteristics compared with the Cu/ZnO catalysts after the cyclic operation. The changes in bulk surface areas of Pt/TiO_2 and Pt/CeO_2 were minimal, suggesting strong thermal stability of the oxide support (Fig 6.6b). Conversely, Pt/ZrO_2 lost 25% of its initial SSA. However, variations in Pt dispersion differed to SSA changes to some extent with Pt/TiO_2 losing 80% of its original Pt dispersion, Pt/ZrO_2 losing 93% of its original Pt dispersion and Pt/CeO_2 retaining its original Pt dispersion. The decrease in activity for Pt/TiO_2 can be attributed solely to the sintering of Pt during the LT-WGS reaction as no pyrophoricity was evident in the cyclic process. Evidence of Pt sintering when loaded

on TiO_2 has been found by others for the LT-WGS process [24, 25]. The loss in activity of Pt/ZrO_2 may be attributed to a combination of loss in SSA as well as loss in Pt dispersion. No sign of Pt sintering was observed when supported on CeO_2 after the oxidative cyclic operation with this mirrored by its LT-WGS stability during the oxidative cycling treatment. The high stability of Pt on CeO_2 in this study agrees with previously reported work from Nagai et al. [55] who specifically compared the stability of metallic Pt on CeO_2 and on Al_2O_3. Nagai et al. [55] observed the metallic phase of Pt on CeO_2 did not sinter even after subjecting the catalysts to oxidative treatment at 800°C. They found the Pt-O-Ce bond (i.e. the Pt and oxide support interaction) had the ability to anchor the metallic Pt by preventing the migration and coalescence of the metal crystallites [55]. The post-characterization results suggest the stability of a Pt catalyst is highly dependent on the degree of Pt sintering.

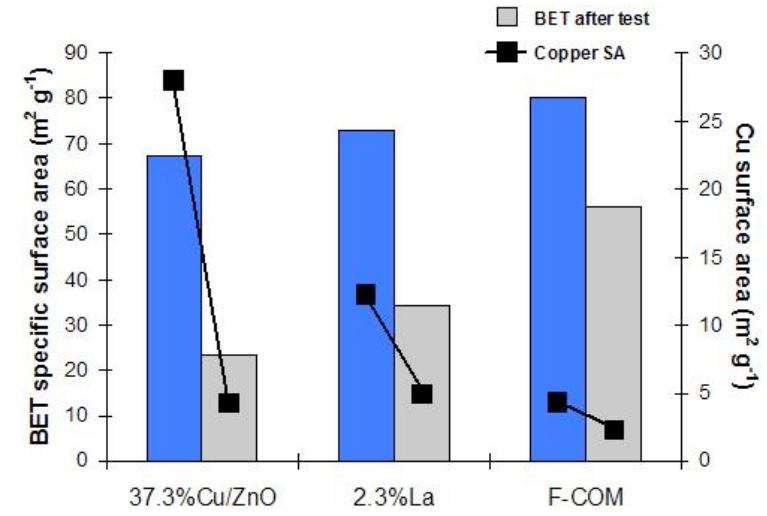

(a)

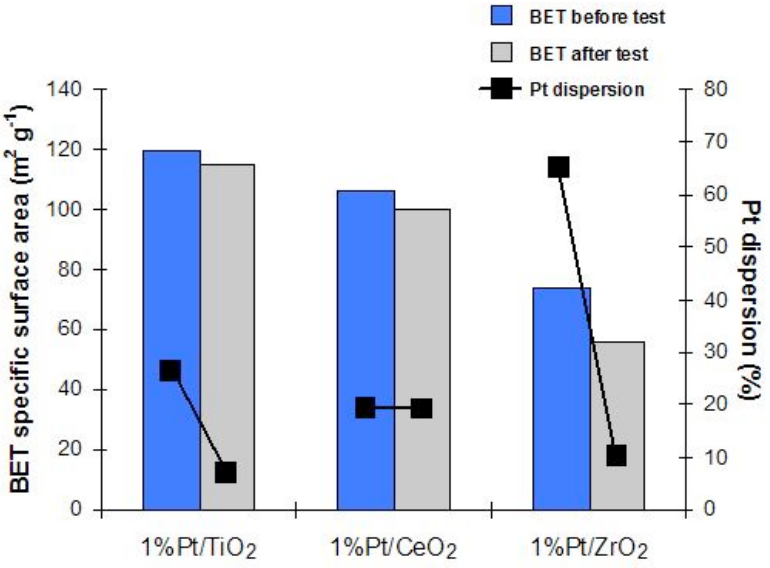

(b)

Fig. 6.6: (a) Specific surface area and Cu surface area changes for: (a) 37.3%Cu/62.7%ZnO, 38.3%Cu/2.3%La/59.4%ZnO and F-COM (37%Cu/54.9%ZnO/8.1%Al_2O_3); (b) surface area and Pt dispersion changes for 1%Pt/TiO_2, 1%Pt/CeO_2 and 1%Pt/ZrO_2 following the shutdown/start-up oxidative LT-WGS reaction for 5 cycles. Reaction temperature = 230°C.

6.3.6 TPO analysis

It is commonly reported that LT-WGS catalyst deactivation also results from the accumulation of carbonaceous species on the catalyst surface leading to blockage of the active sites [27, 35, 51, 56]. To assess whether a build-up of carbonaceous species contributed to catalyst deactivation in this study, TPO experiments were administered to the fresh and spent catalysts. Fig. 6.7a and 6.7b show no accumulation of carbonaceous species on any catalyst surface after the oxidative cyclic LT-WGS reaction. Moreover, it appeared that intrinsic carbonaceous species on the fresh catalyst were removed during the LT-WGS reaction as the CO_2 signal was in most instances substantially much lower for the spent material. This finding indicates catalyst deactivation was not due to the surface accumulation of carbonaceous species hence presenting the product distribution of these carbonaceous species is not necessary.

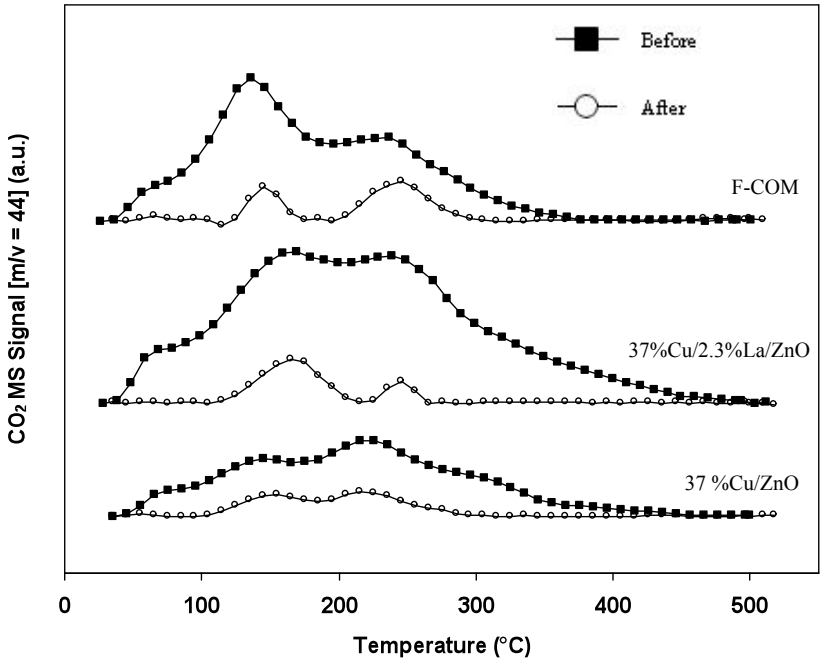

(a)

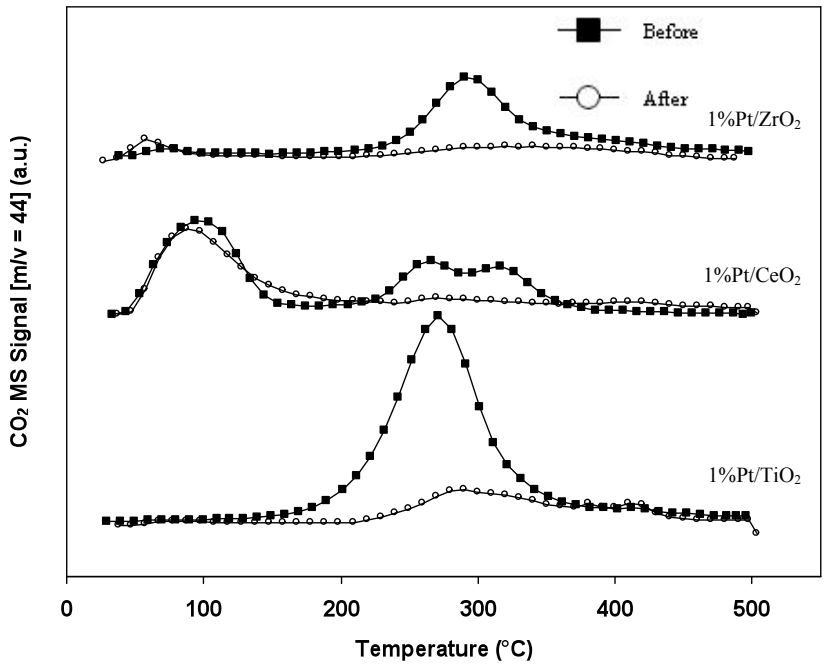

(b)

Fig. 6.7: Comparison of TPO curves for: (**a**) 37%Cu/ZnO-based; (**b**) 1%Pt-based catalysts before and after the 5 cycles of oxidative shut-down/start-up LT-WGS operation.

6.4 Conclusions

The performances of Cu/ZnO-based catalysts were found to be superior compared with 1 wt% Pt-based catalysts for the LT-WGS reaction. La-loaded Cu/ZnO offered the highest activity in terms of CO conversion among the catalysts assessed in this work. The most active Pt catalysts on metal oxide supports followed the order of TiO_2 > CeO_2 > ZrO_2. No evidence was found to correlate the reducibility of the catalyst or specific surface area to their LT-WGS activity. During the oxidative shut-down/start-up LT-WGS operation, the Cu/ZnO-based catalyst displayed pyrophoricity with a marked

increase of temperature in the catalyst bed (up to 360°C) that occurred upon the introduction of air to the system. This pyrophoric property was likely to be responsible for catalyst deactivation, as reflected by the sintering of the bulk and the metallic phases of the materials. In contrast, Pt-based catalysts did not display pyrophoricity with no change in the catalyst bed temperature as air was introduced. Deactivation of the Pt catalysts was mainly due to the loss of active sites, evidenced by the decrease in Pt dispersion. However, the activity of Pt/CeO_2 was maintained throughout the cyclic operation which was congruent with the retention of its original specific surface area and Pt-dispersion making it the most suitable candidate of the materials investigated for fuel cell type operations. TPO studies demonstrated that carbonaceous species, commonly thought to be a source of catalyst deactivation, were not formed as a result of the oxidative shut-down/start-up cyclic operation.

6.5 References

1. J. Larminie and A. Dicks, *Fuel Cell Systems Explained*, Wiley, New York, **2000**.
2. D.L. Trimm and Z.I. Onsan, 'Onboard fuel conversion for hydrogen-fuel-cell-driven vehicles ', *Catalysis Reviews* 43 (**2001**) 31–84.
3. C.H. Bartholomew and R.J. Farrauto, *Fundamentals of Industrial Catalytic Processes*. 2nd Edition ed, John Wiley & Sons, Ltd, Hoboken, NJ, **2006**.
4. C.L. Thomas, 'Catalytic Processes and Proven Catalysts', *Academic Press, New York* (**1970**).
5. D.L. Trimm, 'Minimisation of carbon monoxide in a hydrogen stream for fuel cell application', *Applied Catalysis A: General* 296 (**2005**) 1–11.

6. T. Shishido, M. Yamamoto, I. Atake, D. Li, Y. Tian, H. Morioka, M. Hondac, T. Sano, and K. Takehira, 'Cu/Zn-based catalysts improved by adding magnesium for water–gas shift reaction', *Journal of Molecular Catalysis A: Chemical* 253 (**2006**) 270-278.

7. M.S. Spencer, 'The role of zinc oxide in Cu/ZnO catalysts for methanol synthesis and the water-gas shift reaction', *Topics in Catalysis* 8 (**1999**) 259-266.

8. H. Yahiro, K. Murawaki, K. Saiki, T. Yamamoto, and H. Yamaura, 'Study on the supported Cu-based catalysts for the low-temperature water–gas shift reaction', *Catalysis Today* 126 (**2007**) 436-440.

9. K.G. Azzam, I.V. Babich, K. Seshan, and L. Lefferts, 'Bifunctional catalysts for single-stage water-gas shift reaction in fuel cell applications. Part 1. Effect of the support on the reaction sequence', *Journal of Catalysis* 251 (**2007**) 153-162.

10. I.D. Gonzalez, R.M. Navarro, M.C. Alvarez-Galvan, F. Rosa, and J.L.G. Fierro, 'Performance enhancement in the water–gas shift reaction of platinum deposited over a cerium-modified TiO_2 support', *Catalysis Communications* 9 (**2008**) 1759–1765.

11. P.O. Graf, D.J.M.d. Vlieger, B.L. Mojet, and L. Lefferts, 'New insights in reactivity of hydroxyl groups in water gas shift reaction on Pt/ZrO2', *Journal of Catalysis* 262 (**2009**) 181-187.

12. J.A. Rodriguez, S. Ma, P. Liu, J. Hrbek, J. Evans, and M. Pérez, 'Au(111) in the Water-Gas Shift Reaction Activity of CeO_x and TiO_x Nanoparticles', *Science* 318 (**2007**) 1757-1760.

13. C.H. Kim and L.T. Thompson, 'On the importance of nanocrystalline gold for Au/CeO_2 water–gas shift catalysts', *Journal of Catalysis* 244 (**2006**) 248-250.

14. K.G. Azzam, I.V. Babich, K. Seshan, and L. Lefferts, 'A bifunctional catalyst for the single-stage water–gas shift reaction in fuel cell applications. Part 2. Roles of the support and promoter on catalyst activity and stability', *Journal of Catalysis* 251 (**2007**) 163–171.

15. O. Thinon, F. Diehl, P. Avenier, and Y. Schuurman, 'Screening of bifunctional water-gas shift catalysts', *Catalysis Today* 137 (**2008**) 29-35.

16. Q. Fu, H. Saltsburg, and M. Flytzani-Stephanopoulos, 'Active Nonmetallic Au and Pt Species on Ceria-Based Water-Gas Shift Catalysts', *Science* 301 (**2003**) 935.

17. Q. Fu, W. Deng, H. Saltsburg, and M. Flytzani-Stephanopoulos, 'Activity and stability of low-content gold–cerium oxide catalysts for the water–gas shift reaction', *Applied Catalysis B: Environmental* 56 (**2005**) 57–68.

18. P. Panagiotopoulou and D.I. Kondarides, 'Effect of the nature of the support on the catalytic performance of noble metal catalysts for the water–gas shift reaction', *Catalysis Today* 112 (**2006**) 49–52.

19. R. Burch, 'Gold catalysts for pure hydrogen production in the water–gas shift reaction: activity, structure and reaction mechanism', *Physical Chemistry Chemical Physics* 8 (**2006**) 5483–5500.

20. J.B. Park, J. Graciani, J. Evans, D. Stacchiola, S. Ma, P. Liu, A. Nambu, J.F.n. Sanz, J. Hrbek, and J.A. Rodriguez, 'High catalytic activity of Au/CeOx/TiO2(110) controlled by the nature of the mixed-metal oxide at the nanometer level', *PNAS* 106 (**2009**) 4975–4980.

21. C.H. Kim and L.T. Thompson, 'Deactivation of Au/CeOx water gas shift catalysts', *Journal of Catalysis* 230 (**2005**) 66-74.

22. Y. Denkwitz, A. Karpenko, V. Plzak, R. Leppelt, B. Schumacher, and R.J. Behm, 'Influence of CO_2 and H_2 on the low-temperature water-gas shift reaction on Au/CeO2 catalysts in idealized and realistic reformate', *Journal of Catalysis* 246 (**2007**) 74-90.

23. A. Karpenko, R. Leppelt, J. Cai, V. Plzak, A. Chuvilin, U. Kaiser, and R.J. Behma, 'Deactivation of a Au/CeO_2 catalyst during the low-temperature water–gas shift reaction and its reactivation: A combined TEM, XRD, XPS, DRIFTS, and activity study', *Journal of Catalysis* 250 (**2007**) 139–150.

24. K.G. Azzam, I.V. Babich, K. Seshan, and L. Lefferts, 'Single stage water gas shift conversion over Pt/TiO_2—Problem of catalyst deactivation', *Applied Catalysis A: General* 338 (**2008**) 66–71.

25. X. Zhu, T. Hoang, L.L. Lobban, and R.G. Mallinson, 'Significant Improvement in Activity and Stability of Pt/TiO_2 Catalyst for Water Gas Shift Reaction Via Controlling the Amount of Na Addition', *Catalysis Letters* 129 (**2009**) 135–141.

26. T. Shishido, M. Yamamoto, D. Li, Y. Tian, H. Morioka, M. Honda, T. Sano, and K. Takehira, 'Water-gas shift reaction over Cu/ZnO and Cu/ZnO/Al_2O_3 catalysts prepared by homogeneous precipitation', *Applied Catalysis A: General* 303 (**2006**) 62-71.

27. P.-J. Guo, L.-F. Chen, G.-B. Yu, Y. Zhu, M.-H. Qiao, H.-L. Xu, and K.-N. Fan, 'Cu/ZnO-based water–gas shift catalysts in shut-down/start-up operation', *Catalysis Communications* 10 (**2009**) 1252-1256.

28. W.Y. Teoh, L. Mädler, D. Beydoun, S.E. Pratsinis, and R. Amal, 'Direct (one-step) synthesis of TiO_2 and Pt/TiO_2 nanoparticles for photocatalytic mineralisation of sucrose', *Chemical Engineering Science* 60 (**2005**) 5852 – 5861.

29. M.J.L. Gines, N. Amadeo, M. Laborde, and C.R. Apesteguia, 'Activity and structure-sensitivity of the water-gas shift reaction over Cu-Zn-Al mixed oxide catalysts', *Applied Catalysis A: General* 131 (**1995**) 283-296.

30. J.R. Jensen, T. Johannessen, and H. Livbjerg, 'An improved N_2O-method for measuring Cu-dispersion', *Applied Catalysis A: General* 266 (**2004**) 117-122.

31. J.W. Evans, M.S. Wainwright, A.J. Bridgewater, and D.J. Young, 'On the determination of copper surface area by reaction with nitrous oxide', *Applied Catalysis* 7 (**1983**) 75-83.

32. R. Strobel, W.J. Stark, L. Mädler, S.E. Pratsinis, and A. Baiker, 'Flame-made platinum/alumina: structural properties and catalytic behaviour in enantioselective hydrogenation', *Journal of Catalysis* 213 (**2003**) 296–304.

33. T. Tanabe, Y. Nagai, T. Hirabayashi, N. Takagi, K. Dohmae, N. Takahashi, S.i. Matsumoto, H. Shinjoh, J.N. Kondo, J.C. Schouten, and H.H. Brongersma, 'Low temperature CO pulse adsorption for the determination of Pt particle size in a Pt/cerium-based oxide catalyst', *Applied Catalysis A: General* 370 (**2009**) 108–113.

34. G.C. Chinchen, P.J. Denny, J.R. Jennings, M.S. Spencer, and K.C. Waugh, 'Synthesis of Methanol Part 1. Catalysts and Kinetics', *Applied Catalysis* 36 (**1988**) 1-65.

35. X. Liu, W. Ruettinger, X. Xu, and R. Farrauto, 'Deactivation of Pt/CeO_2 water-gas shift catalysts due to shutdown/startup modes for fuel cell applications', *Applied Catalysis B: Environmental* 56 (**2005**) 69–75.

36. Y. Zhu, C.-H. Sow, T. Yu, Q. Zhao, P. Li, Z. Shen, D. Yu, and J.T.-L. Thong, 'Co-synthesis of ZnO–CuO Nanostructures by Directly Heating Brass in Air', *Advanced Functional Materials* 16(18) (**2006**) 2415 - 2422.

37. W.J. Stark, J.-D. Grunwaldt, M. Maciejewski, S.E. Pratsinis, and A. Baiker, 'Flame-Made Pt/Ceria/Zirconia for Low-Temperature Oxygen Exchange', *Chemistry of Materials* 17 (**2005**) 3352-3358.

38. S.E. Pratsinis, 'Flame aerosol synthesis of ceramic powders ', *Progress in Energy and Combustion Science* 24(3) (**1998**) 197-219.

39. G. Shen, J.H. Cho, J.K. Yoo, G.-C. Yi, and C.J. Lee, 'Synthesis and Optical Properties of S-Doped ZnO Nanostructures: Nanonails and Nanowires', *Journal of Physical Chemistry B* 109 (**2005**) 5491-5496.

40. W. Wang, Y. Zhan, and G. Wang, 'One-step, solid-state reaction to the synthesis of copper oxide nanorods in the presence of a suitable surfactant', *Chemical Communications* (10.1039/b008215p) (**2001**) 727–728.

41. H. Schulz, L. Madler, R. Strobel, R. Jossen, S.E. Pratsinis, and T. Johannessen, 'Independent control of metal cluster and ceramic particle characteristics during one-step synthesis of Pt/TiO_2', *Journal of Materials Research* 20 (**2005**) 2568–2577.

42. R. Kydd, W.Y. Teoh, K. Wong, Y. Wang, Jason Scott, Q.-H. Zeng, A.-B. Yu, J. Zou, and R. Amal, 'Flame-Synthesized Ceria-Supported Copper Dimers for Preferential Oxidation of CO', *Advance Functional Materials* 19 (**2009**) 369-377.

43. W.J. Stark, M. Maciejewski, L. Mädler, S.E. Pratsinis, and A. Baiker, 'Flame-made nanocrystalline ceria/zirconia: structural properties and dynamic oxygen exchange capacity', *Journal of Catalysis* 220 (**2003**) 35–43.

44. K.T. Jacob and K.P. Jayadevan, 'Phase relations in the system Cu-La-O and thermodynamic properties of $CuLaO_2$ and $CuLa_2O_4$', *Journal of Materials Science* 37 (**2002**) 1611 – 1620.

45. W.M. Shaheen, 'Thermal solid-solid interaction and catalytic properties of CuO/Al_2O_3 system treated with ZnO and MoO_3', *Thermochimica Acta* 385(1-2) (**2002**) 105-116.

46. C. Rhodes, G.J. Hutchings, and A.M. Ward, 'Water-gas shift reaction: finding the mechanistic boundary', *Catalysis Today* 23(1) (**1995**) 43-58.

47. T. Imoto, Y. Harano, Y. Nishi, and S. Masuda, 'The Reduction of Zinc Oxide by Hydrogen. III. The Effect of Nitrogen on the Reduction', *Bulletin of the Chemical Society of Japan* 37(4) (**1964**) 441-444.

48. M. Turco, G. Bagnasco, U. Costantino, F. Marmottini, T. Montanari, G. Ramis, and G. Busca, 'Production of hydrogen from oxidative steam reforming of methanol I. Preparation and characterization of $Cu/ZnO/Al_2O_3$ catalysts from a hydrotalcite-like LDH precursor', *Journal of Catalysis* 228 (**2004**) 43-55.

49. P. Panagiotopoulou, J. Papavasiliou, G. Avgouropoulos, T. Ioannides, and D.I. Kondarides, 'Water-gas shift activity of doped Pt/CeO_2 catalysts', *Chemical Engineering Journal* 134 (**2007**) 16-22.

50. S. Letichevsky, C.A. Tellez, R.R.d. Avillez, M.I.P.d. Silva, M.A. Fraga, and L.G. Appel, 'Obtaining CeO_2–ZrO_2 mixed oxides by coprecipitation: role of preparation conditions', *Applied Catalysis B: Environmental* 58 (**2005**) 203–210.

51. A.M.D.d. Farias, P. Bargiela, M.d.G.C. Rocha, and M.A. Fraga, 'Vanadium-promoted Pt/CeO_2 catalyst for water-gas shift reaction', *Journal of Catalysis* 260(1) (**2008**) 93-102.

52. R. Kam, C. Selomulya, R. Amal, and J. Scott, 'The influence of La-doping on the activity and stability of Cu/ZnO catalyst for the low-temperature water–gas shift reaction', *Journal of Catalysis* 273 (**2010**) 73–81.

53. S. Ricote, G. Jacobs, M. Milling, Y. Ji, P.M. Patterson, and B.H. Davis, 'Low temperature water–gas shift: Characterization and testing of binary mixed oxides of ceria and zirconia promoted with Pt', *Applied Catalysis A: General* 303 (**2006**) 35-47.

54. D.S. Newsome, 'The Water-Gas Shift Reaction', *Catalysis Reviews: Science and Engineering* 21(2) (**1980**) 275-318.

55. Y. Nagai, T. Hirabayashi, K. Dohmae, N. Takagi, T. Minami, H. Shinjoh, and S.i. Matsumoto, 'Sintering inhibition mechanism of platinum supported on ceria-based oxide and Pt-oxide–support interaction', *Journal of Catalysis* 242(1) (**2006**) 103–109.

56. A. Gayen, M. Boaro, C.d. Leitenburg, J. Llorca, and A. Trovarelli, 'Activity, durability and microstructural characterization of ex-nitrate and ex-chloride Pt/$Ce_{0.56}Zr_{0.44}O_2$ catalysts for low temperature water gas shift reaction', *Journal of Catalysis* 270(2) (**2010**) 285-298.

CHAPTER SEVEN

Conclusions and Recommendations

7.1 Conclusions

Based on the dry reforming of methane and low-temperature water-gas shift reactions for clean hydrogen generation, a series of platinum and copper supported catalysts were assessed and tested for their reactivity and potential hydrogen production capability under a range of conditions.

Tungsten trioxide (WO_3) system has been observed to be reactive and selective as catalysts for CO-rich syngas and hydrogen in a two-step cyclic steam reforming of methane. Based on this finding, the influence of WO_3 on a Pt/CeO_2 catalyst was investigated in this work for the dry reforming of methane (CH_4). Particular attention was given to the oxygen mobility and capacity of Pt/CeO_2 catalysts owing to the presence of WO_3. TPR analysis showed that the presence of WO_3 improved the redox property of Pt/CeO_2 catalyst by increasing H_2 consumption significantly at temperatures above 700°C. However, at ≥ 30 mol% WO_3 loading, the reduction of surface CeO_2 to Ce_2O_3 was delayed to 400°C as compared to 380°C on a neat Pt/CeO_2 catalyst. This was further supported by XPS assessment which demonstrated a strong Ce-W interaction. Consequently, this behaviour decreased the oxygen mobility on the surface of CeO_2. It was also found that Pt/CeO_2 catalysts loaded with WO_3 at 10 mol% to 20 mol% were

very stable during 20h of dry reforming of methane operation in comparison to a commercial Ni catalyst. However, the catalysts started to loss their activity at 30 mol% WO_3 loading over time, while further addition of WO_3 (>70%) promoted coking on the Pt/CeO_2 sample, ultimately leading to catalyst deactivation.

The influence of metal oxide support (CeO_2, ZnO, TiO_2, SiO_2, Al_2O_3, ZrO_2, MgO and SnO_2) on the performance of Cu-based catalysts synthesized via flame spray pyrolysis was investigated for the low temperature water-gas shift (LT-WGS) reaction. Cu/ZnO attained the highest LT-WGS activity, followed by Cu/MgO, while Cu on other metal supports exhibited minimal or no activity. XPS and H_2-TPR assessments demonstrated interaction between the Cu and oxide support in general although this factor, along with Cu surface area and the support alkalinity, was not found to govern the catalyst activity. CO and H_2O TPD studies showed that the bifunctionality of the catalyst in adsorbing H_2O and CO was crucial in generating LT-WGS activity. Additionally, the findings from this study favoured the occurrence of associative LT-WGS mechanism on Cu/metal oxide catalysts.

The influence of lanthanum (La) doping on the performance of 37 wt% Cu/ZnO catalysts for the low temperature water-gas shift (LT-WGS) reaction was investigated. A 2.3 wt% La loading improved catalyst activity compared to the neat Cu/ZnO and $Cu/ZnO/Al_2O_3$ systems and was accompanied by a lowering of the activation energy. Higher La loadings promoted the adsorption of H_2O at the expense of CO, resulting in a decrease in LT-WGS activity. Additionally, 2.3 wt% La acted to stabilize catalyst activity compared with the neat Cu/ZnO. XPS and H_2-TPR assessment demonstrated a strong interaction between Cu and La components, while data from CO and H_2O TPD

studies favoured the associative WGS mechanism in this instance. Activity and stability findings also suggested metallic Cu was not responsible for LT-WGS activity.

The pyrophoricity of Cu/ZnO-based and Pt-based catalysts was studied during oxidative shut-down/start-up of the low-temperature water-gas shift (LT-WGS) reaction to assess whether these catalysts are suitable for fuel cell application. The Cu/ZnO-based catalysts were observed to display high levels of pyrophoricity manifested as a sharp temperature rise of the catalyst bed upon air introduction. This promoted severe sintering of the bulk and metallic phases of the catalyst facilitating catalyst deactivation. No pyrophoricity was observed for any of the Pt-based catalysts however, sintering of the metallic phase in Pt/TiO_2 and Pt/ZrO_2 persisted, leading to a decrease in activity. It was likely that the sintering of Pt occurred during LT-WGS operation itself. In contrast, Pt/CeO_2 was the only catalyst which retained its activity, displaying no loss in specific surface area or metal dispersion throughout the entire process making it the most suitable candidate of the materials investigated for fuel cell systems. Temperature-programmed oxidation studies indicated deactivation by the oxidative shut-down/start-up operation did not result from the build-up of carbonaceous species.

7.2 Recommendations

In light of the results achieved, the following recommendations for further investigations are suggested:

i. An extensive study of surface adsorption and desorption of involving species, CH_4 and CO_2 over the interface of Pt and CeO_2-WO_3 catalyst. Also, conducting temperature programmed oxidation analysis using CO_2 as a probe molecule on a

reduced Pt/CeO_2-WO_3 catalyst to identify parameters important for dry reforming of methane activity.

ii. Further WGS activity testing on the La/Cu/ZnO catalyst with different feed gas compositions especially gas stream with high CO and CO_2 concentration because such gas stream is related to coal gasification.

iii. The systematic study of other hygroscopic lanthanide oxides formulation (Pr_2O_3, Sm_2O_3, Gd_2O_3, and Dy_2O_3) as promoter for the Cu/ZnO catalyst during low-temperature water-gas shift reaction.

iv. The long term stability and sulphur resistance studies on Pt-based and Cu-based catalyst under various conditions should be studied.

APPENDIX I

Shimadzu 6A integrator was used to determine peak areas and the CO calibration curve was obtained (Fig. S1). The calibration response factor was defined as:

$$R_i = M_i/A_i \qquad \text{(Eq. S1)}$$

Where R_i is the response factor of species i (mol%/peak area)

M_i is the molar percentage of species i (mol%)

A_i is the peak area measured by GC

The catalytic properties were evaluated in terms of CO conversion:

$$\text{CO conversion (\%)} = \frac{(CO)_{in} - (CO)_{out}}{(CO)_{in}} \times 100 \qquad \text{(Eq. S2)}$$

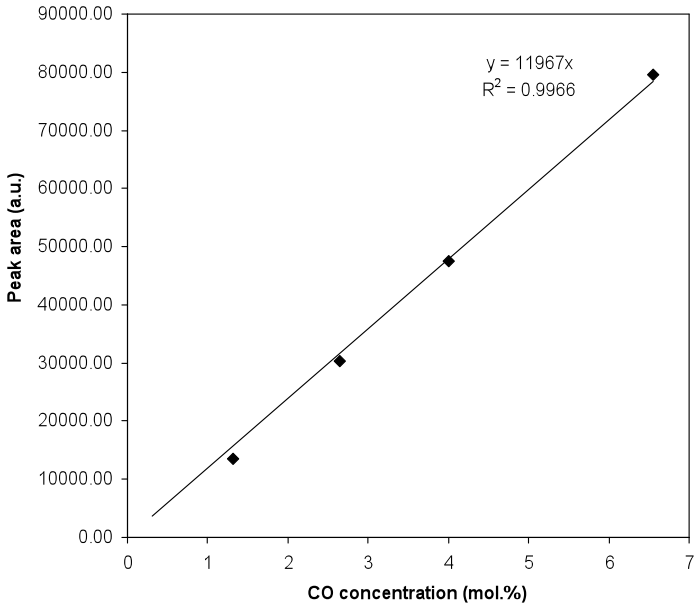

Fig. S1: CO calibration curve obtained from GC equipped with 1.8 m CTR I column (Alltech Associates, Inc).

APPENDIX II

To confirm whether small amounts of carbonaceous species deposited on the catalyst surface during FSP preparation influenced CO-TPD results, CO_2-signals were also monitored for fresh catalyst samples (Fig. S2). The CO_2 profiles from the mass spectrometer show small levels of CO_2 were released at temperatures different to those at which CO desorbed. This indicates carbonaceous species did not contribute to or influence the CO-TPD results.

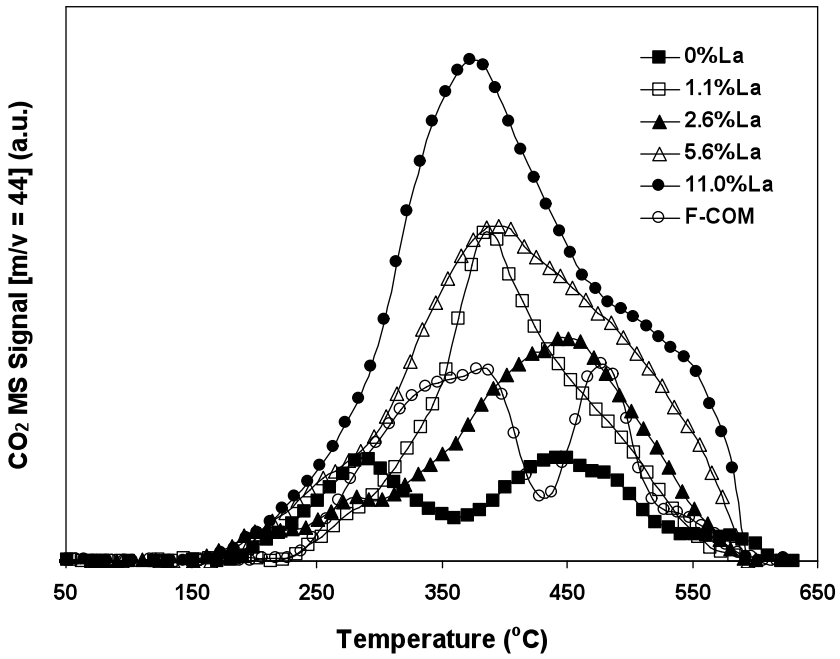

Fig. S2. Accompanying CO_2 signal during CO-TPD of FSP-prepared 37%Cu/ZnO catalysts with increasing La dopant loadings. F-COM represents the Al-doped catalyst and is included for comparison.

APPENDIX III

To assess the effect of gas composition on catalytic activity during the LT-WGS reaction, FSP-prepared 4%Cu/ZnO catalyst was subject to 'ideal' and 'realistic' conditions. Under the ideal condition, no CO_2 and H_2 were present in the gas feed while in the realistic condition the gas composition was as described in Section 2.4. The activity at these two sets of conditions is shown in Fig. S3. We observed the activity of the 4%Cu/ZnO under the ideal condition was considerably higher than under the realistic condition. A gas composition containing CO and H_2O alone is seldom encountered with the ideal situation highly unlikely in practice. Consequently, the more realistic gas composition was used throughout this study. An experimental run without catalyst (control) demonstrated that the stainless steel reactor did not contribute to the LT-WGS activity.

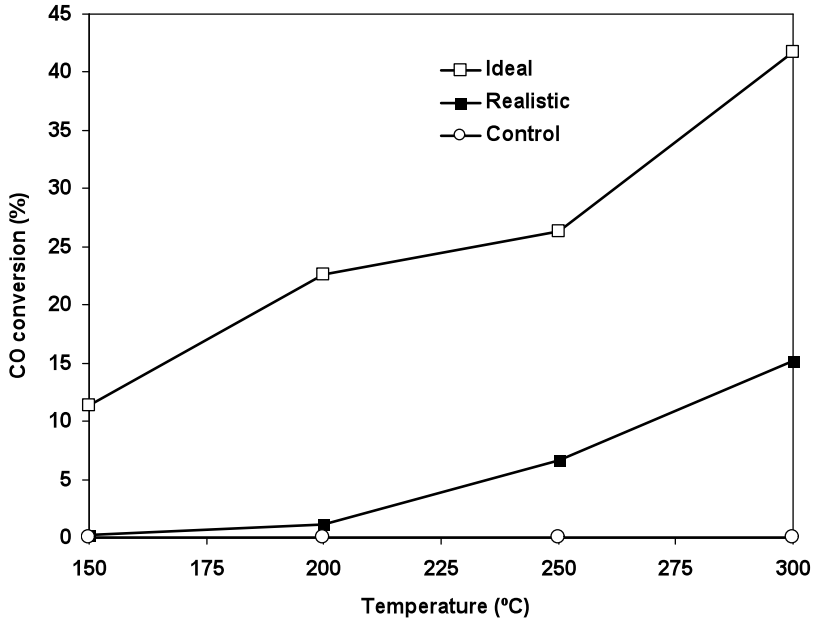

Fig. S3. Effect of gas composition on the activity of 4%Cu/ZnO catalyst for the LT-WGS reaction and the activity of the stainless steel reactor without catalyst (control). Reaction conditions: for ideal system, total flow = 100 mL min^{-1} (7% CO, 23% H_2O, balance N_2); for realistic system, total flow = 100 mL min^{-1} (7% CO, 8.5% CO_2, 23% H_2O, 37.5% H_2, 25% N_2); catalyst loading = 0.10 g; pressure = 1 atm.